Research Article

Brain Conflux

Abnormal intrinsic brain functional network dynamics in amnestic mild cognitive impairment

Authors

Lingling Li, Jiajia Wu, Mouxiong Zheng, Xin Xue, Jie Ma, Xuyun Hua, Jianguang Xu

Correspondence

xjg@shutcm.edu.cn(J. Xu), huaxuyun@shutcm.edu.cn (X. Hua), drmajie@126.com (J. Ma)

Graphical Abstract

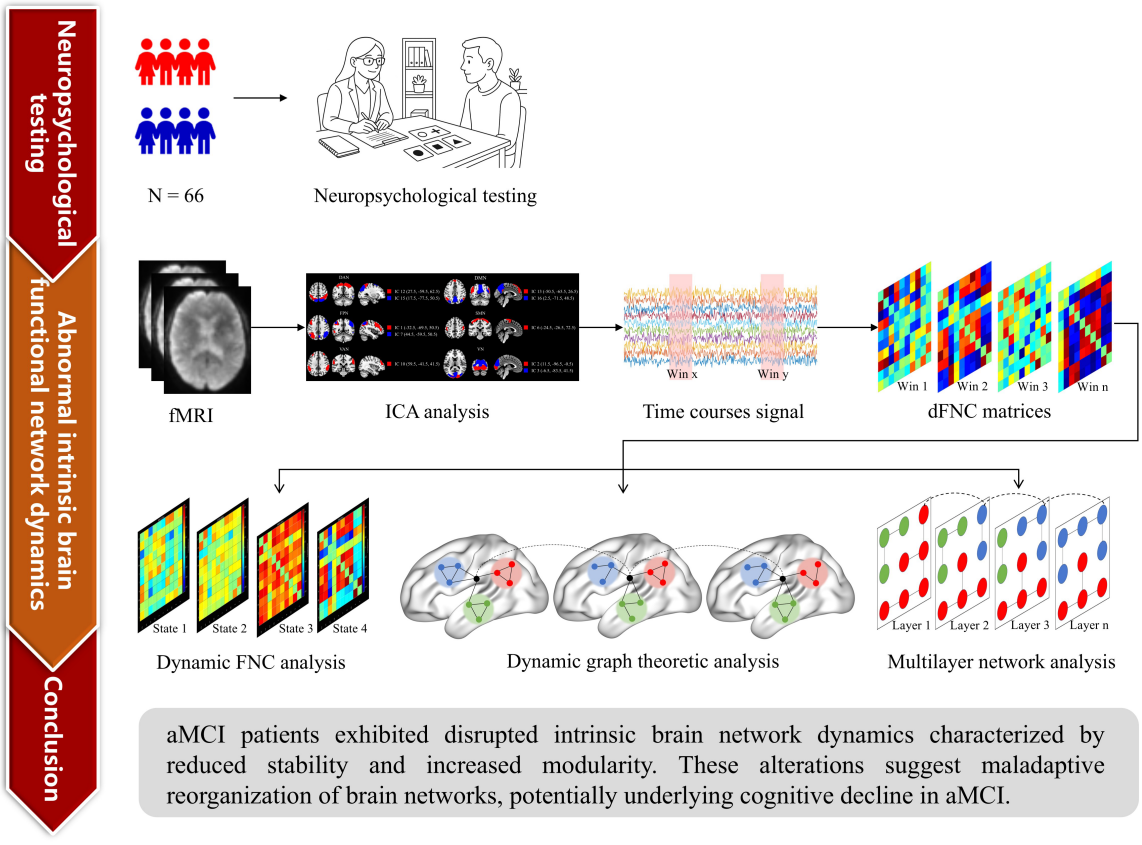

https://doi.org/10.71321/bgaxq397

Research Article Brain Conflux

Abnormal intrinsic brain functional network dynamics in amnestic mild cognitive impairment

Lingling Li [1,2†], Jiajia Wu [1†], Mouxiong Zheng [3†], Xin Xue [1], Jie Ma [1*], Xuyun Hua [3*], Jianguang Xu [1,2,4*]

Received: 2025-07-16 | Accepted: 2025-10-08 | Published online: 2025-10-25

Abstract

Background: Amnestic mild cognitive impairment (aMCI), owing to its high prevalence and significant prognostic relevance for dementia, has become a key focus in the early detection and intervention of neurodegenerative diseases. However, the abnormal intrinsic brain functional network dynamics in aMCI patients remain inadequately understood.

Methods: A total of 66 participants, comprising 31 aMCI patients and 35 age- and education-matched healthy controls (HCs), underwent resting-state fMRI scans and comprehensive neuropsychological assessments. This study examined intrinsic brain network dynamics in aMCI patients via dynamic functional network connectivity (dFNC) analysis, dynamic graph theoretical analysis, and multilayer network analysis.

Results: Compared with HCs, aMCI patients presented a significantly shorter mean dwell time (MDT) in state 2 ($P < 0.05$). In addition, the modularity coefficient Q was significantly greater in aMCI patients (1.40 ± 1.20) than in HCs (0.90 ± 0.46, $P < 0.05$). No significant differences were observed between the groups in terms of network efficiency or network switching rates.

Conclusion: These findings emphasize significant abnormal intrinsic brain functional network dynamics in aMCI patients, with disrupted network stability and increased modularity indicating maladaptive reorganization of brain networks. These results provide valuable biomarkers for early diagnosis and intervention, contributing to a deeper understanding of the neurobiological underpinnings of cognitive decline in aMCI patients.

Keywords: aMCI; dynamic functional network; fMRI; multilayer networks; independent component analysis; graph theory.

Introduction

Mild cognitive impairment (MCI) represents an intermediate stage between normal aging and dementia and is characterized by a progressive decline in memory or other cognitive functions without significant impairment in activities of daily living but does not meet the diagnostic criteria for dementia [1]. Amnestic mild cognitive impairment (aMCI), the most common subtype, is likely to progress to dementia, with an 80% probability of progressing within 6 years of diagnosis [2]. Owing to its high prevalence and strong prognostic relevance for dementia, aMCI has emerged as a critical focus for early detection and intervention in neurodegenerative disease research [3].

Functional magnetic resonance imaging (fMRI), especially resting-state fMRI, has become a powerful tool for investigating the intrinsic brain functional network. Numerous studies have demonstrated that aMCI patients exhibit abnormal intrinsic functional connectivity in specific brain networks, such as the default mode network (DMN) and frontoparietal network (FPN), which are closely associated with cognitive impairments [4]. Despite these findings, most existing studies have focused primarily on static functional network connectivity, often overlooking the dynamic and temporally variable nature of intrinsic brain activity [5]. However, brain networks dynamically reorganize their functional connections over time [5], and these dynamic properties may reveal essential neuropathological mechanisms underlying cognitive dysfunction in aMCI patients.

This study investigated abnormal intrinsic brain functional network dynamics in aMCI patients via dynamic functional network connectivity (dFNC) analysis and multilayer network analysis. Unlike traditional static methods, dFNC enables the examination of temporal fluctuations and state transitions in

1 Department of Rehabilitation Medicine, Yueyang Hospital of Integrated Traditional Chinese and Western Medicine, Shanghai University of Traditional Chinese Medicine, Shanghai 200437, China.

2 School of Rehabilitation Science, Shanghai University of Traditional Chinese Medicine, Shanghai 201203, China.

3 Department of Traumatology and Orthopedics, Shuguang Hospital, Shanghai University of Traditional Chinese Medicine, Shanghai 201203, China.

4 Engineering Research Center of Traditional Chinese Medicine Intelligent Rehabilitation, Ministry of Education, Shanghai 201203, China.

† These authors contributed equally to this work.

* Corresponding Author.

functional connectivity, offering a more nuanced understanding of network instability and adaptability in aMCI patients [6]. These dynamic changes may reflect underlying neuropathological processes that static analyses fail to capture, offering deeper insight into the mechanisms driving cognitive decline. Additionally, examining variability in brain network topology, such as global and local efficiency, reveals disruptions in the brain's capacity for efficient information integration and processing [7]. Disruptions in these topological properties may signal impairments in the ability of the brain to efficiently process and integrate information, which is crucial for maintaining cognitive function [8].

Another key dimension in the study of brain network dynamics is modular organization, which is commonly quantified by the modularity coefficient Q. Modularity reflects the degree to which brain regions are clustered into functionally specialized modules or communities, promoting efficient local processing within modules while enabling integration across the brain [9]. However, alterations in modularity—manifested as either excessive segregation or impaired integration between modules—have been implicated in cognitive decline and neurodegenerative processes [10]. Notably, an increased modularity coefficient Q may signal a shift toward heightened local specialization at the expense of global network coordination, which could hinder the ability of the brain to integrate information and respond adaptively to cognitive demands [9, 11]. In parallel, the rate at which the brain transitions between different network states, termed the network switching rate, serves as an index of network flexibility and adaptability. Frequent and efficient switching is thought to facilitate cognitive flexibility and support dynamic responses to changing environmental or task-related requirements [12]. In aMCI patients, disruptions in modularity and alterations in network switching rates may reflect maladaptive neural reorganization or compensatory mechanisms in response to emerging cognitive deficits.

In summary, this study aims to comprehensively characterize the abnormal intrinsic brain functional network dynamics in aMCI patients via dFNC analysis, dynamic graph theoretic analysis, and multilayer network analysis. These dynamic outcomes have the potential to reveal specific biomarkers for the early detection and monitoring of disease progression, offering new opportunities for personalized interventions. The findings from this study are expected to provide a deeper understanding of how large-scale brain network reorganization contributes to cognitive decline in aMCI patients, thereby informing future clinical strategies for the diagnosis and management of neurodegenerative diseases.

Materials and Methods

Participants

For this case-control study, we initially recruited 110 participants from the Memory Clinic of Yueyang Hospital of Integrated Traditional Chinese and Western Medicine and local communities in Shanghai between January 2022 and October 2022. Ultimately, 31 (28.18%) aMCI patients and 35 (31.82%) healthy controls (HCs) matched for age, sex, and education were included. Approval for the study was obtained from the local ethics committee (NO. 2021-103), and all participants provided informed consent.

The inclusion criteria for the aMCI group were as follows: (1) met the Jak/Bondi diagnostic criteria [13]; (2) had a Mini-Mental State Examination (MMSE) score > 24 points [14]; (3) were aged 55–80 years; (4) had objective memory impairment, Auditory Verbal Learning Test Long-Term Delay Recall (AVLT-N5) and Recognition (AVLT-N7) scores falling below 1.0 standard deviation (SD) from the age-corrected normative mean [15]; (5) had complex Instrumental Activity of Daily Living (IADL) ability that might have been slightly impaired while still maintaining independent daily living [16]; (6) had a Clinical Dementia Rating (CDR) memory score of 0.5 points [17] but did not meet the diagnostic criteria for dementia set by the National Institute on Aging-Alzheimer's Association (NIA-AA) [18]; and (7) were right-handed.

The inclusion criteria for the HCs group were as follows: (1) lacked complaints of cognitive decline; (2) had neuropsychological testing results that did not meet Jak/Bondi's diagnostic criteria [13]; (3) had a normal ability to perform activities of daily living; and (4) lacked a family history of dementia.

The exclusion criteria for all participants were as follows: (1) had a history of mental illness, such as delirium, mania, depression, or anxiety; (2) had contraindications for magnetic resonance imaging (MRI) examination; (3) had less than 6 years of education; (4) had severe aphasia and audio-visual impairment; (5) had severe medical diseases, such as cardiopulmonary insufficiency, liver, or renal insufficiency; and (6) had other diseases that caused cognitive impairment and white matter hyperintensity lesions, such as cerebrovascular disease, craniocerebral trauma, hydrocephalus, brain tumors, or intracranial infection.

Neuropsychological testing

All participants underwent comprehensive neuropsychological testing conducted by two senior neuropsychologists who were blinded to the clinical diagnosis. General cognitive function was assessed via the MMSE, Montreal Cognitive Assessment-Basic (MoCA-B) and Addenbrooke's Cognitive Examination III (ACE-III) [14, 19-20]. Memory function was assessed via the AVLT [21], and attention function was assessed via the Symbol Digit Modalities Test (SDMT) [22]. Language function was assessed via the Boston Naming Test (BNT) [23] and Animal Verbal Fluency Test (AFT) [24]. Executive function was assessed via the Stroop test [25], and spatial function was assessed via the Judgment of Line Orientation (JLO) test [26] and Silhouette Test (ST) [27].

Data acquisition

A 3.0 Tesla Magnetom Prisma scanner (Siemens Healthcare, Erlangen, Germany) was used for fMRI scanning, employing a head coil for scans ranging from the cranial vertex to the level of the foramen magnum. During the scan, they were asked to lie quietly in the scanner, close their eyes without falling asleep, and try to keep their heads as still as possible. The detailed fMRI protocols are provided in Supplemental Table 1.

Data preprocessing

The standard pipeline of Statistical Parametric Mapping version 12 (SPM12, https://www.fil.ion.ucl.ac.uk/spm/software/spm12/) was used for resting-state fMRI data preprocessing. This data preprocessing pipeline included the exclusion of the first 10 volumes, slice timing correction, realignment, normal-

ization and smoothing [15].

Group independent component analysis

Group independent component analysis (ICA) was performed on the preprocessed fMRI data via the Group ICA of the Functional MRI Toolbox (GIFT v3.0c, http://icatb.sourceforge.net) [28]. The detailed processing procedure involves the following steps: (1) Principal component analysis (PCA) is applied twice to perform dimensionality reduction on the preprocessed data [29]. (2) The InfoMax algorithm is applied to perform ICA on the PCA-reduced dataset to extract independent components (ICs) [30]. (3) Independent component analysis and stability selection (ICASSO) was applied for 20 repeated iterations to increase the reliability and stability of the ICA results [31], ultimately yielding 17 ICs. (4) Individual-level ICs were extracted from the group ICA back-reconstruction and subjected to Fisher's Z-transformation [32]. (5) The sorting component GUI module in the GIFT software, in conjunction with the maximum spatial overlap of spatial network templates, was employed to select significant ICs and categorize them into distinct functional networks. The selection criteria for ICs were detailed in Supplementary Material 1.

The time series signals corresponding to the ICs mapped to brain functional networks were postprocessed to reduce noise interference: (1) removal of linear, quadratic, and cubic drifts; (2) removal of spike signals; (3) low-pass filtering with a cutoff frequency of 0.15 Hz; and (4) regression of head motion parameters [33].

Dynamic FNC analysis

The GIFT toolbox (v3.0c, http://icatb.sourceforge.net) was utilized to extract the time series of ICs associated with the functional brain networks for dFNC analysis. The time series were segmented into multiple consecutive time windows via the widely applied sliding window approach, with a window length of 44 seconds (55 TRs) and a step size of 1 TR, as this selection has been reported to provide a good balance between the ability to capture dynamic functional connectivity changes and the quality of correlation matrix estimation [34]. On this basis, k-means clustering methods were employed to perform clustering analysis on the dFNC matrix [35]. The L1 distance (Manhattan distance) function was employed to estimate the similarity between different time windows [36], and 500 iterations and 150 repetitions were used to increase the robustness of the results [37]. The optimal number of clusters was determined via the elbow method (k = 4) [37], which involves partitioning the dFNC into four states. For each state, the following temporal features were computed: (1) fraction time (FT): the frequency with which each state occurs during the total duration; (2) mean dwell time (MDT): the average time the subjects remain in each state; (3) number of transitions (NT): the number of transitions between different dynamic states, reflecting the frequency with which the brain network switches from one state to another [33]. Then, a validation analysis was conducted using a window length of 56 seconds (70 TRs) to evaluate robustness. Additionally, edge analysis was conducted for each state to assess the functional connectivity among different brain networks.

Dynamic graph theoretic analysis

The graph theoretical analysis (GRETNA) toolbox (http://www.nitrc.org/projects/gretna/) [38] was applied to conduct graph theoretical variability analysis on the dFNC matrix in each time window. To ensure the sparsity and comparability of the results, a stepwise thresholding method (0.27: 0.01: 0.48) was employed to compute the variations in the graph theory metrics across different sparsity levels [39]. At each sparsity threshold, two categories of graph theory metrics were calculated: global efficiency and local efficiency. The variability of the area under the curve (AUC) for global and local efficiency across all sparsity levels was used to evaluate the dynamic evolution of the brain's functional network topology, thereby avoiding bias associated with selecting a single sparsity threshold [33].

Multilayer modularity and network switching analysis

The functional network connectivity information of each time window is treated as an individual layer, with layers from different time windows interlinked to form a multilayer network. The iterative ordered Louvain algorithm was applied to perform modularity analysis of the network (with parameters gammas = [0.9, 1, 1.1], omegas = [0.5, 0.75, 1]) [40]. This algorithm can automatically identify functional modules within the network and compute the modularity coefficient Q, which quantifies the density of different modules and the strength of connections between modules. Additionally, the network transition rate of nodes was computed to assess the dynamic changes and switching patterns of the brain network across functional modules. The data processing pipelines are depicted in Figure 1.

Figure 1. Pipelines for data processing.

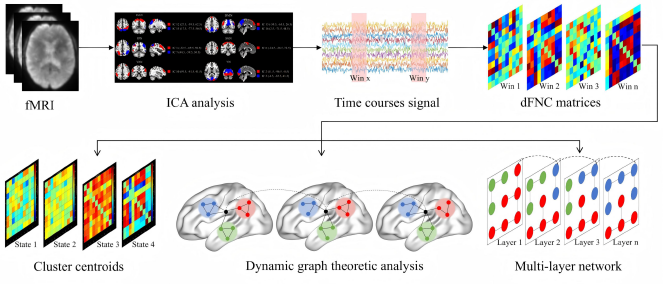

Statistical analysis

Clinical data were analyzed via SPSS software version 27.0 (IBM Corp., Armonk, NY, USA). Intergroup comparisons for continuous variables were performed via the independent two-sample t-test, whereas categorical variables were analyzed via the chi-square (χ^2) test. A significance level of $P < 0.05$ was considered indicative of statistically significant differences between the groups.

The FT, MNT, NT, variability of global and local efficiency, modularity coefficient Q, and network switching analysis were compared between groups via a general linear model, with age, sex, and education included as covariates. Partial correlation analyses were subsequently conducted between the aforementioned group-differentiated network metrics and neuropsychological test scores, with age, sex, and education included as covariates.

https://doi.org/10.71321/bgaxq397

Results

Demographic and clinical characteristics

The baseline characteristics of aMCI patients and HCs are listed in Table 1, including demographic data and cognitive function scores. There was no statistically significant difference in gender, age, height, weight or education between the two groups (P > 0.05). aMCI patients presented impairments in general cognitive function and in multiple specific cognitive domains.

Intrinsic connectivity networks

Ten significant independent components (ICs) were identified and assigned to six brain networks (Figure 2): the dorsal attention network (DAN: IC12 and IC15); the default mode network (DMN: IC13 and IC16); the frontoparietal network (FPN: IC1 and IC7); the somatomotor network (SMN: IC6); the ventral attention network (VAN: IC10); and the visual network (VN: IC2 and IC3).

Dynamic FNC analysis

After applying clustering via the k-means algorithm, the optimal number of clusters was determined via the elbow method, resulting in four states (Figure 3): state 1 (32%), state 2 (44%), state 3 (16%), and state 4 (8%).

Compared with HCs, the MDT in state 2 was significantly lower in aMCI patients ($P < 0.05$), whereas no statistically significant differences were observed in the FT or NT across the four states between the two groups (Figure 4, $P > 0.05$). Partial correlation analysis further revealed a significant positive correlation between MDT in state 2 and completion time on Stroop test A, after controlling for age, sex, and education (r = 0.338, $P = 0.007$).

Additionally, the results of the edge analysis for each state are shown in Supplementary Figure 1.

Figure 2 Spatial patterns of the resting-state networks.

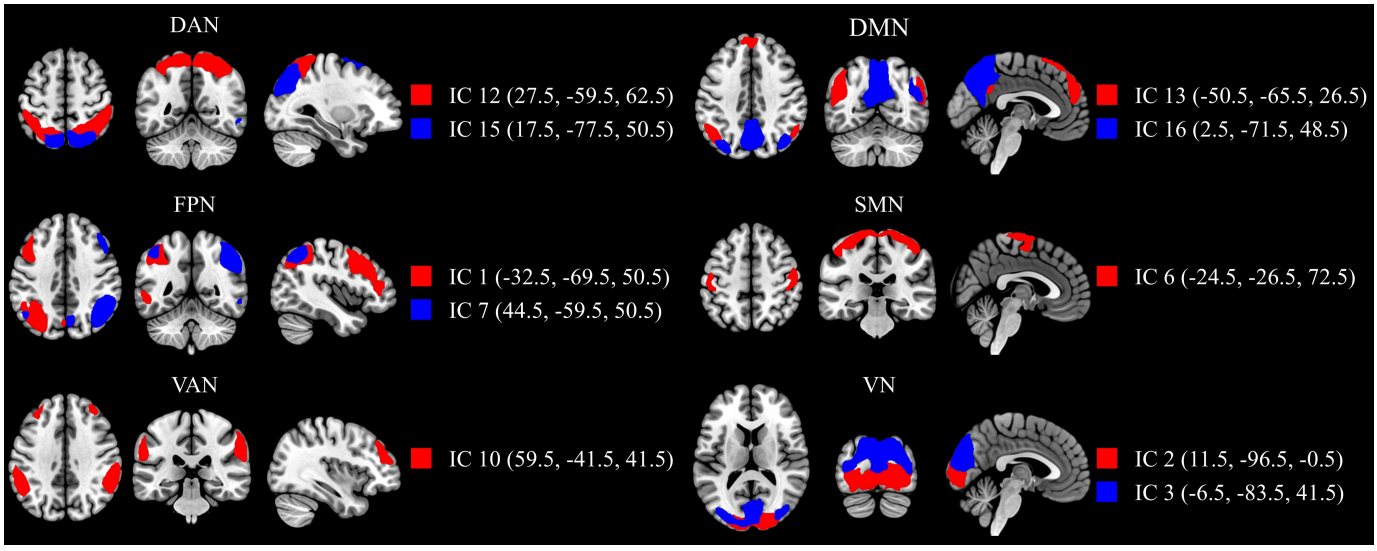

Figure 3. K-means clustering analysis results.

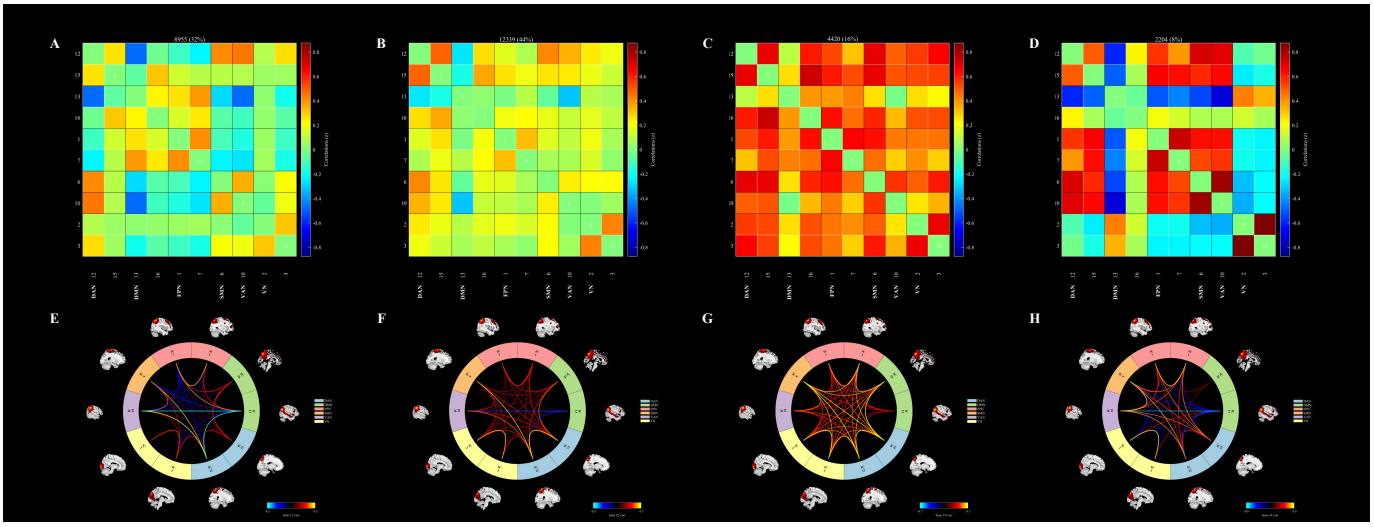

Table 1. Clinical characteristics and neuropsychological testing results.

Characteristics	HCs (N = 35)	aMCI (N = 31)	T/χ^2	*P*
Basic characteristics				
Age (y)	65.09±6.49	67.65±7.32	-1.505	0.137
Education (y)	11.46±3.13	11.74±3.11	-0.37	0.712
Height (cm)	163.51±6.21	161.15±12.17	0.914	0.367
Weight (kg)	61.94±9.58	62.58±12.24	-0.223	0.824
Gender, male (%)	w8 (22.86%)	13 (41.94%)	2.758	0.097
Cognitive performance				
General cognitive function				
MMSE	28.43±1.52	27.13±1.63	3.353	0.001
MoCA-B	26.26±1.99	22.52±3.13	5.863	< 0.001
ACE-III	82.49±8.19	76.32±6.03	3.507	< 0.001
Memory function				
AVLT	60.49±9.63	34.42±8.24	11.738	< 0.001
AVLT-N1	4.06±1.30	2.97±0.89	3.869	< 0.001
AVLT-N2	6.86±1.77	4.47±0.94	6.942	< 0.001
AVLT-N3	8.23±1.59	5.23±1.25	8.487	< 0.001
AVLT-N4	6.69±1.71	2.33±1.37	11.181	< 0.001
AVLT-N5	6.37±1.97	1.57±1.36	11.253	< 0.001
AVLT-N6	6.17±2.42	1.90±1.40	8.861	< 0.001
AVLT-N7	22.11±1.57	17.10±1.77	12.118	< 0.001
Attention function				
SDMT	42.40±8.97	30.10±13.13	4.336	< 0.001
Language function				
BNT	24.24±2.84	22.67±4.08	1.769	0.082
AFT	18.57±4.34	16.35±4.29	2.083	0.041
Executive function				
Stroop test-A	24.00±0.00	23.97±0.19	1.000	0.326
Stroop test-B	23.20±1.86	21.83±2.77	2.279	0.027
Stroop test-A (s)	13.84±3.98	13.30±2.60	0.632	0.530
Stroop test-B (s)	34.78±18.47	41.73±10.33	-1.812	0.075
Spatial function				
JLO	463.11±32.27	380.48±59.78	7.098	< 0.001
ST	235.37±19.41	204.58±43.96	3.754	< 0.001

Figure 4. Dynamic temporal properties of dFNC states. A-D Cluster centroids for each state; E-H Functional connectivity in each state.

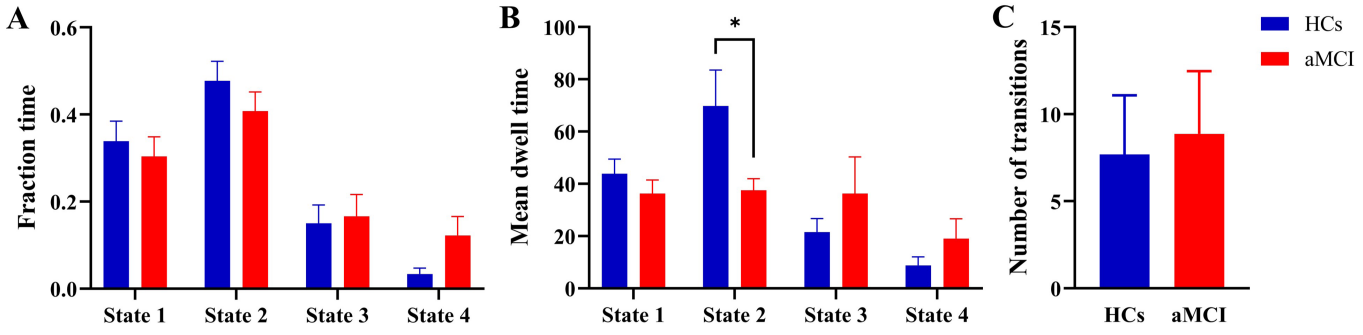

A fraction time; **B** mean dwell time; **C** number of transitions; The middle horizontal line represents the mean value, and the upper and lower horizontal lines represent the standard deviations. aMCI: amnestic mild cognitive impairment; HCs: healthy controls; *: *P* < 0.05.

Dynamic network topology analysis

Dynamic network topology analysis, which is based on the variance of the dFNC matrix, revealed no significant differences in global or local efficiency between the two groups (Supplementary Figure 2, $P > 0.05$).

Multilayer modularity and network switching analysis

Compared with that in HCs (0.90 ± 0.46), the modularity coefficient Q in aMCI patients (1.40 ± 1.20) was significantly greater ($P < 0.05$), with gammas = 1 and omegas = 1. Partial correlation analysis further revealed a significant negative correlation between the modularity coefficient Q and the SDMT score after controlling for age, sex, and education ($r = -0.349$, $P = 0.004$). However, no significant differences were observed in the network switching rates of the six brain networks between the groups (Figure 5, $P > 0.05$). The results for additional parameter combinations (gammas = [0.9, 1, 1.1] and omegas = [0.5, 0.75, 1]) can be found in Supplementary Table 2.

Validation analysis

After applying clustering via the k-means algorithm, the optimal number of clusters was determined via the elbow method, resulting in four states (Supplementary Figure 3): state 1 (44%), state 2 (10%), state 3 (36%), and state 4 (30%).

Compared with that in HCs, the MDT in state 1 was significantly lower in aMCI patients ($P < 0.05$), whereas no statistically significant differences were observed in the FT or NT across the four states between the two groups (Supplementary Figure 4, $P > 0.05$).

Discussion

This study investigated the abnormal intrinsic brain functional network dynamics in aMCI patients through the application of dFNC analysis, dynamic graph theory analysis and multilayer brain network analysis. K-means clustering analysis categorized the brain network into four states, with state 2 occupying the largest proportion (44%), in which aMCI patients demonstrated significantly lower MDTs, indicating the reduced stability of the brain network in this state and its strong correlation with cognitive impairment. Although State 4 occurred infrequently (8% dwell time), it presented sparse and weak internetwork connectivity and resembled a transient low-integration configuration. Furthermore, aMCI patients demonstrated a significant increase in the modularity coefficient Q, suggesting that the modular structure of the brain network underwent alterations, potentially indicating an enhancement in local information transmission and a reduction in the coordination of the brain network. Although no significant differences were observed in graph theory variability analysis or network switching rates among aMCI patients, the changes in the modularity coefficient provide novel insights into brain network reorganization and its role in modulating cognitive function. These findings provide important insights into the changes in the brain networks of aMCI patients and their relationships with cognitive dysfunction, identifying potential biomarkers for future research and clinical diagnosis.

In this study, aMCI patients demonstrated a significant decrease in MDT scores in state 2, indicating reduced stability of brain functional network connectivity in this state and potentially indicating a neural network dysregulation mechanism associated with cognitive dysfunction. Further edge analysis revealed that aMCI patients demonstrated marked alterations in the functional connectivity between several key networks in state 2, with reduced connectivity involving mainly the DMN, FPN, DAN, and SMN. Specifically, the reduced connectivity between the DMN and FPN could disrupt the integration of information across internal thinking, self-referential processing, and higher-order executive functions [41-42], whereas the diminished connectivity between the FPN and SMN may reflect the dissociation between motor execution and cognitive control [43], a dysfunction commonly observed in aMCI patients. Moreover, the reduction in connectivity between the DAN and FPN could further impair the interaction between the regulation of external attention and task-directed control [44]. In contrast, aMCI patients demonstrated enhanced connectivity between the VAN and DMN, potentially indicating a compensatory regulatory mechanism whereby the coupling between the visual-attention system and the spontaneous thinking system is enhanced to sustain some cognitive functions [45]. However, this enhanced VAN–DMN connectivity may reflect a compensatory regulatory mechanism in which the coupling between the stimulus-driven, bottom-up visual attention system and the spontaneous, internally oriented thought system is strengthened to support cognitive function, although its effectiveness and adaptability in aMCI remain uncertain [46-47]. Overall, the abnormal alterations in the connectivity patterns between these networks may underlie the neural mechanisms underlying the reduced time spent in state 2 by aMCI patients, providing crucial insights into the functional dysregulation of their brain networks.

This study demonstrated a significant increase in the modularity coefficient Q in aMCI patients, suggesting that the modular structure of the brain network underwent alterations. The modularity coefficient Q quantifies the degree of clustering between different functional regions of the brain network, and an increase in the Q value could indicate an improvement in local information transfer [9, 48]. However, this enhanced modular structure could be linked to a reduction in coordination between different brain regions, suggesting impairment of the network's functional integration [49]. In aMCI patients, the increase in the modularity coefficient Q could represent an adaptive reorganization strategy by the brain to compensate for cognitive function loss, but localized processing of information might result in reduced global brain coordination, thereby leading to cognitive dysfunction, particularly in complex tasks, such as memory. In clinical practice, changes in the modularity coefficient Q provide promising biomarkers for the early diagnosis of aMCI, particularly when traditional cognitive assessment tools (such as the MMSE and MoCA) fail to identify subtle changes in brain function, as an increase in the Q value reflects early brain network abnormalities. In addition, the increase in the modularity coefficient Q is strongly inversely correlated with the decline in cognitive function, particularly attention, which further suggests that the modular alterations in the brain network are closely linked to cognitive impairment in aMCI patients.

Although significant differences were observed in the modularity coefficient Q, no notable differences were found in the dynamic network topology or network switching rates among aMCI patients. Dynamic network topology analysis provides

assessments of the global and local efficiencies of the brain network as it changes over time, which may reveal the stability of neural connectivity and the efficiency of information transfer [50]. However, our results revealed no significant differences in these metrics between aMCI patients and healthy controls, suggesting that despite alterations in the modular structure of the brain network in aMCI patients, the overall efficiency of network connectivity has not been significantly compromised. This finding could suggest the brain's capacity for adaptation under various cognitive states, particularly since no apparent impairment in task-switching ability or processing speed was observed. This finding may also correlate with the reduction in MDT observed in state 2 of the dFNC analysis, indicating that while aMCI patients exhibit poorer network stability, the brain remains capable of preserving a certain level of network efficiency and adaptability. Therefore, while dynamic network topology analysis did not reveal significant group differences, the changes in the modularity coefficient Q provide a clearer understanding of network functional reorganization and cognitive decline in aMCI patients. Future research should further explore the underlying mechanisms and clinical implications of these findings.

Figure 5. Network switching rates of the six brain networks.

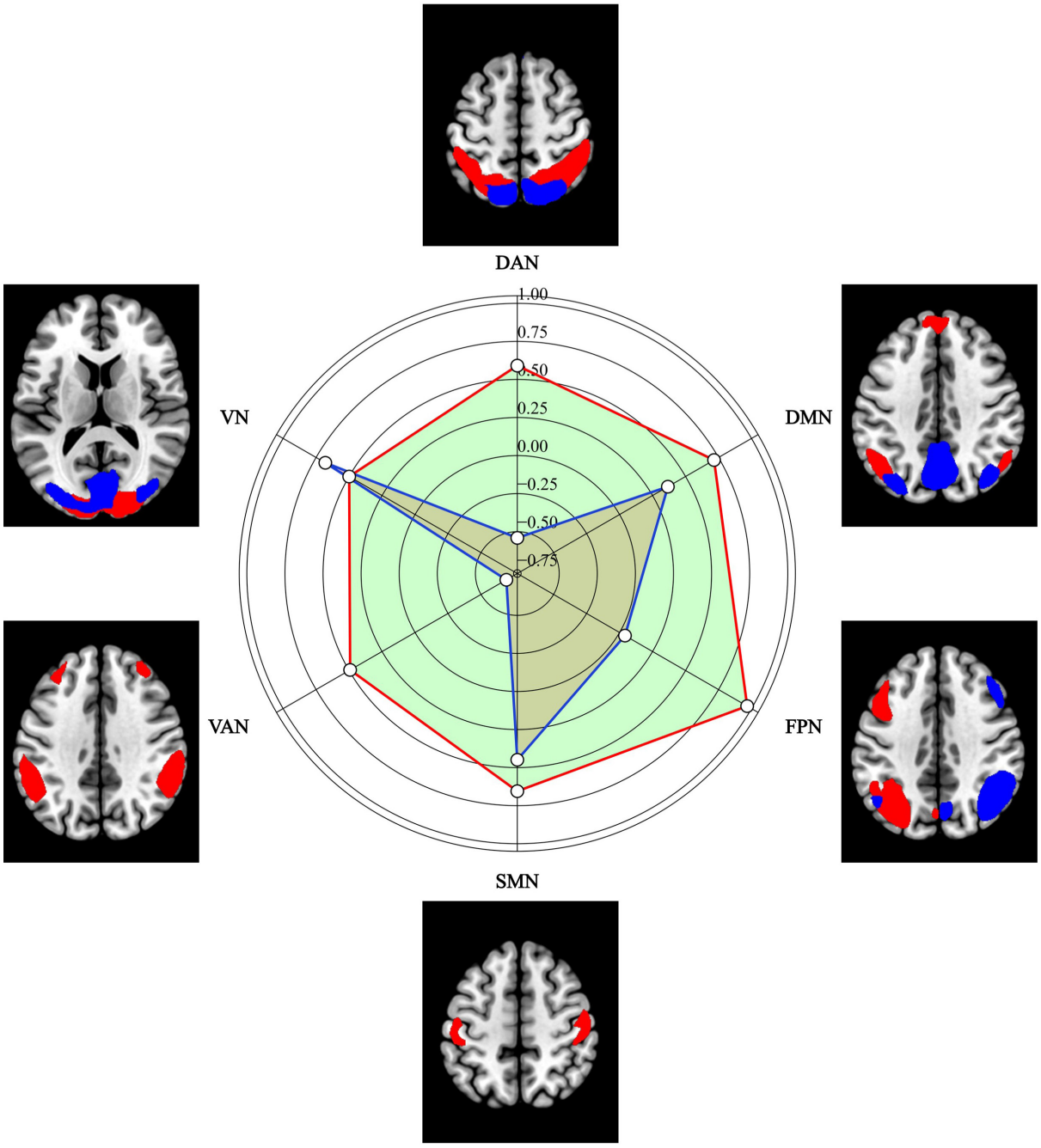

Red lines represent P values, and blue lines represent T values.

Despite the important insights yielded by this study into the abnormal intrinsic brain functional network dynamics in aMCI patients, several limitations should be acknowledged. First, the relatively small sample size may reduce the statistical power and limit the generalizability of the findings. Larger cohorts are needed to validate these observations and explore potential subtype differences within aMCI patients. Second, while this study employed sliding-window analysis to examine dynamic functional connectivity, the cross-sectional design precludes investigation of how these network dynamics evolve over time. Longitudinal studies with repeated neuroimaging and cognitive assessments are necessary to track the temporal trajectory of network changes and clarify their role in predicting disease progression. Third, although age, sex, and education were controlled as covariates, other potentially influential factors—such as genetic risk (e.g., APOE status), vascular health, sleep quality, subthreshold depressive symptoms and lifestyle factors—were not assessed and may confound the observed associations. Finally, the study was conducted at a single center within a limited geographic region, which may introduce selection bias. Future multicenter studies involving more demographically and ethnically diverse populations are warranted to enhance the external validity of the findings.

Conclusion

In conclusion, this study provides valuable insights into the abnormal intrinsic brain functional network dynamics in aMCI patients, highlighting significant alterations in brain network connectivity, particularly in dFNC, the modularity coefficient Q, and network topology. These findings suggest that aMCI patients exhibit reduced stability in certain brain network states, particularly in state 2, as indicated by decreased MDT and alterations in modularity that reflect a shift in the brain's network organization. Despite the lack of significant differences in global network efficiency, the increase in modularity and its correlation with cognitive decline point to the potential of using network metrics, such as the modularity coefficient Q, as biomarkers for the early diagnosis and monitoring of aMCI. These results underscore the importance of dynamic brain network analysis in understanding the neurobiological underpinnings of cognitive dysfunction in aMCI patients and provide a foundation for future longitudinal studies and clinical applications to track disease progression and develop targeted interventions. However, further research with larger, more diverse cohorts and longitudinal designs is needed to validate these findings and explore their clinical utility in real-world settings.

Abbreviations

aMCI: amnestic mild cognitive impairment; HCs: healthy controls; dFNC: dynamic functional network connectivity; MDT: mean dwell time; MCI: mild cognitive impairment; fMRI: functional magnetic resonance imaging; DMN: default mode network; FPN: frontoparietal network; MMSE: mini-mental state examination; AVLT-N5: auditory verbal learning test, long-term delay recall; AVLT-N7: auditory verbal learning test, recognition; SD: standard deviation; IADL: instrumental activity of daily living; CDR: clinical dementia rating; NIAAA: national institute on agingalzheimer's association; MRI: magnetic resonance imaging; MoCAB: montreal cognitive assessment-basic; ACE-III: addenbrooke's cognitive examination III; SDMT: symbol digit modalities test; BNT: boston naming test; AFT: animal verbal fluency test; JLO: judgment of line orientation; ST: silhouette test; ICA: independent component analysis; GIFT: group ICA of the functional MRI toolbox; PCA, principal component analysis; ICs: independent components; ICASSO: independent component analysis and stability selection; FT: fraction time; NT: number of transitions; GRETNA: graph theoretical analysis; AUC: area under the curve.

Author Contributions

Ling-Ling Li (Writing-original draft, Methodology), Jia-Jia Wu (Methodology, Project administration, Writing-review & editing), Mou-Xiong Zheng (Methodology, Project administration, Writing-review & editing), Xin Xue (Formal Analysis, Investigation, Methodology), Jie Ma (Conceptualization, Funding acquisition, Project administration, Supervision), Xu-Yun Hua (Conceptualization, Funding acquisition, Project administration, Supervision), and Jian-Guang Xu (Conceptualization, Funding acquisition, Project administration, Supervision). The authors declare no conflicts of interest.

Acknowledgments

The authors thank all the participants who participated in this study.

Funding Information

This work was supported by the National Key R&D Program of China (Grant Nos.: 2018YFC2001600, and 2018YFC2001604); National Natural Science Foundation of China (Grant Nos.: 82272583, 82172554, 82272589, 81871836, 82302870 and 82472589); Shanghai Health Care Commission (Grant No.: 2022JC026); Shanghai Science and Technology Committee (Grant No.: 22010504200); Shanghai Rising-Star Program (Grant No.: 23QA1409200 and 24QA2709300); Shanghai Youth Top Talent Development Plan; Shanghai "Rising Stars of Medical Talent" - Distinguished Young Medical Talent Program; Shanghai Talent Development Fund (2021074), Science & Technology Development Fund of Shanghai University of Traditional Chinese Medicine (Grant No.: 23KFL112); High-level Chinese Medicine Key Discipline Construction Project (Integrative Chinese and Western Medicine Clinic) of National Administration of TCM (zyyzdxk-2023065); Shanghai Hospital Development Center Foundation-Shanghai Municipal Hospital Rehabilitation Medicine Specialty Alliance (SHDC22023304); Shanghai Oriental Talents Program (QNJY2024077).

Ethics Approval and Consent to Participate

Approval for the study was obtained from the institutional ethics committee (NO. 2021-103), and all participants provided

informed consent.

Competing Interests

The authors declare no conflicts of interest.

Data Availability

The original contributions presented in the study are included in the article/supplementary material; further inquiries can be directed to the corresponding author.

References

[1] Edmonds EC, McDonald CR, Marshall A, Thomas KR, Eppig J, Weigand AJ, et al. (2019). Early versus late MCI: Improved MCI staging using a neuropsychological approach. Alzheimers Dement, 15(5), 699-708. https://doi.org/10.1016/j.jalz.2018.12.009

[2] Gauthier S, Reisberg B, Zaudig M, Petersen RC, Ritchie K, Broich K, et al. (2006). Mild cognitive impairment. Lancet, 367(9518), 1262-1270. https://doi.org/10.1016/s0140-6736(06)68542-5

[3] Mian M, Tahiri J, Eldin R, Altabaa M, Sehar U, & Reddy PH. (2024). Overlooked cases of mild cognitive impairment: Implications to early Alzheimer's disease. Ageing Res Rev, 98, 102335. https://doi.org/10.1016/j.arr.2024.102335

[4] Varela-López B, Zurrón M, Lindín M, Díaz F, & Galdo-Alvarez S. (2025). Compensation versus deterioration across functional networks in amnestic mild cognitive impairment subtypes. Geroscience, 47(2), 1805-1822. https://doi.org/10.1007/s11357-024-01369-9

[5] Golesorkhi M, Gomez-Pilar J, Zilio F, Berberian N, Wolff A, Yagoub MCE, et al. (2021). The brain and its time: intrinsic neural timescales are key for input processing. Commun Biol, 4(1), 970. https://doi.org/10.1038/s42003-021-02483-6

[6] Fu Z, Du Y, & Calhoun VD. (2019). The Dynamic Functional Network Connectivity Analysis Framework. Engineering (Beijing), 5(2), 190-193. https://doi.org/10.1016/j.eng.2018.10.001

[7] Petersen SE, & Sporns O. (2015). Brain Networks and Cognitive Architectures. Neuron, 88(1), 207-219. https://doi.org/10.1016/j.neuron.2015.09.027

[8] Bullmore E, & Sporns O. (2012). The economy of brain network organization. Nat Rev Neurosci, 13(5), 336-349. https://doi.org/10.1038/nrn3214

[9] Sporns O, & Betzel RF. (2016). Modular Brain Networks. Annu Rev Psychol, 67, 613-640. https://doi.org/10.1146/annurev-psych-122414-033634

[10] Chen X, Necus J, Peraza LR, Mehraram R, Wang Y, O'Brien JT, et al. (2021). The functional brain favours segregated modular connectivity at old age unless affected by neurodegeneration. Commun Biol, 4(1), 973. https://doi.org/10.1038/s42003-021-02497-0

[11] Park HJ, & Friston K. (2013). Structural and functional brain networks: from connections to cognition. Science, 342(6158), 1238411. https://doi.org/10.1126/science.1238411

[12] Koch I, Poljac E, Müller H, & Kiesel A. (2018). Cognitive structure, flexibility, and plasticity in human multitasking-An integrative review of dual-task and task-switching research. Psychol Bull, 144(6), 557-583. https://doi.org/10.1037/bul0000144

[13] Bondi MW, Edmonds EC, Jak AJ, Clark LR, Delano-Wood L, McDonald CR, et al. (2014). Neuropsychological criteria for mild cognitive impairment improves diagnostic precision, biomarker associations, and progression rates. J Alzheimers Dis, 42(1), 275-289. https://doi.org/10.3233/jad-140276

[14] Arevalo-Rodriguez I, Smailagic N, Roqué-Figuls M, Ciapponi A, Sanchez-Perez E, Giannakou A, et al. (2021). Mini-Mental State Examination (MMSE) for the early detection of dementia in people with mild cognitive impairment (MCI). Cochrane Database Syst Rev, 7(7), Cd010783. https://doi.org/10.1002/14651858.CD010783.pub3

[15] Li LL, Ma J, Wu JJ, Xue X, Zheng MX, Hua XY, et al. (2025). Impact of effective connectivity within the Papez circuit on episodic memory: moderation by perivascular space function. Alzheimers Res Ther, 17(1), 66. https://doi.org/10.1186/s13195-025-01717-7

[16] Ma J, Zheng MX, Wu JJ, Xing XX, Xiang YT, Wei D, et al. (2023). Mapping the long-term delayed recall-based cortex-hippocampus network constrained by the structural and functional connectome: a case-control multimodal MRI study. Alzheimers Res Ther, 15(1), 61. https://doi.org/10.1186/s13195-023-01197-7

[17] Wilks H, Benzinger TLS, Schindler SE, Cruchaga C, Morris JC, & Hassenstab J. (2024). Predictors and outcomes of fluctuations in the clinical dementia rating scale. Alzheimers Dement, 20(3), 2080-2088. https://doi.org/10.1002/alz.13679

[18] McKhann GM, Knopman DS, Chertkow H, Hyman BT, Jack CR, Jr., Kawas CH, et al. (2011). The diagnosis of dementia due to Alzheimer's disease: recommendations from the National Institute on Aging-Alzheimer's Association workgroups on diagnostic guidelines for Alzheimer's disease. Alzheimers Dement, 7(3), 263-269. https://doi.org/10.1016/j.jalz.2011.03.005

[19] Chen KL, Xu Y, Chu AQ, Ding D, Liang XN, Nasreddine ZS, et al. (2016). Validation of the Chinese Version of Montreal Cognitive Assessment Basic for Screening Mild Cognitive Impairment. J Am Geriatr Soc, 64(12), e285-e290. https://doi.org/10.1111/jgs.14530

[20] Matias-Guiu JA, Cortés-Martínez A, Valles-Salgado M, Rognoni T, Fernández-Matarrubia M, Moreno-Ramos T, et al. (2017). Addenbrooke's cognitive examination III: diagnostic utility for mild cognitive impairment and dementia and correlation with standardized neuropsychological tests. Int Psychogeriatr, 29(1), 105-113. https://doi.org/10.1017/s1041610216001496

[21] Zhao Q, Guo Q, Liang X, Chen M, Zhou Y, Ding D, et al. (2015). Auditory Verbal Learning Test is Superior to Rey-Osterrieth Complex Figure Memory for Predicting Mild Cognitive Impairment to Alzheimer's Disease. Curr Alzheimer Res, 12(6), 520-526. https://doi.org/10.2174/1567205012666150530202729

[22] Silva PHR, Spedo CT, Baldassarini CR, Benini CD, Ferreira DA, Barreira AA, et al. (2019). Brain functional and effec-

tive connectivity underlying the information processing speed assessed by the Symbol Digit Modalities Test. Neuroimage, 184, 761-770. https://doi.org/10.1016/j.neuroimage.2018.09.080
[23] Knesevich JW, LaBarge E, & Edwards D. (1986). Predictive value of the Boston Naming Test in mild senile dementia of the Alzheimer type. Psychiatry Res, 19(2), 155-161. https://doi.org/10.1016/0165-1781(86)90008-9
[24] Zhao Q, Guo Q, & Hong Z. (2013). Clustering and switching during a semantic verbal fluency test contribute to differential diagnosis of cognitive impairment. Neurosci Bull, 29(1), 75-82. https://doi.org/10.1007/s12264-013-1301-7
[25] Chen NC, Chang CC, Lin KN, Huang CW, Chang WN, Chang YT, et al. (2013). Patterns of executive dysfunction in amnestic mild cognitive impairment. Int Psychogeriatr, 25(7), 1181-1189. https://doi.org/10.1017/s1041610213000392
[26] Akkoyun M, Koçoğlu K, Boz HE, Tüfekci IY, Ekin M, Akdal GJAs, et al. (2023). Eye movements during the judgment of line orientation test in patients with Alzheimer's disease and amnestic mild cognitive impairment. 19, e075697.
[27] Huang L, Chen KL, Lin BY, Tang L, Zhao QH, Li F, et al. (2019). An abbreviated version of Silhouettes test: a brief validated mild cognitive impairment screening tool. Int Psychogeriatr, 31(6), 849-856. https://doi.org/10.1017/s1041610218001230
[28] Calhoun VD, Adali T, Pearlson GD, & Pekar JJ. (2001). A method for making group inferences from functional MRI data using independent component analysis. Hum Brain Mapp, 14(3), 140-151. https://doi.org/10.1002/hbm.1048
[29] Fiorenzato E, Strafella AP, Kim J, Schifano R, Weis L, Antonini A, et al. (2019). Dynamic functional connectivity changes associated with dementia in Parkinson's disease. Brain, 142(9), 2860-2872. https://doi.org/10.1093/brain/awz192
[30] Bell AJ, & Sejnowski TJ. (1995). An information-maximization approach to blind separation and blind deconvolution. Neural Comput, 7(6), 1129-1159. https://doi.org/10.1162/neco.1995.7.6.1129
[31] Himberg J, Hyvärinen A, & Esposito F. (2004). Validating the independent components of neuroimaging time series via clustering and visualization. Neuroimage, 22(3), 1214-1222. https://doi.org/10.1016/j.neuroimage.2004.03.027
[32] Wang D, Qin W, Liu Y, Zhang Y, Jiang T, & Yu C. (2014). Altered resting-state network connectivity in congenital blind. Hum Brain Mapp, 35(6), 2573-2581. https://doi.org/10.1002/hbm.22350
[33] Kim J, Criaud M, Cho SS, Díez-Cirarda M, Mihaescu A, Coakeley S, et al. (2017). Abnormal intrinsic brain functional network dynamics in Parkinson's disease. Brain, 140(11), 2955-2967. https://doi.org/10.1093/brain/awx233
[34] Allen EA, Damaraju E, Plis SM, Erhardt EB, Eichele T, & Calhoun VD. (2014). Tracking whole-brain connectivity dynamics in the resting state. Cereb Cortex, 24(3), 663-676. https://doi.org/10.1093/cercor/bhs352
[35] Lloyd SJltoit. (1982). Least squares quantization in PCM. 28(2), 129-137.
[37] Malhi GS, Das P, Outhred T, Bryant RA, & Calhoun V. (2019). Resting-state neural network disturbances that underpin the emergence of emotional symptoms in adolescent girls: resting-state fMRI study. Br J Psychiatry, 215(3), 545-551. https://doi.org/10.1192/bjp.2019.10
[38] Wang J, Wang X, Xia M, Liao X, Evans A, & He Y. (2015). GRETNA: a graph theoretical network analysis toolbox for imaging connectomics. Front Hum Neurosci, 9, 386. https://doi.org/10.3389/fnhum.2015.00386
[39] Achard S, & Bullmore E. (2007). Efficiency and cost of economical brain functional networks. PLoS Comput Biol, 3(2), e17. https://doi.org/10.1371/journal.pcbi.0030017
[40] Pedersen M, Zalesky A, Omidvarnia A, & Jackson GD. (2018). Multilayer network switching rate predicts brain performance. Proc Natl Acad Sci U S A, 115(52), 13376-13381. https://doi.org/10.1073/pnas.1814785115
[41] Menon V. (2021). Dissociation by Network Integration. Am J Psychiatry, 178(2), 110-112. https://doi.org/10.1176/appi.ajp.2020.20121728
[42] Spreng RN, Stevens WD, Chamberlain JP, Gilmore AW, & Schacter DL. (2010). Default network activity, coupled with the frontoparietal control network, supports goal-directed cognition. Neuroimage, 53(1), 303-317. https://doi.org/10.1016/j.neuroimage.2010.06.016
[43] Hsu CL, Best JR, Voss MW, Handy TC, Beauchet O, Lim C, et al. (2019). Functional Neural Correlates of Slower Gait Among Older Adults With Mild Cognitive Impairment. J Gerontol A Biol Sci Med Sci, 74(4), 513-518. https://doi.org/10.1093/gerona/gly027
[44] Kessler D, Angstadt M, & Sripada C. (2016). Growth Charting of Brain Connectivity Networks and the Identification of Attention Impairment in Youth. JAMA Psychiatry, 73(5), 481-489. https://doi.org/10.1001/jamapsychiatry.2016.0088
[45] Ignatavicius A, Matar E, & Lewis SJG. (2025). Visual hallucinations in Parkinson's disease: spotlight on central cholinergic dysfunction. Brain, 148(2), 376-393. https://doi.org/10.1093/brain/awae289
[46] Li R, Wu X, Fleisher AS, Reiman EM, Chen K, & Yao L. (2012). Attention-related networks in Alzheimer's disease: a resting functional MRI study. Hum Brain Mapp, 33(5), 1076-1088. https://doi.org/10.1002/hbm.21269
[47] Pini L, de Lange SC, Pizzini FB, Boscolo Galazzo I, Manenti R, Cotelli M, et al. (2022). A low-dimensional cognitive-network space in Alzheimer's disease and frontotemporal dementia. Alzheimers Res Ther, 14(1), 199. https://doi.org/10.1186/s13195-022-01145-x
[48] Bertolero MA, Yeo BT, & D'Esposito M. (2015). The modular and integrative functional architecture of the human brain. Proc Natl Acad Sci U S A, 112(49), E6798-6807. https://doi.org/10.1073/pnas.1510619112
[49] Baum GL, Ciric R, Roalf DR, Betzel RF, Moore TM, Shinohara RT, et al. (2017). Modular Segregation of Structural Brain Networks Supports the Development of Executive Function in Youth. Curr Biol, 27(11), 1561-1572.e1568. https://doi.org/10.1016/j.cub.2017.04.051
[50] Avena-Koenigsberger A, Misic B, & Sporns O. (2017). Communication dynamics in complex brain networks. Nat Rev Neurosci, 19(1), 17-33. https://doi.org/10.1038/nrn.2017.149

Case Report

Brain Conflux

Rapid Progress of Unilateral Cerebral Microbleeds: A Novel Imaging Finding in Cerebral Amyloid Angiopathy-Related Inflammation

Authors

Lili Tang, Yujia Jin, Bingqian Wang, Yin Hu, Lusha Tong, Qiang Du

Correspondence

2310040@zju.edu.cn (L. Tong), duqiang0510@zju.edu.cn (Q. Du)

Graphical Abstract

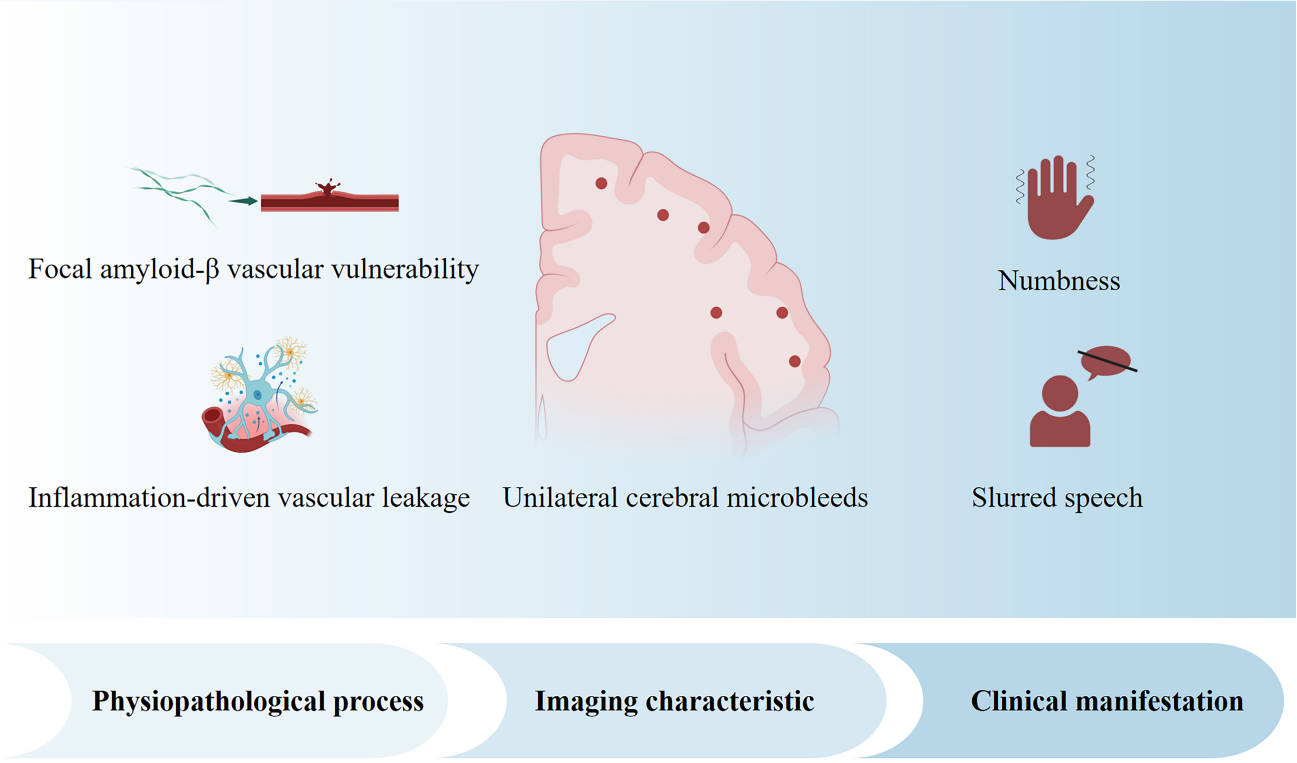

https://doi.org/10.71321/v8zybz49

Rapid Progress of Unilateral Cerebral Microbleeds: A Novel Imaging Finding in Cerebral Amyloid Angiopathy-Related Inflammation

Lili Tang[1†], Yujia Jin[1†], Bingqian Wang[2], Yin Hu[1], Lusha Tong[1*], Qiang Du[1*]

Received: 2025-09-13 | Accepted: 2025-09-21 | Published online: 2025-10-26

Abstract

Cerebral amyloid angiopathy-related inflammation (CAA-ri) is a rare but treatable CAA subtype characterized by reversible inflammatory mechanisms, offering unique diagnostic and therapeutic potential. We report a CAA-ri case featuring left-dominant cerebral microbleeds (CMBs) (baseline: 38 left vs. 2 right; 13-month progression to 65 left) with rapid clinical improvement post-corticosteroid therapy. This case expands the phenotypic spectrum of CAA-ri by demonstrating asymmetric CMBs with unilateral progression—a previously underrecognized pattern. This presentation requires heightened awareness in clinical practice to avert misdiagnosis and overlooked diagnoses.

Keywords: Cerebral Amyloid Angiopathy-Related Inflammation; Unilateral Cerebral Microbleeds.

Introduction

Cerebral amyloid angiopathy-related inflammation (CAA-ri) is defined as a pathological condition characterized by perivascular and intravascular inflammation, which is triggered by the deposition of vascular amyloid-beta (Aβ), leading to local blood-brain barrier leakage and culminating in vascular rupture. Common features of CAA-ri are rapid progressive dementia, epileptic seizures, headaches, and magnetic resonance imaging (MRI) findings showing single or multiple focal white matter hyperintensities on T2-weighted sequences and cortical microbleeds [1]. It is important to note that in the case of CAA-ri, the cerebral microbleeds (CMBs) distribution pattern is predominantly bilateral and asymmetric [2]. No cases of CAA-ri with strictly unilateral progress have been reported to date. So recognizing the rare clinical manifestations of CAA-ri is of great significance. Since its treatment differs significantly from that of typical CAA, and CAA-ri exhibits a favorable response to immunosuppressive therapy.

Here, we report a case of CAA-ri with strict unilateral rapid progressive CMBs as the main manifestation and the chief complaint was recurrent and transient numbness in the right limbs. The patient's condition was successfully managed with methylprednisolone pulse therapy.

Case Presentation

A 60-year-old male patient presented to our hospital multiple times within 15 months due to recurrent episodes of slurred speech and right limb numbness. Each episode lasted 5-8 minutes and resolved completely without residual symptoms. Head susceptibility-weighted imaging (SWI) revealed multiple CMBs in the left hemisphere. There was no relevant family history (e.g. cerebrovascular disease, dementia, and hereditary small vessel disease).

The patient first sought medical attention in November 2023 due to "Recurrent numbness in the right limbs and slurred speech for 3 months". MRI with T1, T2, and SWI sequences showed multiple microbleeds in the left cerebral hemisphere (frontal, parietal, occipital and temporal lobe), periventricular white matter hyperintensity (Fazekas grade II), and scattered lacunar lesions in the lateral ventricles and semioval center. To evaluate venous drainage abnormalities, MR venography (MRV) showed superior drainage in the left transverse sinus

1 Department of Neurology, The Second Affiliated Hospital of Zhejiang University, School of Medicine, Hangzhou, Zhejiang, China

2 Department of Encephalopathy, Yixing Traditional Chinese Medicine Hospital, Yixing, China

† These authors contributed equally to this work.

* Corresponding Author.

and sigmoid sinus, with local stenosis in the distal ends of both transverse sinuses. To confirm venous stenosis and exclude arteriovenous malformation, digital subtraction angiography (DSA) was performed, and the results were bilateral transverse sinus stenosis (left > right), no evidence of shunting or vascular malformations. The patient's follow-up head MRI during the 12-month follow-up showed a progressive increase in microbleeds (from 38 to 65 lesions) within the left hemisphere, suggesting ongoing vascular pathology (Figure 1A-F). However, no significant progression of WMH (white matter hyperintensity) lesions was observed (Figure 2A-F). To exclude infectious, inflammatory, or neurodegenerative etiologies, cerebrospinal fluid (CSF) analysis including GFAP and Alzheimer's disease (AD) biomarkers was performed and the results showed pathological manifestations related to AD (Number of nucleated cells: 1 × 10^6 /L, GFAP: 8.44 pg/mL [normal ≤ 30], Aβ42: 140.15pg/mL [normal > 609.4 pg/mL], Aβ42/Aβ40: 0.024pg/mL [normal>0.055]). Moreover, whole-exome sequencing (20858 genes) and mitochondrial genome analysis (37 genes) ruled out pathogenic variants in hereditary small-vessel disease genes (NOTCH3, COL4A1, TREX1) and mitochondrial disorders, confirming the absence of monogenic causation. According to the Criteria for the Diagnosis of CAA-ri, our case meets probable CAA - ri (Table 1) [1]. However, the attack characteristics of patients (transient, repetitive, and stereotyped episodes) align with transient focal neurological episodes (TFNE), necessitating differentiation from CAA-ri [3]. TFNE typically follows a self-limiting pattern, with symptoms improving and resolving over days to weeks. Besides, TFNE shows no improvement with corticosteroids. The patient subsequently received methylprednisolone pulse therapy and slow tapering to oral prednisone. During the follow-up after hormone therapy, the patient reported complete resolution of episodic slurred speech and no recurrence of right limbs numbness. The follow-up brain MRI (Figure 1G-I and Figure 2G-I) performed in April 2025 demonstrated stable cerebral microbleed burden.

Discussion

This case delineates a novel CAA-ri phenotype characterized by predominantly unilateral progression of cerebral microbleeds (CMBs) alongside definitive amyloid pathology (CSF Aβ42: 140.15 pg/mL [normal > 609.4 pg/mL]; Aβ42/Aβ40: 0.024 [normal > 0.055]). While classic CAA-ri exhibits bilateral lobar CMBs with vasogenic edema, the striking left hemispheric burden (38 baseline → 65 lesions) and delayed contralateral microbleeds (2 static lesions) suggest compartmentalized perivascular inflammation superimposed on diffuse amyloidosis.

CSF profiles were consistent with cerebral amyloidosis, reflecting cerebral amyloid-β deposition, these changes also characterize cerebral amyloid angiopathy (CAA) and its inflammatory subtype (CAA-ri). It typically associated with bilateral lobar CMBs in CAA and CAA-ri. However, the strictly left-sided predominance of microbleeds defies this pattern. We hypothesize two non-exclusive mechanisms: (1) Focal amyloid-β vascular vulnerability: Regional differences in vascular Aβ clearance or inflammatory activation may lead to asymmetric CMBs despite global amyloid burden. The specific distribution of the microbleeds provides evidence for a localized Aβ deposition that triggered the focal inflammatory response. Autopsy studies have shown patchy Aβ distribution in CAA [4]. (2) Inflammation-driven vascular leakage: The patient's steroid-responsive symptoms suggest superimposed perivascular inflammation, which could exacerbate erythrocyte extravasation in amyloid-laden vessels, disproportionately affecting one hemi-

Table 1. Criteria for the diagnosis of cerebral amyloid angiopathy-related inflammation (CAA-ri)

Diagnosis	Criteria
Probable CAA-ri	1. Age ≥40 years 2. At least one clinical manifestation from the following: headache, decreased consciousness, behavioral change, or focal neurological signs and seizures; symptoms cannot be attributed to acute intracerebral hemorrhage (ICH) 3. Magnetic resonance imaging (MRI) demonstrates asymmetric unifocal or multifocal white matter hyperintensities (WMH) lesions (corticosubcortical or deep), extending to the immediate subcortical white matter; asymmetry not secondary to prior ICH 4. Presence of ≥1 cortico-subcortical hemorrhagic lesion: cerebral macrobleed, cerebral microbleed, or cortical superficial siderosis 5. Exclusion of neoplastic, infectious, or other causes
Possible CAA-ri	1. Age ≥40 years 2. At least one clinical manifestation from the following: headache, decrease in consciousness, behavioral change, or focal neurological signs and seizures; the presentation is not directly attributable to an acute ICH 3. MRI reveals WMH lesions extending to the immediate subcortical white matter 4. Presence of ≥1 cortico-subcortical hemorrhagic lesion: cerebral macrobleed, cerebral microbleed, or cortical superficial siderosis 5. Exclusion of neoplastic, infectious, or other causes

Figure 1. Longitudinal susceptibility-weighted imaging (SWI) demonstrating unilateral progression of cerebral microbleeds (CMBs) in the left hemisphere.
(**A-C**) Baseline SWI (November 2023). (**D-F**) Follow-up SWI (December 2024, without immunosuppressive therapy). (**G-I**) Follow-up SWI (April 2025, with immunosuppressive therapy).

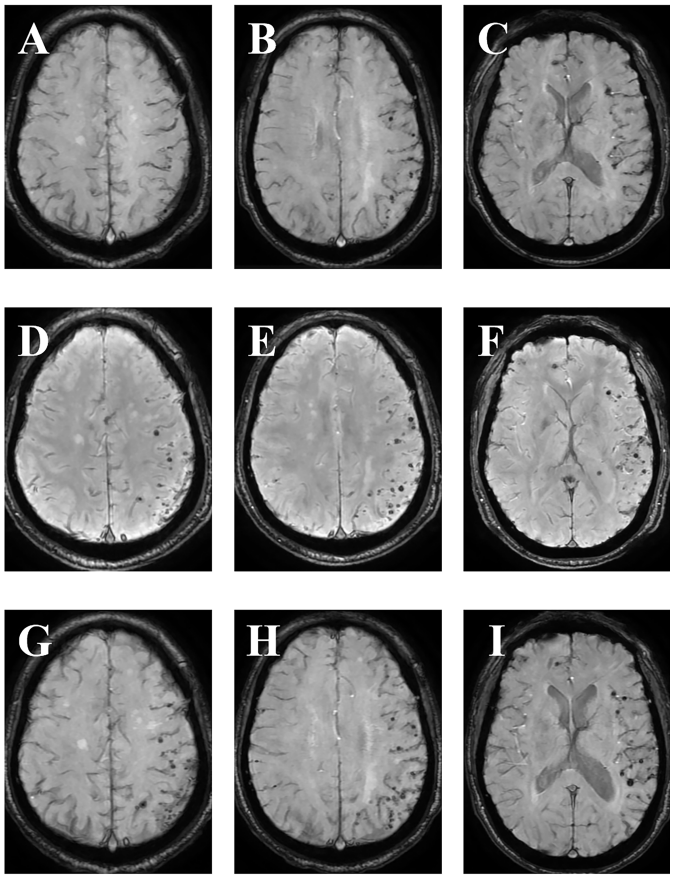

Figure 2. Longitudinal asymmetric white matter hyperintensities (WMH) on T2 imaging.
(**A-C**) Baseline T2-FLAIR images (November 2023). (**D-F**) Follow-up T2-weighted images (December 2024, without immunosuppressive therapy). (**G-I**) Follow-up T2-weighted images (April 2025, with immunosuppressive therapy).

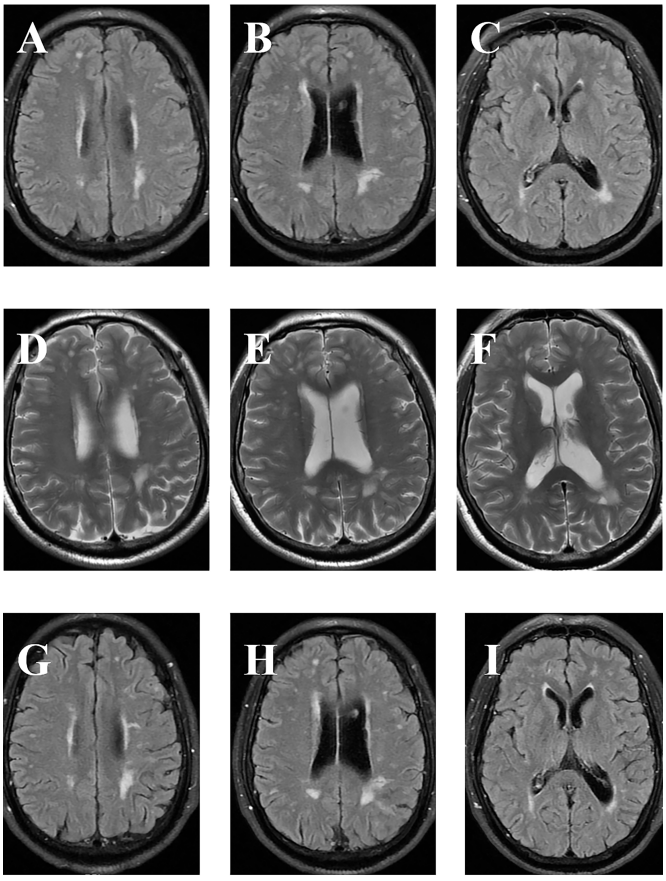

sphere. The extensive T2/FLAIR hyperintensities, which co-localized with the cluster of progressing microbleeds, provide a radiological correlate for this localized inflammation and associated vasogenic edema [5]. Such lateralized progression may represent an early stage of CAA-ri, wherein unilateral blood-brain barrier (BBB) breakdown precedes bilateral involvement. Longitudinal SWI monitoring is critical to capture this dynamic evolution.

Although brain biopsy is the diagnostic gold standard for CAA-ri, its invasive nature and risk of hemorrhagic complications limit routine clinical use. This underscores the value of recognizing distinctive clinical and imaging features, such as subacute cognitive decline, epilepsy, asymmetric white matter/cortical changes, dominant unilateral microbleeds (a less common but suggestive finding) to support non-invasive diagnosis. Immunosuppressive therapy has demonstrated efficacy in improving clinical and radiographic outcomes while reducing relapse rates in CAA-ri. After 6-month follow-up, immunosuppressive therapy effectively controlled the patient's right limb numbness.

Conclusion

In this report, we have described a unique case of CAA-ri characterized by a previously unreported pattern of strictly unilateral, rapidly progressing cerebral microbleeds. This case demonstrates that the neuroimaging spectrum of CAA-ri is broader than traditionally perceived. The key clinical implication is that the presence of such an asymmetric, progressive pattern of microbleeds should raise a high index of suspicion for the highly treatable diagnosis of CAA-ri. This awareness is critical to prevent misdiagnosis and to facilitate the timely initiation of corticosteroid therapy.

Abbreviations

Aβ: amyloid-beta; AD: Alzheimer's disease; BBB: blood brain barrier; CAA-ri: cerebral amyloid angiopathy-related inflammation; CMBs: cerebral microbleeds; CSF: cerebrospinal fluid; DSA: digital subtraction angiography; ICH: intracerebral hemorrhage; MRI: magnetic resonance imaging; MRV: MR venography; SWI: susceptibility-weighted imaging; TFNE: transient focal neurological episode; WMH: white matter hyperintensity.

Author Contributions

Lili Tang and Yujia Jin collected data and drafted the manuscript. Bingqian Wang and Yin Hu created the figures. Lusha Tong and Qiang Du revised the manuscript and conceived the study.

Acknowledgments

Not applicable.

Funding Information

None.

Ethics Approval and Consent to Participate

This study was approved by the Ethics Committee of The Second Affiliated Hospital of Zhejiang University School of Medicine (Approval Number: (2025) No. 1017).

Competing Interests

The authors declare no competing interests.

Data Availability

Not applicable.

References

[1] Auriel, Eitan, Andreas Charidimou, M. Edip Gurol, Jun Ni, Ellis S. Van Etten, Sergi Martinez-Ramirez, Gregoire Boulouis, et al (2016) Validation of Clinicoradiological Criteria for the Diagnosis of Cerebral Amyloid Angiopathy-Related Inflammation. JAMA Neurology 73 (2): 197–202. https://doi.org/10.1001/jamaneurol.2015.4078.

[2] Biffi, Alessandro, and Steven M. Greenberg (2011) Cerebral Amyloid Angiopathy: A Systematic Review. Journal of Clinical Neurology 7 (1): 1. https://doi.org/10.3988/jcn.2011.7.1.1.

[3] Kozberg, Mariel G, Irvin Yi, Whitney M Freeze, Corinne A Auger, Ashley A Scherlek, Steven M Greenberg, and Susanne J Van Veluw (2022) Blood–Brain Barrier Leakage and Perivascular Inflammation in Cerebral Amyloid Angiopathy. Brain Communications 4 (5): fcac245. https://doi.org/10.1093/braincomms/fcac245.

[4] Smith, Eric E., Andreas Charidimou, Cenk Ayata, David J. Werring, and Steven M. Greenberg (2021) Cerebral Amyloid Angiopathy–Related Transient Focal Neurologic Episodes. Neurology 97 (5): 231–38. https://doi.org/10.1212/WNL.0000000000012234.

[5] Theodorou, Aikaterini, Lina Palaiodimou, Konark Malhotra, Christina Zompola, Aristeidis H. Katsanos, Ashkan Shoamanesh, Efstathios Boviatsis, et al (2023) Clinical, Neuroimaging, and Genetic Markers in Cerebral Amyloid Angiopathy-Related Inflammation: A Systematic Review and Meta-Analysis. Stroke 54 (1): 178–88. https://doi.org/10.1161/STROKEAHA.122.040671.

Review Article

Brain Conflux

Stage-Specific Multimodal Imaging–Guided Non-Invasive Brain Stimulation for Post-Stroke Aphasia: A Structured Narrative Review

Authors

Liting Chen, Zhenye Luo, Xiaoling Wu, WenYing Chen, Xiaole Fan

Correspondence

975249386@qq.com (X. Fan)

Graphical Abstract

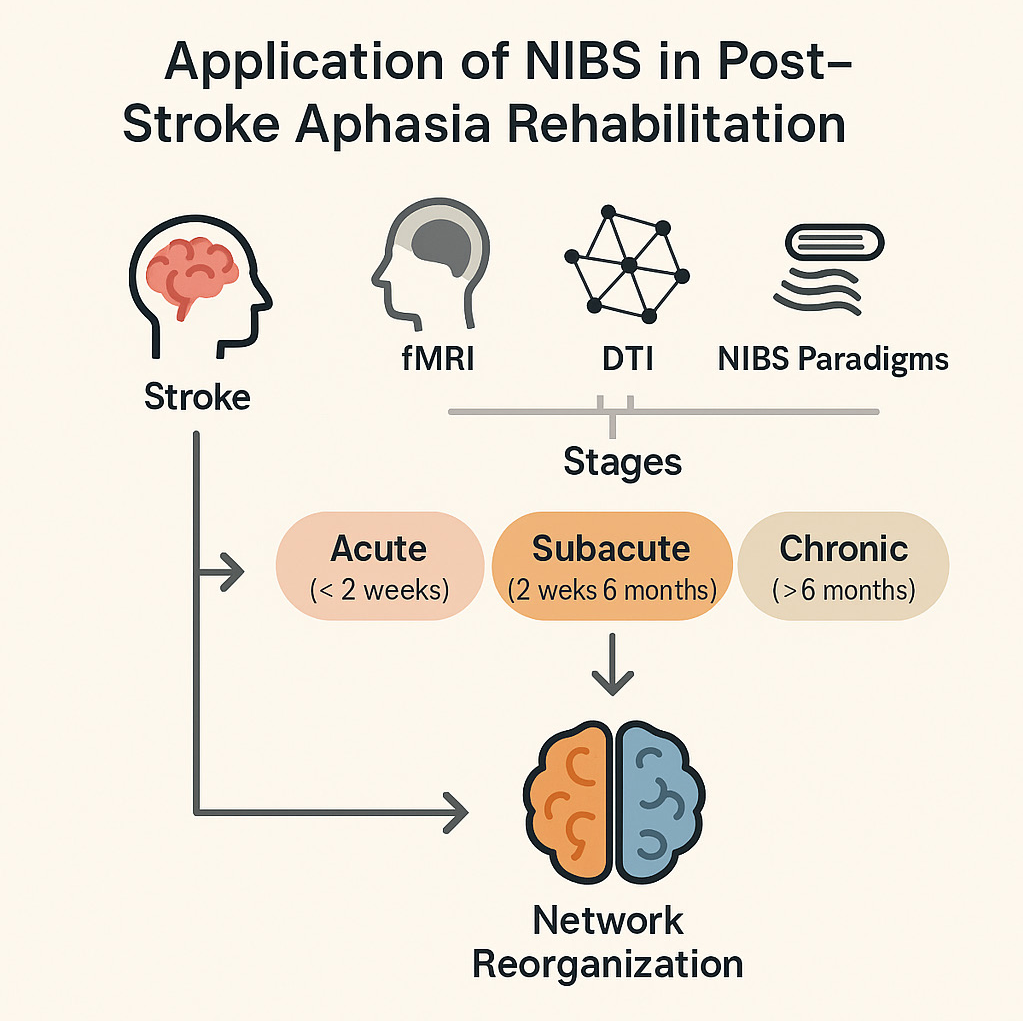

https://doi.org/10.71321/sxgrxh75

Review Article

Brain Conflux

Stage-Specific Multimodal Imaging–Guided Non-Invasive Brain Stimulation for Post-Stroke Aphasia: A Structured Narrative Review

Liting Chen [1†], Zhenye Luo [1†], Xiaoling Wu [1], WenYing Chen [3], Xiaole Fan [2*]

Received: 2025-07-30 | Accepted: 2025-10-25 | Published online: 2025-11-20

Abstract

Non-invasive brain stimulation (NIBS) modalities—including transcranial magnetic stimulation (TMS), theta-burst stimulation (TBS), and transcranial direct current stimulation (tDCS)—have emerged as promising approaches to promote language recovery in post-stroke aphasia by engaging both functional and structural neuroplasticity. This structured narrative review integrates recent multimodal evidence from functional magnetic resonance imaging (fMRI), DTI, and connectome analyses to delineate the stage-dependent mechanisms underlying NIBS-induced modulation of language networks. Findings across studies suggest a dynamic pattern of reorganization: acute-phase hypoactivation of left-hemisphere language areas and diffuse right-hemisphere disinhibition give way to bilateral upregulation in the subacute phase, followed by gradual restoration of left-dominant connectivity during the chronic stage, which may be limited by persistent contralesional hyperactivity. Low-frequency TMS or continuous TBS targeting right-hemisphere homologues can suppress maladaptive overcompensation, whereas high-frequency TMS or intermittent TBS applied to residual left-hemisphere sites enhances excitability and network centrality. Bilateral or neuronavigation-guided tDCS, particularly when combined with language training, rebalances interhemispheric excitability and supports sustained gains in naming and fluency. DTI-derived increases in arcuate and uncinate fasciculi integrity correlate with clinical improvement, while contralesional temporoparietal cortical thickening reflects concurrent structural remodeling.

Keywords: Non-invasive brain stimulation; Post-stroke aphasia; Functional magnetic resonance imaging.

Introduction

Post-stroke aphasia (PSA) is one of the most common and debilitating neurological complications following cerebrovascular accidents, with an incidence rate of approximately 30%–40% [31]. The underlying pathology primarily involves neuronal dysfunction or structural damage in the perisylvian language network of the left cerebral hemisphere—most notably in Broca's area (Brodmann areas 44/45), Wernicke's area (Brodmann area 22), and their subcortical connecting pathways such as the arcuate fasciculus—resulting from acute ischemic or hemorrhagic events [26]. Based on lesion location and clinical presentation, PSA can be classified into several subtypes, including expressive aphasia (Broca's), receptive aphasia (Wernicke's), conduction aphasia, mixed aphasia, and anomic aphasia. Patients typically exhibit multidimensional impairments in language function, such as non-fluent speech, word-finding difficulties (anomia), simplified grammar, disrupted syntax, impaired auditory comprehension, repetition deficits, alexia, and agraphia, with anomia and impaired repetition being the most commonly observed features [35]. Moreover, individuals with PSA often present with associated cognitive deficits, including impaired executive function, attention, and working memory, which further exacerbate communication difficulties and negatively impact rehabilitation outcomes [42]. Previous studies have demonstrated that early and accurate aphasia subtype classification and functional localization, when combined with individualized speech-language interventions (e.g., constraint-induced therapy, semantic-specific training) and neuromodulation techniques (e.g., transcranial magnetic stimulation, transcranial direct current stimulation), can significantly promote language network reorganization and recovery, improve patients' quality of life, and facilitate social reintegration [12].

1 Medical Imaging Center, The First Affiliated Hospital of Jinan University, Guangzhou 510630, China

2 Department of Ultrasound, The First Affiliated Hospital of Jinan University, Guangzhou 510000, China

3 Department of Radiology, The Third Affiliated Hospital of Sun Yat-sen University, Guangzhou 510000, China

† These authors contributed equally to this work.

* Corresponding Author.

Stage-Specific Reorganization of Language Networks

However, the natural recovery of language function in PSA follows a dynamic, three-phase process. Numerous longitudinal functional imaging studies support a triphasic model of language network reorganization encompassing acute, subacute, and chronic stages (Figure 1). During the acute phase (a few days to two weeks post-onset), acute neuronal dysfunction within the lesion site leads to a significant reduction in activation across left-hemispheric language centers—primarily Broca's area, Wernicke's area, and the arcuate fasciculus. Simultaneously, interhemispheric inhibition is weakened, resulting in a relative "disinhibition" of contralesional homologous regions in the right hemisphere (RH). However, RH activation during this stage is typically weak and spatially nonspecific. Its role appears preparatory, laying the foundation for subsequent neuroplasticity rather than directly substituting for language functions [19]. In the subacute phase (2 weeks to 6 months post-stroke), partial reperfusion and metabolic recovery within the infarcted area initiate neuroplastic mechanisms such as synaptic remodeling and axonal regeneration. fMRI and positron emission tomography (PET) studies have demonstrated reorganization-related upregulation in both the RH homologous language network (e.g., right Broca–Wernicke circuit) and the residual and perilesional cortex of the left hemisphere. This reorganization is positively associated with early improvements in speech fluency, naming ability, and auditory comprehension and is modifiable through interventions like constraint-induced language therapy (CILT) and neuromodulation [34]. In the chronic phase (>6 months), if the left-hemispheric language network and its subcortical tracts are sufficiently restored, it gradually regains dominance, with activation patterns approaching those of healthy controls. In contrast, persistent RH overactivation, especially in the context of limited left-hemispheric engagement, is associated with poorer long-term outcomes. Predictive models from longitudinal studies suggest that optimal chronic-stage recovery depends more on early preservation of left perilesional cortex and perfusion than on continued RH compensation [19, 23, 34].

Interhemispheric Balance: Facilitation vs. Maladaptation

This triphasic framework highlights the dual role of RH homologous regions: facilitatory disinhibition during early phases, and potentially inefficient compensation during later stages. In acute and subacute phases, RH activation may support

Figure 1. Stage-specific multimodal imaging–guided non-invasive brain stimulation (NIBS) framework for post-stroke aphasia. Multimodal imaging (fMRI, DTI, EEG) delineates dynamic language network reorganization across recovery stages, guiding targeted NIBS strategies. In the acute phase, inhibitory stimulation modulates right-hemisphere hyperactivity; in the subacute phase, bilateral facilitation supports network rebalancing; and in the chronic phase, excitatory stimulation enhances left perilesional plasticity. This framework integrates stage-dependent imaging biomarkers with tailored neuromodulation to optimize individualized language recovery.

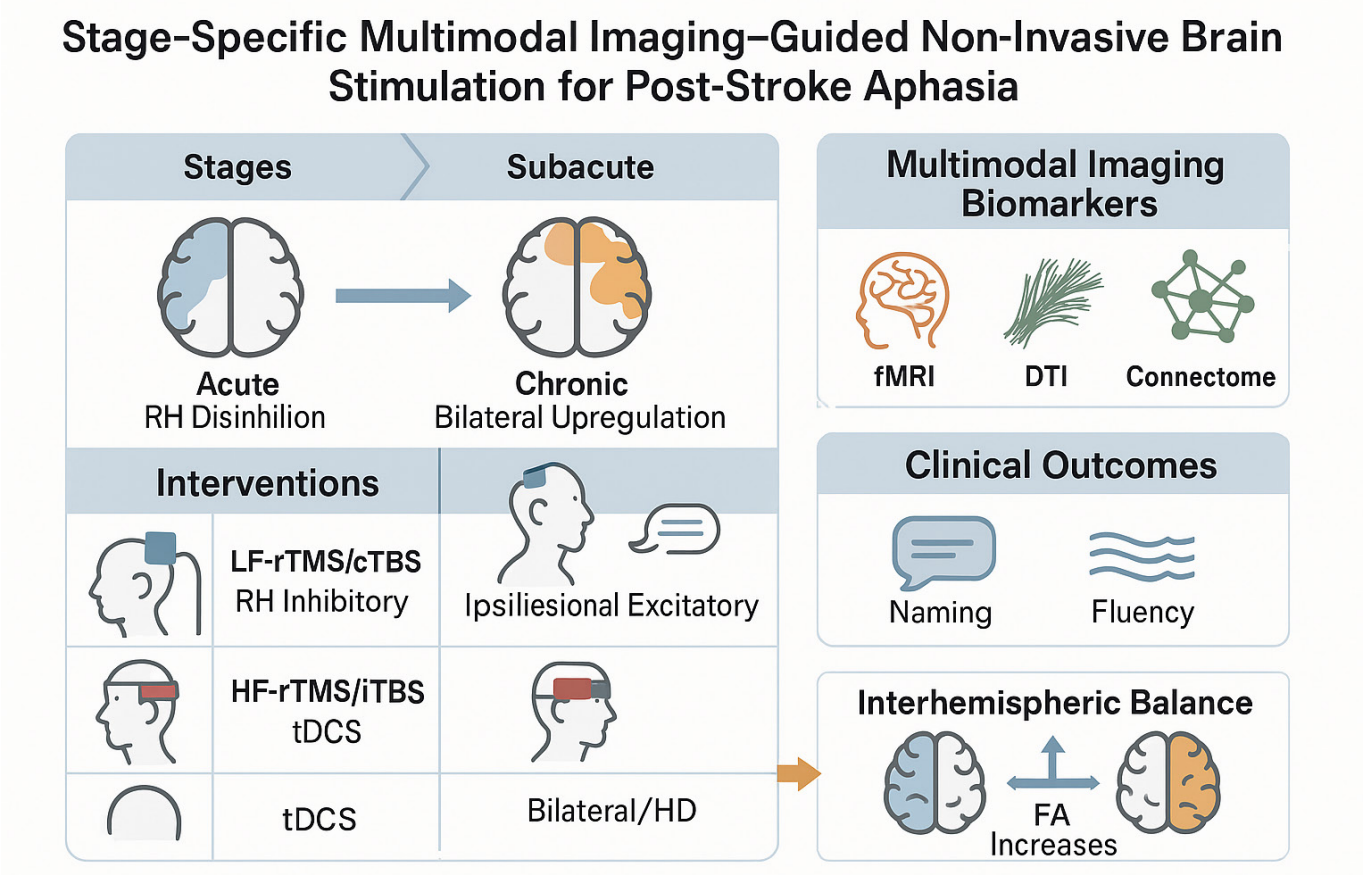

early recovery, particularly when the left network is severely impaired. For example, initial gains in language function have been linked to increased activation in the right inferior frontal gyrus and insular cortex [46]. However, in cases where the left hemisphere retains reorganization potential, persistent RH overactivation may disrupt interhemispheric balance and hinder left-sided recovery, negatively affecting long-term prognosis [25, 34]. Indeed, sustained RH hyperactivation in the chronic phase has been associated with poorer language performance and increased naming errors [36].

Multiple functional imaging and transcranial stimulation studies have shown that excessive activation in the right hemisphere is often associated with poorer recovery outcomes. Conversely, suppressing such compensatory overactivation—such as through inhibitory transcranial magnetic stimulation (TMS) targeting right-hemispheric homologous regions—may facilitate reorganization of the left-hemispheric language network and improve language performance. This "dual-role" model is commonly conceptualized within the framework of the interhemispheric inhibition model, which posits that early disinhibition of RH circuits may transiently support function, but persistent hyperactivation in the chronic phase may exert maladaptive inhibitory effects on perilesional regions in the left hemisphere. NIBS studies have further validated findings from functional imaging. Evidence indicates that applying inhibitory stimulation to right-hemispheric language areas in patients with chronic PSA can lead to modest improvements in language abilities. While low-frequency repetitive transcranial magnetic stimulation (rTMS) to the RH has demonstrated efficacy in chronic PSA, the optimal time window for intervention is dependent on the patient's recovery phase [20]. Therefore, selecting the ideal intervention window should be guided by multimodal fMRI metrics and standardized language assessment scales.

Aim and Scope of This Structured Narrative Review

In recent years, NIBS—including TMS and tDCS—has emerged as a prominent area of interest in post-stroke aphasia (PSA) rehabilitation due to its favorable safety profile and reproducibility. A growing body of work shows that NIBS can modulate both hemispheric language networks and domain-general control systems, influencing cortical plasticity alongside measurable changes in network function and microstructural architecture. However, the differential efficacy and mechanisms of various stimulation modalities remain incompletely understood. To avoid redundancy, we summarize shared mechanisms once (interhemispheric rebalance; ipsilesional facilitation) and emphasize stage-adapted applications within each modality section below. Multimodal neuroimaging offers a critical window into NIBS-induced functional and structural reorganization, including fMRI, DTI, and high-resolution T1-weighted imaging. Our primary aim is to provide a conceptual, stage-specific synthesis that integrates multimodal imaging with neuromodulation strategies for individualized translation, presenting a structured narrative across fMRI, DTI/structural connectivity, and functional connectivity.

1. Common Non-Invasive Brain Stimulation Techniques

This section summarizes commonly used NIBS modalities and emphasizes how their mechanisms and optimal applications vary across the acute, subacute, and chronic stages of post-stroke language recovery.

Repetitive Transcranial Magnetic Stimulation: Stage-Adapted Overview

Stage-adapted overview. The application and therapeutic efficacy of rTMS in post-stroke aphasia are highly stage-dependent. During the acute phase, low-frequency inhibitory rTMS targeting contralesional homologues may help limit maladaptive hyperexcitability and preserve perilesional function. In the subacute phase, bilateral reorganization predominates; accordingly, either inhibitory stimulation of the right hemisphere or excitatory stimulation of residual left-hemispheric regions can enhance cross-hemispheric balance and promote network reintegration. By the chronic stage, rTMS is primarily used to restore left-dominant activation and reinforce residual perilesional connectivity through excitatory paradigms such as high-frequency rTMS or iTBS. These stage-tailored strategies align with the evolving mechanisms of neural plasticity underlying post-stroke language recovery.

rTMS protocols include conventional stimulation paradigms—such as 1 Hz inhibitory and 10 Hz excitatory protocols—as well as more recent patterned approaches, such as iTBS [7]. For PSA, two primary strategies have been proposed: low-frequency rTMS applied to the right-hemispheric homologous language area to suppress excessive interhemispheric inhibition exerted on the damaged left-hemisphere language network [18, 29]; and high-frequency rTMS or iTBS targeting residual language areas in the left hemisphere to directly enhance their functional engagement. Many studies have cited the interhemispheric inhibition hypothesis to explain these effects: following left-hemisphere language network damage, the RH may become hyperactive due to loss of transcallosal inhibition. This hyperactivation may then exert symmetrical inhibition back onto the left hemisphere via the corpus callosum, paradoxically impeding recovery [11, 22]. Accordingly, applying low-frequency rTMS to the right Broca's area homologue can "release the brake" by attenuating right-to-left interhemispheric inhibition, thereby promoting reactivation and reorganization of the left-hemispheric language network [22]. In clinical practice, low-frequency rTMS is typically applied using neuronavigation to localize the right Broca homologue, with a stimulation frequency of 1 Hz, session duration of approximately 20 minutes, and a typical treatment course lasting 1 to 2 weeks. This intervention is often combined with concurrent speech-language therapy and has been shown to significantly improv. For instance, Medina et al. (2012) and Hamilton et al. (2010) [18, 29] demonstrated that in patients with, low-frequency rTMS applied to the RH significantly improved discourse productivity and verbal fluency and functional imaging studies suggest that the therapeutic mechanism involves suppression of maladaptive overactivation in the right prefrontal cortex, thereby facilitating re-engagement of left-hemisphere language regions. This neuromodulatory approach remains effective even in the chronic phase of stroke recovery, with evidence supporting sustained clinical benefits for at least six months post-intervention. A study by Harvey et al. (2017) [22] demonstrated that low-frequency rTMS targeting the right Broca homologue

can lead to sustained naming improvements in individuals with chronic aphasia. The intervention protocol involved navigated stimulation of the right inferior frontal gyrus (Broca homologue), delivered at 1 Hz for approximately 20 minutes per session over a course of 1–2 weeks. Functional MRI data further revealed that rTMS induced a posterior shift in activation within the right prefrontal cortex—from the anterior part of the Broca homologue (Brodmann area 45) to more motor-related regions (Brodmann areas 6, 44, and 46). Concurrently, there was a significant increase in activation of left-hemispheric regions involved in naming. These findings highlight the potential of rTMS to promote functional reorganization and facilitate long-term language recovery, even in the chronic phase post-stroke, with improvements persisting for at least six months after treatment

High-frequency rTMS or iTBS targeting the left hemisphere is designed to directly strengthen residual language areas and is particularly suited for patients in whom portions of the left-hemispheric language cortex remain functionally intact. Case reports have shown that high-frequency stimulation of the left inferior frontal gyrus or motor-related regions may enhance language output, with neuroimaging evidence indicating improved connectivity within the left-hemispheric language network [49]. However, compared to low-frequency inhibitory stimulation of the right hemisphere, clinical reports on high-frequency rTMS for aphasia are relatively scarce. This is largely due to challenges in precisely targeting intact left-hemispheric regions while avoiding lesioned areas. To address this issue, a personalized targeting approach has recently emerged, integrating functional neuroimaging guidance to identify stimulation sites. Even without navigation equipment, function-specific targets derived from task fMRI can be localized and applied clinically [50]. In a randomized controlled trial, researchers identified language-relevant activation hotspots in the left superior frontal gyrus (SFG) via individual functional imaging and applied rTMS at those targets. Results demonstrated that both excitatory iTBS to the left hemisphere and inhibitory continuous theta-burst stimulation (cTBS) to the right hemisphere, when combined with language therapy, yielded significantly better outcomes than sham stimulation [33]. These findings suggest that non-classical language areas, such as the SFG, may also serve as effective stimulation targets. Notably, high-frequency rTMS, particularly iTBS, offers the advantage of short stimulation durations—approximately 3 minutes per session in the classical iTBS protocol—thus imposing minimal burden on patients. However, to consolidate treatment effects, extended stimulation protocols or increased session counts may be required.

Moreover, large-sample studies and systematic reviews have provided higher levels of evidence supporting the use of rTMS in the treatment of aphasia. A recent systematic review and meta-analysis included 47 randomized controlled trials (RCTs) involving 2,190 patients with non-fluent aphasia, and demonstrated that rTMS significantly improves post-stroke language function, including abilities in repetition, naming, and spontaneous speech. Severity scores for aphasia were significantly reduced, and some studies also reported increased serum brain-derived neurotrophic factor (BDNF) levels and reduced depression incidence in the rTMS groups [7]. Another double-blind RCT targeting chronic non-fluent aphasia applied 1 Hz low-frequency rTMS to the right inferior frontal gyrus (triangular part), combined with multimodal aphasia therapy (M-MAT). Compared to the sham stimulation + training group, the real rTMS + training group showed an additional improvement of approximately 4.6 points in the WAB Aphasia Quotient at 15-week follow-up. Patients who received rTMS exhibited fewer word-finding difficulties and produced longer, more complete sentences. The study was graded as Class III evidence by Neurology, suggesting that rTMS may provide additional therapeutic benefit when used as an adjunct to conventional speech-language training [27]. Taken together, the overall efficacy of rTMS for aphasia has been supported by multiple randomized controlled trials.

Nevertheless, significant variability exists across rTMS protocols, and some findings are even contradictory. For example, low-frequency inhibitory stimulation of the right hemisphere may have limited efficacy in certain patients—such as those with severe global aphasia—in whom right-hemispheric compensation may still be contributing to residual language function; in such cases, excessive suppression of the RH may be counterproductive. Conversely, high-frequency stimulation of the left hemisphere requires the presence of sufficient residual functional cortex, which may be lacking in patients with extensive left-hemispheric lesions, limiting its utility [11]. In addition, there is considerable inter-individual variability in brain network reorganization patterns following stroke, making it a current challenge—and research focus—to personalize rTMS parameters and stimulation targets based on lesion location and recovery stage.

Theta Burst Stimulation: intermittent TBS and continuous TBS

The rationale for using TBS in post-stroke aphasia also follows a stage-specific pattern. In the early acute stage, cTBS may suppress maladaptive contralesional overactivation and prevent inhibitory dominance from the right hemisphere. During the subacute period, excitatory iTBS [24] over perilesional or residual left-hemispheric areas can amplify ongoing neuroplastic changes and facilitate bilateral reorganization. In the chronic stage, TBS protocols are increasingly employed to strengthen stable left-hemispheric circuits and consolidate language network re-engagement, often in combination with behavioral language training. iTBS [24] is a rapid pattern of rTMS that delivers short bursts of high-frequency pulses at a theta rhythm (~5 Hz). Each burst consists of three 50 Hz pulses, repeated every 200 milliseconds (i.e., at 5 Hz). A standard iTBS protocol includes 2 seconds of stimulation followed by 8 seconds of rest, repeated in cycles for a total of approximately 190 seconds, delivering 600 pulses in total. Stimulation intensity is typically set at 80% of the active motor threshold (AMT). This rhythmic alternation is believed to induce theta-frequency brain oscillations, which may simulate endogenous cortical rhythms and regulate activity within neural networks [39]. iTBS exerts excitatory effects on the cortex and is commonly used to enhance excitability in the lesioned language areas of patients with aphasia. The target region is usually the posterior inferior frontal gyrus (Broca's area) in the left (dominant) hemisphere, aiming to enhance both local and network-level activation. A randomized controlled trial by Bai et al. (2025) confirmed that iTBS combined with language training significantly improves language production functions in patients with post-stroke aphasia, including spontaneous speech, naming,

and repetition, as well as increasing the Aphasia Quotient (AQ) [2]. The study revealed that, compared to baseline, patients in the iTBS group showed significant improvements in all aforementioned language domains, with gains in naming, repetition, and AQ significantly greater than in the sham-stimulation group. Further fMRI analyses suggested a potential mechanism: resting-state fMRI comparisons before and after treatment revealed significant increases in fractional amplitude of low-frequency fluctuations (fALFF) [44] and degree centrality in several language-related areas of the left frontal and temporal lobes. These findings indicate that iTBS may strengthen the activation and network centrality of left-hemisphere language circuits, thereby enhancing functional connectivity efficiency and supporting language recovery. Consequently, promoting neuroplasticity within the lesioned (left) hemisphere is regarded as a key mechanism by which iTBS facilitates language rehabilitation. Through rhythmic stimulation, iTBS induces localized neuronal excitation and network reorganization, thereby reinforcing residual left-hemispheric language activity and facilitating functional restoration. Moreover, some studies have observed that iTBS can entrain theta-frequency neural oscillations that persist for several hundred milliseconds after stimulation, suggesting that iTBS may "imprint" frequency-specific rhythms into brain networks [39]. These oscillations may facilitate the modulation of speech-related cognitive processes, offering an additional explanatory pathway for the therapeutic benefits of iTBS in aphasia.

cTBS shares the same fundamental stimulation unit as iTBS—namely, bursts of three 50 Hz pulses—but is delivered continuously without interruption. A typical cTBS protocol administers 600 pulses over approximately 40 seconds (i.e., 200 bursts delivered consecutively without intervals), with stimulation intensity set at 80% of the active motor threshold (AMT). In contrast to iTBS, cTBS produces an inhibitory aftereffect on cortical excitability: a single session of cTBS can result in reduced excitability of the target cortex lasting up to 60 minutes [3]. Clinically, cTBS is commonly employed to suppress hyperactivity in the contralesional (right) hemisphere, particularly in language-homologous regions, to rebalance interhemispheric inhibition. For instance, cTBS may be targeted to the right posterior superior temporal gyrus (pSTG)—the homolog of Wernicke's area—or to the right pars triangularis—the counterpart of Broca's area—to reduce compensatory overactivation in these areas and release inhibitory pressure on the left-hemispheric language network. This approach is grounded in the interhemispheric imbalance model of post-stroke recovery, which posits that damage to the left-hemispheric language areas often leads to compensatory overactivation in the right hemisphere. This right-sided hyperexcitability, in turn, exerts excessive transcallosal inhibition on the left hemisphere, thereby impairing recovery of language functions [5, 24]. By suppressing the overactive right hemisphere with cTBS, a more favorable environment is created for functional reorganization in the left hemisphere. Empirical evidence supports this mechanism. In a randomized controlled trial, Zheng et al. [48] applied cTBS to the right pSTG (homologous to Wernicke's area) in patients with post-stroke aphasia and found significant improvements in auditory comprehension and repetition. Functional imaging revealed a notable reduction in overactivation of the right pars triangularis, along with increased spontaneous neural activity in the left frontal lobe. These findings suggest that suppressing hyperactivity in right-hemispheric language regions reduces their interference with left-hemispheric language circuits, thereby enhancing cortical activation in the lesioned hemisphere and facilitating functional recovery. Further support comes from a study by Harvey et al. [21], who applied cTBS to the right pars triangularis in patients with chronic aphasia. The intervention led to notable improvements in object naming, primarily by reducing errors related to phonological access deficits. The authors proposed that right-sided cTBS facilitated the phonological encoding stage, thereby enhancing the retrieval of word forms in these patients. These findings highlight the potential of cTBS to modulate maladaptive neural activity in the right hemisphere and support targeted interventions based on the specific nature of language impairments, such as phonological deficits in naming.

Notably, the short-term effects of cTBS are not limited to local changes in cortical excitability but also extend to the modulation of network connectivity. Yoo et al. conducted a study using combined transcranial magnetic stimulation and electroencephalography (TMS-EEG) to examine network-level effects of cTBS in healthy participants [43]. Neuronavigated cTBS was delivered to the left pars opercularis—a subregion of Broca's area—and the researchers observed a significant enhancement of phase synchrony between bilateral Broca areas in the gamma frequency band (250–350 ms time window). In addition, increased intrahemispheric synchrony was detected between the left pars opercularis and other left-hemisphere language-related regions (e.g., left supramarginal gyrus, left superior temporal gyrus) in both the gamma and theta/delta bands across various time windows. In contrast, the sham stimulation group exhibited no such increases in synchrony; in some cases, synchrony even decreased in specific frequency bands. These findings suggest that cTBS can modulate both inter- and intrahemispheric connectivity within the language network, facilitating coordinated activity between bilateral language areas as well as enhancing intra-network synchrony within the left hemisphere. This modulation of network dynamics indicates that cTBS may promote language recovery by reorganizing the temporal and spatial architecture of the language system. In addition, a recent systematic review summarized all available RCTs investigating TBS for post-stroke functional deficits [24]. The review concluded that TBS exhibits a favorable trend toward superior rehabilitation outcomes compared to conventional rTMS, across multiple domains including motor recovery, aphasia, and spatial neglect. Specifically, iTBS enhances cortical excitability in the lesioned hemisphere to promote functional restoration, while cTBS suppresses excessive contralesional activity to restore network balance.

In summary, TBS represents a powerful neuromodulatory tool for language network reorganization in post-stroke aphasia. Compared to conventional rTMS, TBS offers advantages such as lower stimulation intensity, shorter administration time, and longer-lasting aftereffects [24]. However, due to the limited number and heterogeneity of existing studies, there is currently insufficient evidence to recommend a single optimal TBS protocol. Variability in stimulation targets, dosages, and timing across studies has led to inconsistent efficacy outcomes. Therefore, future research should focus on large-scale, high-quality multicenter RCTs, combined with multimodal neuroimaging assessments, to determine the most effective stimulation parameters and optimal intervention windows for

TBS in aphasia rehabilitation.

Transcranial Direct Current Stimulation

tDCS is a non-invasive brain stimulation technique that modulates cortical excitability through the application of low-intensity direct current. Compared with TMS, tDCS devices are more compact and portable, and the stimulation procedure is simpler, making tDCS a widely used intervention in aphasia rehabilitation. The method involves placing a pair of electrodes (anode and cathode) on the scalp to deliver a constant low current that subtly alters neuronal membrane potentials. Cathodal stimulation typically leads to membrane hyperpolarization and decreased excitability, while anodal stimulation induces depolarization and increased excitability of the underlying cortex [4, 17, 37]. In the treatment of post-stroke aphasia, the most common electrode configuration is bilateral tDCS, which aims to restore interhemispheric balance. Typically, the anode is positioned over the left inferior frontal gyrus (Broca's area) or the left primary motor cortex (M1) to enhance excitability of the lesioned hemisphere, while the cathode is placed over the homologous region on the right hemisphere (e.g., right Broca's area or right M1) to suppress contralesional overactivity [37]. This approach mirrors the interhemispheric modulation model employed in rTMS, combining excitation of the lesioned side with inhibition of the intact side. In post-stroke aphasia interventions, a commonly employed electrode montage for tDCS is the "bilateral-balanced" configuration, in which the anode is placed over the left inferior frontal gyrus (Broca's area) or the left primary motor cortex (M1) to enhance excitability of the lesioned hemisphere's language center, while the cathode is positioned over the corresponding area in the contralateral hemisphere (right Broca's homolog or right M1) to suppress excitability in the intact hemisphere. This approach aims to achieve a balanced modulation of hemispheric excitability, mirroring the strategy of "inhibiting the contralesional side and exciting the ipsilesional side" commonly used in rTMS protocols [15, 16, 32]. For instance, Soliman et al. applied anodal stimulation over the left Broca's area and cathodal stimulation over the right Broca's homolog, and demonstrated that this bilateral tDCS montage could promote language recovery in patients with aphasia [37]. tDCS is commonly administered in conjunction with language training, typically for 20 minutes per session, once daily for 1–2 weeks (approximately 10 sessions). During stimulation, patients perform naming, repetition, or other language-related tasks. This simultaneous training leverages the neuroplastic "window of opportunity" induced by tDCS, allowing the therapeutic effects of training to be more effectively integrated into functional brain networks. Multiple studies, including randomized controlled trials, have shown that tDCS combined with behavioral training yields more significant and lasting improvements in language function than behavioral training alone. For example, Meinzer et al. conducted a double-blind RCT involving patients with chronic aphasia and found that applying anodal tDCS over the left M1 (twice daily, 20 minutes each session) at the start of each intensive naming session over a two-week period significantly enhanced naming performance for trained words. Moreover, the improvement generalized to untrained vocabulary, and performance remained stable at 6-month follow-up in the tDCS group, whereas the sham group exhibited partial decline. Naming accuracy for untrained words also improved significantly only in the tDCS group, with no change in the control group. Functional communication skills, such as conversational ability, were likewise significantly better in the tDCS group [30]. This study provided the first RCT evidence demonstrating that tDCS not only improves core language functions (e.g., naming accuracy) but also facilitates long-term retention and generalization of therapy outcomes. In other words, tDCS accelerates immediate language recovery while promoting broader network plasticity that supports sustained and generalized language improvement following the end of training.

From a neuroimaging perspective, the effects of tDCS on the brain of patients with aphasia can be described as "broad yet subtle" modulation. On one hand, tDCS reduces unnecessary overactivation in non-language regions; on the other hand, it enhances the coordinated activity within language-related networks. Darkow et al [10]. investigated the immediate effects of tDCS on brain activity in aphasic patients using concurrent fMRI. Compared to sham stimulation, anodal tDCS over the left hemisphere significantly reduced task-related overactivation in higher-order cognitive control areas unrelated to naming (suggesting suppression of these "interfering" regions), while activation within the core language network—primarily the left frontal, temporal, and parietal areas—increased. Functional connectivity analyses further revealed increased low-frequency synchronization within the language network, indicating more efficient communication among its constituent nodes. In a 6-week extended intervention, Cherney et al. (2021) demonstrated that both anodal and cathodal fMRI-guided tDCS combined with language therapy led to greater improvements in functional language and clinical ratings compared to therapy alone. Notably, cathodal stimulation was associated with increased perilesional cortical activation [8]. Taken together, these findings suggest that tDCS may function by "reducing noise and amplifying signal"—that is, by suppressing extraneous brain activity unrelated to language processing while simultaneously enhancing the functional coupling within language-relevant areas, thereby creating a more optimized neural environment for language processing. Beyond changes in functional activity, structural plasticity induced by tDCS has also been reported. In a DTI study, Soliman et al. [37] found that short-term repeated tDCS led to observable plastic changes in white matter tracts involved in language. Specifically, they reported a significant post-treatment increase in the fractional anisotropy (FA) of the right uncinate fasciculus (UNC)—a major white matter tract connecting the temporal and frontal lobes, including key language regions. This suggests that tDCS may promote remodeling of white matter and myelin integrity, thereby enhancing structural connectivity within and between hemispheric language areas. Interestingly, in that study, although the electrode was placed over the left hemisphere, the observed white matter changes were predominantly in the right hemisphere. The authors hypothesized that left-hemisphere stimulation may have modulated contralateral regions via interhemispheric networks—indicating that tDCS can promote bilateral cooperative plasticity. Unlike TMS, which directly induces excitatory neural firing, tDCS exerts a gentler influence. It operates with low current intensity and broad diffusion, without immediately triggering neuronal discharges. However, it is precisely this low-intensity, sustained modulation—especially when paired with behavioral training—that enhances the plastic potential of neural circuits. This enables the brain to re-

organize its networks in a “quietly guided” manner. Rather than directly replacing impaired language functions, tDCS elevates the brain’s baseline capacity for executing language tasks. It thereby increases the efficiency of language processing and allows patients to derive greater and more enduring benefits from subsequent language therapy.

In recent years, several modified transcranial electrical stimulation techniques—such as high-definition transcranial direct current stimulation (HD-tDCS) and transcranial alternating current stimulation (tACS)—have been introduced into the field of aphasia rehabilitation. These methods aim to achieve more precise or deeper neuromodulation by altering electrode configurations or current waveforms. However, current evidence regarding their use in aphasia remains limited, and their clinical efficacy requires further validation. Notably, while traditional approaches emphasize suppression of the right hemisphere to relieve its inhibitory effect on the lesioned left hemisphere, some studies have proposed alternative strategies. For patients with extensive left-hemispheric lesions and minimal residual language network capacity, enhancing right hemisphere activity may serve as a compensatory approach. A recent meta-analysis [51] evaluated the effect of anodal tDCS applied to the right hemisphere on naming performance in individuals with post-stroke aphasia. The results indicated that patients receiving right-anodal tDCS demonstrated a greater trend toward improvement in naming accuracy compared to those receiving sham stimulation or conventional therapy. Based on these findings, the authors suggested that anodal stimulation over the right hemisphere could be a promising intervention, particularly in cases where the left-hemispheric language areas are severely damaged. This view diverges somewhat from the classic "right-suppression" model. The study proposed that right-hemisphere anodal tDCS may serve as a compensatory adjunct for patients with large left-sided lesions and limited residual plasticity. However, for patients with a partially preserved left-hemispheric language network, left-sided stimulation should remain the priority, while prolonged right-hemisphere overactivation should be avoided. In addition, several studies have focused on bihemispheric tDCS protocols, which combine anodal stimulation to the left hemisphere with cathodal stimulation to the right, aiming to concurrently increase left-hemispheric excitability while suppressing right-sided overactivation [13]. More recently, a novel tDCS approach has targeted the right cerebellum for aphasia treatment [28]. Meta-analytic evidence shows that cerebellar TMS improves balance and limb motor outcomes and modulates motor-related rs-fMRI networks, indicating that cerebello-cortical circuits are plastic and may serve as analogues for cross-network interventions in language recovery [45]. This region has both structural and functional connections with the left-hemispheric language areas, which is particularly important in patients with large left-hemisphere lesions where it may be difficult to identify viable perilesional cortex for direct stimulation.

tDCS: Stage-Specific Considerations and Take-Home Message

In summary, tDCS offers a safe and feasible “foundational modulation” strategy for post-stroke aphasia. By balancing cortical excitation and inhibition and promoting neural network reorganization, tDCS exerts a mild yet profound influence on the remodeling of the language network, thereby creating a more favorable neural environment for language rehabilitation. Looking ahead, as stimulation parameters are further optimized and integrated with neuroimaging and physiological markers, it may become possible to more precisely identify suitable candidates for tDCS and develop personalized stimulation protocols. Such advances are expected to enhance the efficacy of tDCS and broaden its application in aphasia rehabilitation. The therapeutic role of tDCS also evolves across recovery stages. In the acute phase, early bilateral or contralesional-anodal montages may facilitate global excitability and prevent network diaschisis. The subacute phase benefits most from bihemispheric configurations that balance interhemispheric inhibition and enhance task-specific learning when paired with speech therapy. In the chronic phase, left-anodal or bilateral tDCS targeting residual cortical regions promotes long-term restoration of left-dominant network integrity. These temporal shifts underscore the importance of stage-adapted stimulation paradigms within a precision neuromodulation framework.

Functional MRI Evidence of NIBS-Induced Reorganization

fMRI has been widely used to measure changes in brain activation and network connectivity before and after NIBS. Multiple small-sample studies have demonstrated that interventions using TMS or tDCS can induce plastic reorganization of functional activation patterns in the brain.

Immediate and Short-Term Effects: iTBS, a highly efficient TMS protocol, can induce immediate changes in brain function after a single session of intervention [38]. Xu et al. (2021) [41] applied a single session of iTBS over the left primary motor cortex (M1) in 16 patients with post-stroke aphasia, followed by resting-state fMRI immediately before and after stimulation. The results showed significant changes in local neural activity and functional connectivity after a single session of iTBS: degree centrality increased in the right middle frontal gyrus and left parietal lobe, while fractional amplitude of low-frequency fluctuations decreased in parts of the frontal and occipital lobes, and functional connectivity between the left M1 and the left superior frontal gyrus weakened. These findings suggest that even a single session of TMS can modulate brain network activity acutely, providing insights into how to facilitate language network plasticity and laying a neurophysiological foundation for subsequent language rehabilitation training.

Concurrent Stimulation-Imaging Studies: Darkow et al. (2017) conducted a simultaneous tDCS-fMRI study using a double-blind crossover design, in which patients with chronic aphasia received either real or sham tDCS during a naming task inside the MRI scanner. Results showed that anodal stimulation reduced over-reliance on higher-order cognitive control regions during naming, enhanced activation within the core language network, and promoted low-frequency oscillations. Furthermore, the functional activation patterns of patients receiving real stimulation became more similar to those of healthy controls [10].

These results indicate that a single session of tDCS can modulate residual language networks in aphasia, reduce un-

necessary cognitive control, and enhance intra-network coordination—providing a potential mechanism for subsequent individualized behavioral interventions.

Long-Term Reorganization Effects: fMRI has also been employed to investigate lasting functional reorganization following repeated NIBS interventions. For example, a protocol using low-frequency rTMS to inhibit the right inferior frontal gyrus (IFG) has been applied to reduce maladaptive right-hemisphere compensation, aiming to release suppressed functions of the left-hemisphere language areas. Harvey et al. (2017) [22] applied 1 Hz rTMS to the right IFG pars triangularis (homologous to Broca's area) in 9 patients with chronic aphasia for 10 consecutive days. Naming performance improved significantly, peaking at 6-month follow-up. Corresponding fMRI revealed a posterior shift in activation within the right IFG: whereas naming-related activation was localized to BA45 (pars triangularis) before intervention, this region was no longer active after 6 months. Instead, activation appeared in more posterior right IFG subregions, such as the pars opercularis (BA6/44/46). Furthermore, activation patterns shifted from right-hemisphere dominance to increased involvement of left-hemisphere regions, including the supplementary motor area, medial frontal cortex, and cingulate gyrus. In other words, rTMS promoted a shift in compensatory activation within the right frontal cortex from anterior (BA45) to posterior areas (BA6/44/46), along with increased recruitment of the left hemisphere—reflecting a dynamic reorganization of the bilateral language network. These changes coincided with sustained language improvement, supporting the therapeutic strategy of reducing excessive right frontal compensation while enhancing left-hemisphere engagement. Similarly, in a study by Chang et al. (2022) [6], high-frequency rTMS was delivered to the most active residual left-hemisphere language region identified by functional near-infrared spectroscopy (fNIRS), combined with 10 days of speech therapy in 5 patients with chronic non-fluent aphasia. Significant improvement in the Aphasia Quotient (WAB) was observed within one month. Network analysis using fNIRS showed enhanced functional connectivity among left-hemisphere speech production and processing areas, with significantly increased local clustering coefficients. In contrast, the clustering coefficient in the right hemisphere decreased, slightly reducing global network efficiency. This suggests that enhancing left-hemisphere integration while reducing maladaptive right-hemisphere compensation may be a mechanism for language recovery.

Numerous neuroimaging studies have demonstrated that the mechanisms underlying language recovery align with existing theories of neural plasticity. Patients with better outcomes often exhibit reestablishment of left-hemisphere language network dominance, while right-hemisphere compensation is either suppressed (e.g., via low-frequency rTMS to reduce interhemispheric inhibition) or reorganized into a more supportive role (e.g., posterior shift of compensatory activation to more efficient regions) [19, 22]. These neuroplastic changes are often observed concurrently with improvements in language performance, suggesting that the restoration of function is indeed grounded in reorganization of the brain's language network. Conversely, patients who fail to exhibit such neuroimaging-based markers of plasticity often show limited language improvement. When clinical gains are not paralleled by expected imaging changes, this may indicate the need for adjusting stimulation strategies to optimize treatment efficacy.

Most of the aforementioned fMRI studies are small-scale pre-post comparisons or preliminary RCTs, with sample sizes ranging from fewer than 10 to approximately 20 participants, and some incorporating sham stimulation as controls [37]. Despite these limitations, the findings consistently demonstrate that NIBS can induce favorable functional reorganization of the brain—characterized by increased activation and connectivity in left-hemisphere (ipsilesional) language regions and reduced maladaptive overactivation in the right hemisphere (contralesional), thereby aligning brain activity patterns more closely with those seen in healthy language networks. Such functional neuroimaging evidence provides a mechanistic foundation supporting the use of NIBS to facilitate aphasia recovery. Nonetheless, given the heterogeneity of participants and methodological constraints, these conclusions require further validation in large-scale, rigorously designed clinical trials.

Structural Imaging Studies: White Matter and Gray Matter Plasticity

White Matter Plasticity

DTI has been primarily used to assess the structural integrity and connectivity of white matter (WM) fiber tracts, offering a unique perspective on plasticity induced by brain stimulation. Compared with fMRI, which reflects functional changes, DTI reveals remodeling of the underlying anatomical connections within the neural network. Soliman et al. (2021) [37] conducted a randomized trial in 21 subacute post-stroke aphasia patients, comparing a real tDCS group (anodal over the left inferior frontal gyrus [IFG], cathodal over the right IFG) and a sham group, both receiving 10 sessions of stimulation. While the sham group showed no significant language changes, the real tDCS group demonstrated marked improvement in HSS aphasia scores. Seven patients in the real tDCS group underwent pre- and post-intervention DTI scans. Tractography of language-related white matter bundles revealed that, compared with sham stimulation, real tDCS significantly increased FA in the right uncinate fasciculus and decreased mean diffusivity (MD) in the right fronto-insular tract—suggesting enhanced fiber integrity and reduced extracellular diffusivity. Notably, the increase in FA of the right uncinate fasciculus positively correlated with gains in speech fluency, supporting the idea that greater structural remodeling parallels greater functional recovery. Zhao et al. (2021) [47] examined 39 patients with primary progressive aphasia (PPA) who received 15 sessions of naming therapy combined with left IFG tDCS, and analyzed DTI metrics of ventral (uncinate/inferior longitudinal fasciculi) and dorsal (arcuate fasciculus) pathways prior to intervention. Their results showed that the tDCS group outperformed the sham group in naming accuracy for both trained and untrained words. Higher FA in ventral pathways predicted greater gains in trained items, while higher FA in dorsal pathways predicted better generalization to untrained words. This suggests that the structural integrity of language-related WM tracts may serve as a predictive biomarker of therapeutic responsiveness to tDCS in PPA patients—those with more preserved WM structures tended to benefit more from stimulation. Allendorfer et al. (2012) [1] reported that following 10 days of excitatory iTBS over the

left hemisphere in chronic aphasia patients, FA significantly increased in several left-hemispheric regions, including the inferior and superior frontal gyri and the anterior corpus callosum. Additional FA increases were observed in the right midbrain, bilateral temporoparietal cortex, and posterior cingulate gyrus, whereas decreases appeared in the bilateral fusiform gyri and left cerebellum. These changes overlapped with activation regions identified in previous fMRI studies of iTBS-induced language facilitation, suggesting that excitatory rTMS may enhance synaptic connectivity via mechanisms such as long-term potentiation (LTP), which is reflected structurally as improved WM integrity. Recent studies combining NIBS and language therapy have also reported microstructural WM plasticity in perilesional or contralesional tracts, such as increased FA or decreased MD in the right uncinate and fronto-insular fasciculi following bilateral tDCS [37]. These structural changes have been closely linked to improvements in speech fluency. Collectively, these findings highlight the parallel nature of structural and functional plasticity, supporting the concept that NIBS facilitates coordinated reorganization at both anatomical and functional levels of the language network.

Gray Matter Plasticity

Although relatively fewer studies have focused on gray matter (GM) volume changes, emerging evidence suggests a link between GM remodeling and functional language recovery. Some studies have reported that increased GM volume in the right temporoparietal junction is significantly associated with improved language outcomes in post-stroke aphasia patients—even though this region lies in the contralesional hemisphere and is not homologous to the lesioned left-hemispheric language areas [40]. This finding implies that cortical GM remodeling—such as hypertrophy in language-related regions of the intact hemisphere—may also represent a form of neuroplasticity that contributes to compensatory mechanisms supporting language recovery.

Integrated Multimodal Imaging Framework for Stage-Specific Neuromodulation

Based on the synthesis of multimodal neuroimaging findings, Han et al. (2024) [19] proposed a plasticity framework of the post-stroke language network grounded in the dual-stream model, providing a systematic summary of recovery mechanisms across different stages. They mapped specific white matter pathways—such as those related to fluency, repetition, comprehension, naming, and reading—to corresponding subcomponents of language, highlighting the plasticity characteristics of these tracts during recovery. The model emphasizes that in the acute stage, due to severe functional disruption in the lesioned left hemisphere and limited capacity for white matter reconstruction, language recovery relies predominantly on functional reorganization within residual cortical areas and perilesional zones. In the subacute phase, with the initiation of neuroplastic and metabolic processes, compensatory remodeling can be observed in both the right-hemispheric homologous pathways and left perilesional networks, supporting intermediate-term functional gains. In the chronic phase, if the left hemisphere gradually regains its dominance in the language network, the global activation pattern tends to normalize and resemble that of healthy individuals. Conversely, persistent over-reliance on right-hemispheric pathways—although offering temporary compensation—may suppress more efficient reorganization in the left hemisphere, leading to suboptimal outcomes. The framework also advocates for dynamic monitoring using multimodal imaging at different recovery stages, and stresses the importance of tailoring the timing and targets of intervention. For instance, the authors identified regions such as the medial superior frontal gyrus and dorsal anterior cingulate cortex as promising neuromodulatory targets due to their involvement in higher-order cognitive control networks. However, multi-target stimulation did not outperform optimized single-target stimulation; notably, rMFG targeting effectively downregulated dACC activity [14]. This conceptual model provides a structured guideline for future clinical decision-making and study design; however, its assumptions warrant further validation through longitudinal and multimodal interventional research. Collectively, these multimodal imaging findings not only delineate the dynamic reorganization of post-stroke language networks but also provide a practical rationale for tailoring NIBS interventions. Functional hypoactivation and interhemispheric imbalance identified through fMRI, together with DTI-derived measures of tract integrity, can inform the selection of stimulation targets, polarity, and timing across different recovery stages, thereby establishing a clinically meaningful imaging-guided neuromodulation framework.

Future Directions and Perspectives

Future research on NIBS for aphasia should focus on several key directions to further enhance its therapeutic efficacy and translational relevance. Despite encouraging progress, significant challenges remain, including the lack of standardized imaging biomarkers, small sample sizes, heterogeneous stimulation timing and parameters, and limited reproducibility across studies. Addressing these limitations will be essential for achieving methodological consistency and clinical generalizability.

First, integrating multiple neuroimaging modalities—such as fMRI, DTI, and electroencephalography (EEG)—is essential for dynamically monitoring the remodeling of language networks and capturing both functional and structural changes during recovery. EEG, with its high temporal resolution, can complement MRI-based approaches by revealing real-time oscillatory and network-level changes induced by stimulation, thereby improving the temporal precision of multimodal imaging frameworks. Such multimodal fusion will enable real-time assessment of neuroplasticity induced by NIBS and facilitate a deeper understanding of the neural signatures associated with each recovery stage.

Second, the application of machine learning and artificial intelligence techniques should be expanded to comprehensively analyze patients' baseline neuroimaging and clinical data. This approach allows for predictive modeling of language recovery trajectories and supports the optimization of individualized intervention strategies. Data-driven models that incorporate structural and functional MRI, as well as DTI parameters, can estimate patient-specific responsiveness to different stimulation paradigms and assist in evidence-based decision-making [9].

Third, the development of personalized NIBS protocols that adapt to each patient's stage of recovery—guided by predictive models and imaging biomarkers—could align stimulation intensity and pattern with the evolving neuroplastic potential of the brain. A phase-specific, progressive stimulation strategy may maximize functional gains and improve the long-term stability of outcomes.

In addition to the well-established TMS and tDCS paradigms, several emerging neuromodulation techniques—including transcranial alternating current stimulation, transcranial random noise stimulation, and focused ultrasound neuromodulation—are gaining increasing attention for their potential to deliver more frequency-specific, spatially precise, and depth-selective modulation of neural activity. Although empirical evidence in post-stroke aphasia remains limited, incorporating these novel modalities into multimodal imaging–guided frameworks represents a promising frontier for advancing precision neuromodulation. Future research should explore how these innovative stimulation techniques can be integrated with neuroimaging and computational modeling to improve personalization and reproducibility in language rehabilitation.

Finally, translating neuroimaging-based mechanistic insights into standardized clinical protocols remains a critical challenge. Large-scale, multicenter trials are needed to establish consensus on stimulation parameters, timing, and intervention paradigms, thereby facilitating integration into routine clinical practice. Developing standardized imaging biomarkers and reproducible stimulation frameworks will be crucial for bridging the gap between mechanistic studies and clinical application. Bridging the gap between experimental and clinical implementation will depend on the development of replicable, guideline-based NIBS frameworks that ensure accessibility, consistency, and clinical benefit across diverse patient populations [9]. Future studies should also integrate molecular biomarkers such as BDNF and synaptic plasticity indices with multimodal imaging metrics to better elucidate how cellular mechanisms translate into macroscopic network reorganization and clinical improvement.

Evidence Synthesis and Consistency Across Studies

Although considerable heterogeneity exists among study designs, stimulation parameters, and imaging methods, several consistent patterns have emerged. Across multiple pilot and randomized controlled trials, inhibitory NIBS applied to right-hemispheric homologues and excitatory stimulation targeting left perilesional or residual language areas have repeatedly demonstrated beneficial effects) on naming, fluency, and comprehension [7, 33]. Meta-analyses [7] further support the superiority of bihemispheric or imaging-guided protocols compared to conventional approaches. However, controversies remain regarding the optimal timing of stimulation, the durability of long-term effects, and inter-individual variability in response patterns [19]. Overall, the level of evidence has progressed from small-scale exploratory studies to a growing number of well-controlled clinical trials, reflecting an encouraging trend toward standardization and higher methodological rigor.

Conclusion

In summary, non-invasive brain stimulation offers renewed hope for post-stroke aphasia rehabilitation, while multimodal neuroimaging provides a powerful means to elucidate its mechanisms and therapeutic effects. Recent evidence shows that NIBS can promote neuroplastic changes at multiple levels—from the reorganization of functional networks to potential strengthening of structural pathways. Nonetheless, it is increasingly evident that each patient's path to recovery is unique, requiring more precise and individualized intervention strategies. Future advances in neuroimaging and data analytics are expected to further refine our understanding of language network remodeling, enabling clinicians to design more targeted, stage-specific treatment plans. With continued scientific exploration, the field is moving toward a more complete blueprint of language recovery, offering tangible improvements in communication ability and quality of life for patients with aphasia.

Abbreviations

NIBS=Non-invasive brain stimulation; TMS=Transcranial magnetic stimulation; rTMS=Repetitive transcranial magnetic stimulation; TBS=Theta burst stimulation; iTBS=Intermittent theta burst stimulation; cTBS=Continuous theta burst stimulation; tDCS=Transcranial direct current stimulation; HD-tDCS=High-definition transcranial direct current stimulation; tACS=Transcranial alternating current stimulation; PSA=Post-stroke aphasia; RH=Right hemisphere; fMRI=Functional magnetic resonance imaging; DTI=Diffusion tensor imaging; PET=Positron emission tomography; fNIRS=Functional near-infrared spectroscopy; EEG=Electroencephalography; IFG=Inferior frontal gyrus; SFG=Superior frontal gyrus; pSTG=Posterior superior temporal gyrus; BA=Brodmann area; M1=Primary motor cortex; AQ=Aphasia Quotient; WAB=Western Aphasia Battery; CILT=Constraint-induced language therapy; M-MAT=Multimodal aphasia therapy; BDNF=Brain-derived neurotrophic factor; PPA=Primary progressive aphasia; FA=-Fractional anisotropy; MD=Mean diffusivity; UNC=Uncinate fasciculus; CC=Corpus callosum; WM=White matter; GM=Gray matter; AI=Artificial intelligence; RCT=Randomized controlled trial.

Author Contributions

Liting Chen: Conceptualization, literature search, data compilation, manuscript drafting. Zhenye Luo: Literature search, data analysis, manuscript drafting. Xiaoling Wu: Literature search support, figure/table preparation. WenYing Chen:manuscript revision. Xiaole Fan: Project supervision, study design, final manuscript approval.

Acknowledgment

We acknowledge the participants of our study for their contribution and our team members for their support.

Funding Information

We acknowledge financial support from the Medical Science and Technology Research Fund of Guangdong Province, China (No. A2023144) and Guangdong Provincial Young Innovative Talents Project (Grant No. 2025KQNCX005).

Ethics Approval and Consent to Participate

This study was approved by the Ethics Committee of the First Affiliated Hospital of Jinan University (Approval No. KY-2024-096).

Competing Interests

Competing financial interests: The authors declare no competing financial interests.

Data Availability

No new datasets were generated or analyzed in this review article. All data cited in this manuscript are from previously published studies, which are properly referenced in the text.

References

[1] Jane B. Allendorfer, Judd M. Storrs, and Jerzy P. Szaflarski. 2012. Changes in white matter integrity follow excitatory rTMS treatment of post-stroke aphasia. Restorative neurology and neuroscience 30, 2: 103–113. https://doi.org/10.3233/RNN-2011-0627

[2] Guangtao Bai, Liang Jiang, Qi Li, and Peiju Qiu. 2025. Study on intermittent theta burst stimulation improves expression function and mechanism in patients with aphasia after stroke. The Neurologist 30, 4: 204–211. https://doi.org/10.1097/NRL.0000000000000622

[3] Zhongfei Bai, Jiaqi Zhang, and Kenneth N. K. Fong. 2022. Effects of transcranial magnetic stimulation in modulating cortical excitability in patients with stroke: a systematic review and meta-analysis. Journal of NeuroEngineering and Rehabilitation 19, 1: 24. https://doi.org/10.1186/s12984-022-00999-4

[4] M. Bikson, Abhishek Datta, Asif Rahman, and Jen Scaturro. 2010. Electrode montages for tDCS and weak transcranial electrical stimulation: role of "return" electrode's position and size. Clinical Neurophysiology 121, 12: 1976–1978. https://doi.org/10.1016/j.clinph.2010.05.020

[5] L.J. Boddington and J.N.J. Reynolds. 2017. Targeting interhemispheric inhibition with neuromodulation to enhance stroke rehabilitation. Brain Stimulation 10, 2: 214–222. https://doi.org/10.1016/j.brs.2017.01.006

[6] Won Kee Chang, Jihong Park, Ji-Young Lee, Sungmin Cho, Jongseung Lee, Won-Seok Kim, and Nam-Jong Paik. 2022. Functional network changes after high-frequency rTMS over the most activated speech-related area combined with speech therapy in chronic stroke with non-fluent aphasia. Frontiers in Neurology 13: 690048. https://doi.org/10.3389/fneur.2022.690048

[7] Jing Cheng, Yijing Jiang, Ting Rao, Yihan Yang, Yanping Liu, Ying Zhan, and Shanli Yang. 2024. Repetitive transcranial magnetic stimulation for post-stroke non-fluent aphasia: a systematic review and meta-analysis of randomized controlled trials. Frontiers in Neurology 15: 1348695. https://doi.org/10.3389/fneur.2024.1348695

[8] Leora R. Cherney, Edna M. Babbitt, Xue Wang, and Laura L. Pitts. 2021. Extended fMRI-Guided Anodal and Cathodal Transcranial Direct Current Stimulation Targeting Perilesional Areas in Post-Stroke Aphasia: A Pilot Randomized Clinical Trial. Brain sciences 11, 3. https://doi.org/10.3390/brainsci11030306

[9] Bruce Crosson, Amy D Rodriguez, David Copland, Julius Fridriksson, Lisa C Krishnamurthy, Marcus Meinzer, Anastasia M Raymer, Venkatagiri Krishnamurthy, and Alexander P Leff. 2019. Neuroplasticity and aphasia treatments: new approaches for an old problem. Journal of Neurology, Neurosurgery and Psychiatry 90, 10: 1147–1155. https://doi.org/10.1136/jnnp-2018-319649

[10] Robert Darkow, Andrew Martin, Anna Würtz, Agnes Flöel, and Marcus Meinzer. 2017. Transcranial direct current stimulation effects on neural processing in post-stroke aphasia. Human brain mapping 38, 3: 1518–1531. https://doi.org/10.1002/hbm.23469

[11] Andrew T. DeMarco, Elizabeth Dvorak, Elizabeth Lacey, Catherine J. Stoodley, and Peter E. Turkeltaub. 2021. An exploratory study of cerebellar transcranial direct current stimulation in individuals with chronic stroke aphasia. Cognitive and Behavioral Neurology 34, 2: 96–106. https://doi.org/10.1097/WNN.0000000000000270

[12] Bernhard Elsner (ed.). 2013. Transcranial direct current stimulation (tDCS) for improving function and activities of daily living in patients after stroke. In Cochrane Database of Systematic Reviews. John Wiley & Sons, Ltd, Chichester, UK. https://doi.org/10.1002/14651858.cd009645.pub2

[13] Sarah Feil, Peter Eisenhut, Frauke Strakeljahn, Sarah Müller, Claude Nauer, Jens Bansi, Stefan Weber, Alexandra Liebs, Jean-Pascal Lefaucheur, Jürg Kesselring, Roman Gonzenbach, and Veit Mylius. 2019. Left shifting of language related activity induced by bihemispheric tDCS in postacute aphasia following stroke. Frontiers in Neuroscience 13: 295. https://doi.org/10.3389/fnins.2019.00295

[14] Zi-Jian Feng, Xin-Ping Deng, Na Zhao, Jing Jin, Juan Yue, Yun-Song Hu, Ying Jing, Hong-Xiao Wang, Thomas R Knösche, Yu-Feng Zang, and Jue Wang. 2022. Resting-state fMRI functional connectivity strength predicts local activity change in the dorsal cingulate cortex: a multi-target focused rTMS study. Cerebral Cortex 32, 13: 2773–2784. https://doi.org/10.1093/cercor/bhab380

[15] Agnes Flöel. 2014. tDCS-enhanced motor and cognitive function in neurological diseases. Neuroimage 85: 934–947. https://doi.org/10.1016/j.neuroimage.2013.05.098

[16] Julius Fridriksson, Jessica D. Richardson, Julie M. Baker, and Chris Rorden. 2011. Transcranial direct current stimulation improves naming reaction time in fluent aphasia: a double-blind, sham-controlled study. Stroke 42, 3: 819–821. https://doi.org/10.1161/STROKEAHA.110.600288

[17] Ivor B. Gartside. 1968. Mechanisms of sustained increas-

es of firing rate of neurones in the rat cerebral cortex after polarization: role of protein synthesis. Nature 220, 5165: 383–384. https://doi.org/10.1038/220383a0

[18] Roy H. Hamilton, Linda Sanders, Jennifer Benson, Olufunsho Faseyitan, Catherine Norise, Margaret Naeser, Paula Martin, and H. Branch Coslett. 2010. Stimulating conversation: enhancement of elicited propositional speech in a patient with chronic non-fluent aphasia following transcranial magnetic stimulation. Brain and Language 113, 1: 45–50. https://doi.org/10.1016/j.bandl.2010.01.001

[19] Yue Han, Yuanyuan Jing, Yanmin Shi, Hongbin Mo, Yafei Wan, Hongwei Zhou, and Fang Deng. 2024. The role of language-related functional brain regions and white matter tracts in network plasticity of post-stroke aphasia. Journal of Neurology 271, 6: 3095–3115. https://doi.org/10.1007/s00415-024-12358-5

[20] Takatoshi Hara and Masahiro Abo. 2021. New treatment strategy using repetitive transcranial magnetic stimulation for post-stroke aphasia. Diagnostics 11, 10: 1853. https://doi.org/10.3390/diagnostics11101853

[21] Denise Y. Harvey, Joely A. Mass, Priyanka P. Shah-Basak, Rachel Wurzman, Olufunsho Faseyitan, Daniela L. Sacchetti, Laura DeLoretta, and Roy H. Hamilton. 2019. Continuous theta burst stimulation over right pars triangularis facilitates naming abilities in chronic post-stroke aphasia by enhancing phonological access. Brain and language 192: 25–34. https://doi.org/10.1016/j.bandl.2019.02.005

[22] Denise Y. Harvey, Jamie Podell, Peter E. Turkeltaub, Olufunsho Faseyitan, H. Branch Coslett, and Roy H. Hamilton. 2017. Functional Reorganization of Right Prefrontal Cortex Underlies Sustained Naming Improvements in Chronic Aphasia via Repetitive Transcranial Magnetic Stimulation. Cognitive and Behavioral Neurology: Official Journal of the Society for Behavioral and Cognitive Neurology 30, 4: 133–144. https://doi.org/10.1097/WNN.0000000000000141

[23] W.-D. Heiss and A. Thiel. 2006. A proposed regional hierarchy in recovery of post-stroke aphasia. Brain and language 98, 1: 118–123. https://doi.org/10.1016/j.bandl.2006.02.002

[24] Tingting Jiang, Xiupan Wei, Mingzhu Wang, Jiang Xu, Nan Xia, and Min Lu. 2024. Theta burst stimulation: what role does it play in stroke rehabilitation? A systematic review of the existing evidence. BMC Neurology 24, 1: 52. https://doi.org/10.1186/s12883-023-03492-0

[25] Zafer Keser, Rajani Sebastian, Khader M. Hasan, and Argye E. Hillis. 2020. Right hemispheric homologous language pathways negatively predicts poststroke naming recovery. Stroke 51, 3: 1002–1005. https://doi.org/10.1161/STROKEAHA.119.028293

[26] Swathi Kiran and Cynthia K. Thompson. 2019. Neuroplasticity of language networks in aphasia: advances, updates, and future challenges. Frontiers in Neurology 10. https://doi.org/10.3389/fneur.2019.00295

[27] Trevor A. Low, Kevin Lindland, Adam Kirton, Helen L. Carlson, Ashley D. Harris, Bradley G. Goodyear, Oury Monchi, Michael D. Hill, Miranda L. Rose, and Sean P. Dukelow. 2025. Transcranial magnetic stimulation combined with multimodality aphasia therapy for chronic poststroke aphasia: a randomized clinical trial. Neurology 104, 6: e213424. https://doi.org/10.1212/WNL.0000000000213424

[28] Paola Marangolo, Valentina Fiori, Umberto Sabatini, Giada De Pasquale, Carmela Razzano, Carlo Caltagirone, and Tommaso Gili. 2016. Bilateral transcranial direct current stimulation language treatment enhances functional connectivity in the left hemisphere: preliminary data from aphasia. Journal of Cognitive Neuroscience 28, 5: 724–738. https://doi.org/10.1162/jocn_a_00927

[29] Jared Medina, Catherine Norise, Olufunsho Faseyitan, H. Branch Coslett, Peter E. Turkeltaub, and Roy H. Hamilton. 2012. Finding the right words: transcranial magnetic stimulation improves discourse productivity in non-fluent aphasia after stroke. Aphasiology 26, 9: 1153–1168. https://doi.org/10.1080/02687038.2012.710316

[30] Marcus Meinzer, Robert Darkow, Robert Lindenberg, and Agnes Flöel. 2016. Electrical stimulation of the motor cortex enhances treatment outcome in post-stroke aphasia. Brain : a journal of neurology 139, Pt 4: 1152–1163. https://doi.org/10.1093/brain/aww002

[31] Alina Menichelli, Giovanni Furlanis, Arianna Sartori, Mariana Ridolfi, Marcello Naccarato, Paola Caruso, Valentina Pesavento, and Paolo Manganotti. 2019. Thrombolysis' benefits on early post-stroke language recovery in aphasia patients. Journal of Clinical Neuroscience 70: 92–95. https://doi.org/10.1016/j.jocn.2019.08.064

[32] Alessia Monti, Roberta Ferrucci, Manuela Fumagalli, Francesca Mameli, Filippo Cogiamanian, Gianluca Ardolino, and Alberto Priori. 2013. Transcranial direct current stimulation (tDCS) and language. Journal of neurology, neurosurgery, and psychiatry 84, 8: 832–842. https://doi.org/10.1136/jnnp-2012-302825

[33] Jianxun Ren, Weijing Ren, Ying Zhou, Louisa Dahmani, Xinyu Duan, Xiaoxuan Fu, Yezhe Wang, Ruiqi Pan, Jingdu Zhao, Ping Zhang, Bo Wang, Weiyong Yu, Zhenbo Chen, Xin Zhang, Jian Sun, Mengying Ding, Jianting Huang, Liu Xu, Shiyi Li, Weiwei Wang, Wuxiang Xie, Hao Zhang, and Hesheng Liu. 2023. Personalized functional imaging-guided rTMS on the superior frontal gyrus for post-stroke aphasia: a randomized sham-controlled trial. Brain Stimulation 16, 5: 1313–1321. https://doi.org/10.1016/j.brs.2023.08.023

[34] Dorothee Saur, Rüdiger Lange, Annette Baumgaertner, Valeska Schraknepper, Klaus Willmes, Michel Rijntjes, and Cornelius Weiller. 2006. Dynamics of language reorganization after stroke. Brain : a journal of neurology 129, Pt 6: 1371–1384. https://doi.org/10.1093/brain/awl090

[35] Shannon M. Sheppard and Rajani Sebastian. 2021. Diagnosing and managing post-stroke aphasia. Expert Review of Neurotherapeutics 21, 2: 221–234. https://doi.org/10.1080/14737175.2020.1855976

[36] Laura M. Skipper-Kallal, Elizabeth H. Lacey, Shihui Xing, and Peter E. Turkeltaub. 2017. Right hemisphere remapping of naming functions depends on lesion size and location in poststroke aphasia. Neural Plasticity 2017: 1–17. https://doi.org/10.1155/2017/8740353

[37] Radwa K. Soliman, Chantal M. W. Tax, Noha Abo-Elfetoh, Ahmed A. Karim, Ayda Youssef, Doaa Kamal, and Eman M. Khedr. 2021. Effects of tDCS on Language Recovery in Post-Stroke Aphasia: A Pilot Study Investigating Clinical Parameters and White Matter Change with Diffusion Imaging. Brain sciences 11, 10. https://doi.org/10.3390/brainsci11101277

[38] Nico Sollmann and Petro Julkunen. 2022. Modern developments in transcranial magnetic stimulation: the edito-

rial. Brain Sciences 12, 5: 628. https://doi.org/10.3390/brainsci12050628
[39] Ethan A. Solomon, Michael R. Sperling, Ashwini D. Sharan, Paul A. Wanda, Deborah F. Levy, Anastasia Lyalenko, Isaac Pedisich, Daniel S. Rizzuto, and Michael J. Kahana. 2021. Theta-burst stimulation entrains frequency-specific oscillatory responses. Brain Stimulation 14, 5: 1271–1284. https://doi.org/10.1016/j.brs.2021.08.014
[40] Shihui Xing, Elizabeth H. Lacey, Laura M. Skipper-Kallal, Xiong Jiang, Michelle L. Harris-Love, Jinsheng Zeng, and Peter E. Turkeltaub. 2016. Right hemisphere grey matter structure and language outcomes in chronic left hemisphere stroke. Brain : a journal of neurology 139, Pt 1: 227–241. https://doi.org/10.1093/brain/aww323
[41] Shuo Xu, Qing Yang, Mengye Chen, Panmo Deng, Ren Zhuang, Zengchun Sun, Chong Li, Zhijie Yan, Yongli Zhang, and Jie Jia. 2021. Capturing Neuroplastic Changes after iTBS in Patients with Post-Stroke Aphasia: A Pilot fMRI Study. Brain sciences 11, 11. https://doi.org/10.3390/brainsci11111451
[42] Zhijie Yan, Shuo Xu, Dongshuai Wei, Xinyuan He, Chong Li, Yongli Zhang, Mengye Chen, Jingna Zhang, Xiaofang Li, Qing Yang, and Jie Jia. 2022. Comparison of three cognitive assessment methods in post-stroke aphasia patients. Frontiers in Psychology 13. https://doi.org/10.3389/fpsyg.2022.896095
[43] Woo-Kyoung Yoo, Marine Vernet, Jung-Hoon Kim, Anna-Katharine Brem, Shahid Bashir, Fritz Ifert-Miller, Chang-Hwan Im, Mark Eldaief, and Alvaro Pascual-Leone. 2020. Interhemispheric and Intrahemispheric Connectivity From the Left Pars Opercularis Within the Language Network Is Modulated by Transcranial Stimulation in Healthy Subjects. Frontiers in Human Neuroscience 14: 63. https://doi.org/10.3389/fnhum.2020.00063
[44] Juan Yue, Na Zhao, Yang Qiao, Zi-Jian Feng, Yun-Song Hu, Qiu Ge, Tian-Qing Zhang, Zhu-Qian Zhang, Jue Wang, and Yu-Feng Zang. 2023. Higher reliability and validity of WAVELET-ALFF of resting-state FMRI : from multicenter database and application to RTMS modulation. Human Brain Mapping 44, 3: 1105–1117. https://doi.org/10.1002/hbm.26142
[45] Yuheng Zeng, Zujuan Ye, Wanxin Zheng, and Jue Wang. 2024. Efficacy of cerebellar transcranial magnetic stimulation for post-stroke balance and limb motor function impairments: meta-analyses of random controlled trials and resting-state fMRI studies. Cerebellum 23, 4: 1678–1696. https://doi.org/10.1007/s12311-024-01660-7
[46] Marina Zettin, Caterina Bondesan, Giulia Nada, Matteo Varini, and Danilo Dimitri. 2021. Transcranial Direct-Current Stimulation and Behavioral Training, a Promising Tool for a Tailor-Made Post-stroke Aphasia Rehabilitation: A Review. Frontiers in human neuroscience 15: 742136. https://doi.org/10.3389/fnhum.2021.742136
[47] Yi Zhao, Bronte Ficek, Kimberly Webster, Constantine Frangakis, Brian Caffo, Argye E. Hillis, Andreia Faria, and Kyrana Tsapkini. 2021. White matter integrity predicts electrical stimulation (tDCS) and language therapy effects in primary progressive aphasia. Neurorehabilitation and Neural Repair 35, 1: 44–57. https://doi.org/10.1177/1545968320971741
[48] Kai Zheng, Xinlei Xu, Yingying Ji, Hui Fang, Fanglan Gao, Guilan Huang, Bin Su, Li Bian, Guofu Zhang, and Caili Ren. 2023. Continuous theta burst stimulation-induced suppression of the right fronto-thalamic-cerebellar circuit accompanies improvement in language performance in poststroke aphasia: A resting-state fMRI study. Frontiers in Aging Neuroscience 14: 1079023. https://doi.org/10.3389/fnagi.2022.1079023
[49] Zhong Sheng Zheng, Jing Wang, Sharon Lee, Kevin Xing-Long Wang, Ben Zhang, Melissa Howard, Emily Rosario, and Caroline Schnakers. 2025. Cerebellar transcranial direct current stimulation improves quality of life in individuals with chronic poststroke aphasia. Scientific Reports 15, 1: 6898. https://doi.org/10.1038/s41598-025-90927-y
[50] Bingbing Zhou, Jiajia Qi, Kangjia Chen, Hong Li, Jiahui Liu, Qian Zhou, Zujuan Ye, and Jue Wang. 2025. Localizing Function-specific Targets for Transcranial Magnetic Stimulation in the Absence of Navigation Equipment. Journal of Visualized Experiments, 219: 67888. https://doi.org/10.3791/67888
[51] Wenwen Cheng, Yufeng Li, Bin Cheng, Ying Chen, Zhiwen Chen, Liyan Cui, et al. Effects of transcranial direct current stimulation over the right hemisphere on naming ability in patients with poststroke aphasia: a meta-analysis. Journal of Neurolinguistics 58: 100986. https://doi.org/10.1016/j.jneuroling.2021.100986

Research Article Brain Conflux

Cell Type- and Developmental Stage–Specific Mapping of Polygenic Risk Across Schizophrenia, Depression, and Bipolar Disorder

Authors

Nana Liu, Yuting Liu, Sijia Wang, Jie Tang

Correspondence

tangjie@tmu.edu.cn (J. Tang)

Graphical Abstract

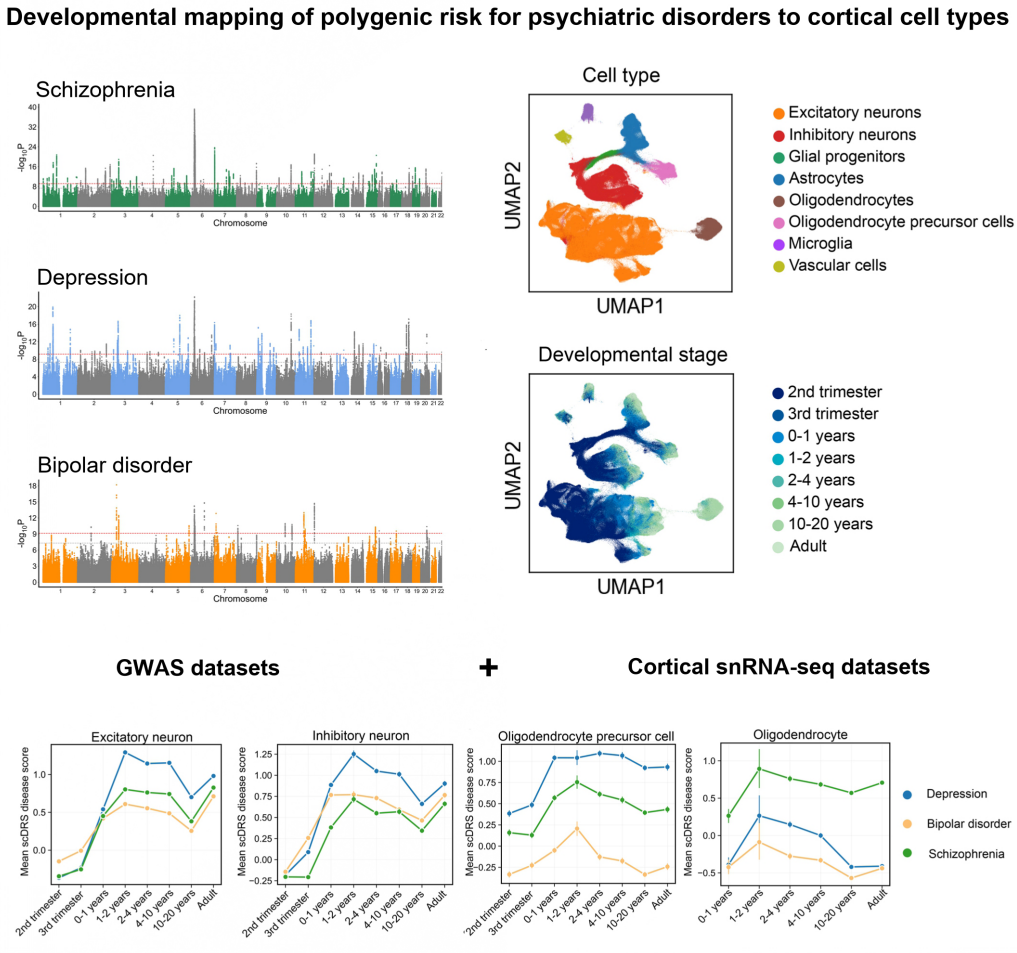

https://doi.org/10.71321/ftnk8985

Research Article Brain Conflux

Cell Type- and Developmental Stage–Specific Mapping of Polygenic Risk Across Schizophrenia, Depression, and Bipolar Disorder

Nana Liu [1] , Yuting Liu [2] , Sijia Wang [1] , Jie Tang [1*]

Received: 2025-09-20 | Accepted: 2025-10-27 | Published online: 2025-11-11

Abstract

Schizophrenia, depression, and bipolar disorder are highly heritable psychiatric illnesses that share overlapping symptoms but also exhibit disorder-specific features. To dissect the cellular and developmental mechanisms underlying genetic risk, we integrated large-scale genome-wide association study (GWAS) data with human cortical single-nucleus RNA sequencing (snRNA-seq) data spanning gestation to adulthood (>700,000 nuclei from 106 donors). Gene-based analyses revealed 104 shared genes across disorders and convergent enrichment in synaptic pathways, alongside disorder-specific signals such as metal ion transport in schizophrenia. Using the single-cell disease relevance score (scDRS), we mapped polygenic risk across cortical cell types and developmental windows. Excitatory neurons were consistently implicated across all disorders from postnatal stages through adulthood, while inhibitory neurons showed broader vulnerability in depression and bipolar disorder, extending into the fetal period. Glial cells demonstrated disorder specificity: astrocytes were implicated across disorders during early postnatal synaptogenesis, oligodendrocyte precursor cells (OPCs) showed prolonged associations in depression, and mature oligodendrocytes were uniquely implicated in schizophrenia during childhood. These findings highlighted excitatory-inhibitory imbalance as a shared mechanism, alongside distinct glial and developmental trajectories contributing to disorder-specific pathophysiology. Our findings help to highlight the cortical cell types and developmental windows through which psychiatric genetic risk may act, offering insights into potential critical periods for intervention.

Keywords: Psychiatric disorders; Genome-wide association study ; Single-nucleus RNA sequencing; Cell type-specific risk; Neurodevelopmental trajectories.

Introduction

Schizophrenia, depression and bipolar disorder are highly burdensome psychiatric illnesses [1]. Despite their clinical heterogeneity, these disorders frequently exhibit comorbidity and overlapping symptoms [2, 3], which aligns with the dimensional-continuum models of psychiatric risk. These models conceptualize psychiatric illnesses along continuous dimensions rather than as discrete categories, emphasizing that multiple interacting domains, such as cognition and emotion, jointly contribute to psychiatric symptoms and their shared neurobiological basis [4-6]. Large-scale genome-wide association studies (GWASs) have revealed substantial genetic correlations across psychiatric disorders, suggesting a shared polygenic architecture as well as disorder-specific components [7-13]. While these genetic studies have uncovered hundreds of associated loci, the mechanisms by which risk variants act on specific cell types and developmental windows, as well as the similarities and differences of these mechanisms across diseases, remain incompletely understood.

The cerebral cortex constitutes a fundamental pathophysiological substrate for psychiatric disorders. It is essential for higher-order cognitive and emotional processes, and converging evidence from neuroimaging studies has demonstrated cortical abnormalities across schizophrenia, depression, and bipolar disorder [14-17]. Increasing evidence indicates that the effects of psychiatric risk variants are dependent on neurodevelopmental context, particularly during fetal and early postnatal stages [18-21]. For example, genetic risk factors for schizophrenia primarily act during early cortical development, perturbing neuronal circuit formation and synaptic organization in ways that predispose to later disease manifestation [18]. Moreover, shared genetic risk across psychiatric disorders has been shown to regulate genes expressed in developing neocortex during midgestation [21]. Therefore, linking polygenic risk to cortical cell types across developmental stages helps

1 Department of Radiology and Tianjin Key Laboratory of Functional Imaging, Tianjin Medical University General Hospital, 300052 Tianjin, China

2 Department of Radiology, Jinling Hospital, Affiliated Hospital of Medical School, Nanjing University, Nanjing, 210002, China

* Corresponding Author.

identify when and where genetic risk arises, providing insight into how psychiatric disorders develop.

Advances in single-nucleus RNA sequencing (snRNA-seq) now provide improved resolution to map gene expression across diverse cortical cell types and developmental stages [22, 23]. These datasets enable dissection of how disease-associated genes are expressed across different cell types and developmental stages. Integrating GWAS with single-cell transcriptomic data has emerged as a powerful approach to link genetic risk with cellular contexts [24, 25]. In particular, the single-cell disease relevance score (scDRS) framework allows polygenic risk to be projected onto individual cells, thereby quantifying disease relevance across cell types and developmental time [26].

In this study, we integrated GWAS summary statistics of schizophrenia, depression, and bipolar disorder with large-scale human cortical snRNA-seq data spanning from the second trimester of gestation to adulthood. We aimed to identify shared and disorder-specific genes and pathways, determine the cellular and developmental distribution of polygenic risk, and disentangle common versus distinct biological mechanisms across major psychiatric disorders.

Materials and Methods

GWAS datasets

To investigate the cellular mechanisms through which genetic risk contributes to major psychiatric disorders, we analyzed GWAS summary statistics of European ancestry for depression (N_{case} = 294,322, $N_{control}$ = 741,438) [8], bipolar disorder (N_{case} = 41,917, $N_{control}$ = 371,549) [9] and schizophrenia (N_{case} = 53,386, $N_{control}$ = 77,258) [7]. For depression, cases were defined based on multiple criteria, including the International Classification of Diseases (ICD), self-reported depression, or questionnaire-based assessments. Control participants were drawn from population-based cohorts, excluding individuals with any diagnosis of depression. For bipolar disorder, all cases met international diagnostic criteria, including the Diagnostic and Statistical Manual of Mental Disorders (DSM) and ICD, while controls had no psychiatric history. For schizophrenia, diagnoses were based on DSM or ICD criteria, structured clinical interviews, medical record reviews, consensus diagnoses, and scale-assisted assessment. Controls were individuals without a history of psychiatric disorders or were randomly selected from the population. As these GWAS represent meta-analyses of multiple cohorts, detailed information on study design, diagnostic procedures, and quality control is available in the original publications.

Human cortex single-nucleus RNA sequencing dataset from gestation to adulthood

We used snRNA-seq gene expression data from human cerebral cortex, spanning developmental stages from the second trimester of gestation to adulthood (fourth last menstrual period month human stage to 54 years old). The study analyzed >700,000 single-nucleus RNA sequencing profiles from 106 donors (45 female and 61 male subjects) [23]. The developmental stages included the second trimester of gestation (31 donors), the third trimester of gestation (12 donors), 0-1 years (11 donors), 1-2 years (4 donors), 2-4 years (10 donors), 4-10 years (8 donors), 10-20 years (17 donors) and adulthood (>20 years,13 donors). Preprocessing of the snRNA-seq data was carried out using Scanpy (single-cell analysis in python, v 1.10.1, http://scanpy.readthedocs.io/en/stable/index.html) [27]. Each cell was assigned a predefined cell type and developmental stage [23]. The cell types included excitatory neurons, inhibitory neurons, glial progenitors, astrocytes, oligodendrocyte precursor cells (OPCs), oligodendrocytes, microglia, and vascular cells. We filtered out cells expressing fewer than 250 genes and genes expressed in fewer than 50 cells, 704,080 single nuclei transcriptome profiles × 17,589 genes remained in the snRNA-seq data. Following the filtering, we normalized the snRNA-seq data matrix. Each cell was normalized by total counts over all genes, enabling comparison of gene expression levels across cells. The normalized data matrix was then logarithmized to stabilize variance for further analyses. Batch correction was applied to the dataset [23], with gene counts and sex included as covariates for the scDRS analysis.

MAGMA

MAGMA (v1.10, https://cncr.nl/research/magma/) [28] was used to construct gene sets for schizophrenia, depression, and bipolar disorder based on GWAS summary statistics. We performed these analyses using genome-wide summary data. Gene boundaries were defined based on Ensembl release 102 (GRCh37) and extended by 35 kb upstream and 10 kb downstream to incorporate potential regulatory regions. Linkage disequilibrium was estimated from the European reference panel of the 1000 Genomes Project (Phase 3) [29]. Gene-based association testing was performed in MAGMA using the SNP-wise Mean model. Gene-level *P*-values were derived from the exact distribution of the sum of squared z-scores using the Imhof method and were subsequently converted to gene-level z-scores. For each disorder, the top 1,000 genes with the highest MAGMA gene-level z-scores were selected, restricting to genes that passed quality control in the snRNA-seq dataset.

Over-representation analysis

To investigate the functional enrichment of disorder-associated genes, over-representation analysis was conducted for each disorder using the ToppGene Suite (https://toppgene.cchmc.org/) [30]. For each over-representation analysis, the input gene set comprised the top 1,000 genes ranked by MAGMA gene-level z-scores, which were tested against the ToppGene Suite's default background of all genes annotated for Gene Ontology (GO) biological process terms (n = 20,557). In this analysis, we specifically selected the GO biological process database, as our primary objective was to clarify and compare the biological processes underlying the genetic architecture of schizophrenia, depression, and bipolar disorder. Restricting the analysis to a single database also helped minimize gene set redundancy and reduced the inflated burden of multiple testing. Statistical significance was assessed using a hypergeometric test, and *P*-values were adjusted for multiple testing using the Bonferroni correction.

Single-cell disease relevance score (scDRS)

We used scDRS (v1.0.4, https://github.com/martinjzhang/scDRS) [26] to investigate the cellular targets of schizophrenia, depression, and bipolar disorder through polygenic score at

single-cell resolution. For each snRNA-seq cell, scDRS computed a disease relevance score by aggregating the expression of the top 1,000 associated genes (default parameter setting in scDRS), followed by normalization. To determine statistical significance, 1,000 sets of Monte Carlo control scores were generated and normalized. One-sided cell-level *P* values were computed by comparing each cell's normalized disease relevance score to the empirical distribution of control scores. Uniform Manifold Approximation and Projection (UMAP, v0.5.6) [31] is a nonlinear dimensionality reduction technique, which was used for visualizing the structure of snRNA-seq data in two dimensions. Cell type-level analyses aggregated individual cell-level results to identify cell types associated with the three psychiatric disorders. Although scDRS retains sufficient power even for small cell numbers [26], we excluded cell types in specific developmental stages with fewer than 50 cells. Consequently, scDRS results for 704,072 single nuclei were retained for cell type-level analyses. Each cell was assigned to a unique combination of cell type and developmental stage based on its annotation; therefore, no cell was counted in more than one category. *P* values for both cell-level and cell type-level analyses were adjusted using false discovery rate (FDR) correction to control for multiple hypothesis testing.

Sensitivity analysis of gene selection threshold

To assess the robustness of our results to gene selection criteria, we performed sensitivity analyses using alternative threshold for MAGMA-prioritized genes per disorder. In the original scDRS study [26], six strategies were evaluated, including the top 100, 500, 1,000, 2,000, as well as those based on family-wise error rate (FWER) < 5%, and FDR < 1%. The default top 1,000 gene set substantially outperformed all other versions, except for the top 2,000 gene set, which showed comparable performance but slightly poorer calibration. Therefore, we selected the top 2,000 gene set for sensitivity analysis to further validate the robustness of our findings.

Results

Disease-associated genes and pathways

For each disorder, we extracted the top 1,000 associated genes and assessed their overlap (Supplementary Table 1 and Figure 1a). A total of 104 genes were shared across schizophrenia, depression, and bipolar disorder, highlighting their pleiotropic genetic architecture, whereas 517, 642, and 563 genes were disorder-specific for schizophrenia, depression, and bipolar disorder, respectively. Pathway enrichment analysis (Bonferroni-corrected $P < 0.05$) identified 34 pathways for schizophrenia (Supplementary Table 2), 50 for depression (Supplementary Table 3), and 21 for bipolar disorder (Supplementary Table 4), with nine shared pathways primarily related to synaptic processes (Figure 1b-e), such as synapse organization ($Pc = 1.52 \times 10^{-7}$ for schizophrenia, $Pc = 2.67 \times 10^{-10}$ for depression, $Pc = 1.24 \times 10^{-2}$ for bipolar disorder) and synaptic signaling ($Pc = 1.85 \times 10^{-7}$ for schizophrenia, $Pc = 4.19 \times 10^{-9}$ for depression, $Pc = 3.18 \times 10^{-6}$ for bipolar disorder). Depression- and schizophrenia-associated pathways were enriched for generation of neurons ($Pc = 2.17 \times 10^{-8}$ for schizophrenia, $Pc = 1.87 \times 10^{-10}$ for depression) and neuron differentiation ($Pc = 7.80 \times 10^{-9}$ for schizophrenia, $Pc = 2.66 \times 10^{-10}$ for depression), while schizophrenia- and bipolar disorder shared enrichment in regulation of synaptic plasticity ($Pc = 8.87 \times 10^{-3}$ for schizophrenia, $Pc = 2.79 \times 10^{-2}$ for bipolar disorder). Schizophrenia-specific pathways were significantly enriched in GABAergic synaptic transmission ($Pc = 1.09 \times 10^{-2}$) and metal ion transport ($Pc = 1.67 \times 10^{-2}$). These findings reveal both shared and disorder-specific molecular mechanisms, with convergent enrichment in synaptic pathways across disorders, and schizophrenia showing additional specificity in GABAergic transmission and ion transport.

Developmental and cell-type specificity of risk genes

We next applied scDRS analysis to snRNA-seq data spanning eight major brain cell types (Figure 2a) across eight developmental stages (Figure 2b). First, we calculated a scDRS for each cell in the snRNA-seq datasets based on the genes associated with schizophrenia, depression, and bipolar disorder, and projected these scores onto UMAP plot (Figure 2c). At the single-cell level, scDRS showed that genes associated with all three psychiatric disorders were highly expressed in excitatory and inhibitory neurons, particularly during postnatal stages. Schizophrenia and depression genes also exhibited elevated scDRS in OPCs, while schizophrenia genes showed higher scDRS in mature oligodendrocytes compared with depression and bipolar disorder.

We then performed cell-type-level analyses to associate predefined cell types at different developmental stages with these disorders. In total, the analyses identified 19 significant cell type-schizophrenia pairs, 21 for depression, and 14 for bipolar disorder (FDR < 0.05, Monte Carlo test; Supplementary Tables 5-7). The analysis demonstrated that excitatory neurons were associated with schizophrenia, depression, and bipolar disorder spanning the postnatal period through adulthood. All three disorders were also significantly associated with inhibitory neurons, but with distinct temporal windows. In schizophrenia, inhibitory neuron associations were mainly postnatal, whereas in depression and bipolar disorder, associations extended from the third trimester through adulthood (Figure 2d). These results emphasized that excitatory and inhibitory neuronal dysfunction was recognized as a foundational element across major psychiatric disorders. The broader vulnerability window may reflect the early involvement of GABAergic interneurons in depression and bipolar disorder. Our findings emphasized the temporal association of excitatory and inhibitory neurons with schizophrenia, depression, and bipolar disorder during the postnatal period. This observation aligned with the developmental trajectories of glutamatergic synapse density, dendritic arborization, and mesocortical dopaminergic projections, all of which continue to mature after birth [18], thereby underscoring the critical role of neural circuit development in the pathophysiology of schizophrenia, depression, and bipolar disorder.

Glial cells demonstrated disorder-specific associations. Astrocytes were consistently associated with all three disorders during the 1-2 years stage, a period coinciding with active synaptogenesis [32, 33] and gliogenesis [34, 35], highlighting the importance of early postnatal glial maturation for neurodevelopmental vulnerability to psychiatric disorders. OPCs were linked to schizophrenia and depression, with depression spanning from the third trimester through adulthood, while schizophrenia was restricted to 0-4 years (Figure 2d). Mature oligodendrocytes were only associated with schizophrenia during

1-10 years. OPCs could differentiate into mature oligodendrocytes to form myelin sheaths, support axonal metabolism, and participate in neuroplasticity [36]. The distinct temporal patterns observed for oligodendrocyte lineage cells suggest disorder-specific vulnerabilities in white matter development. The prolonged association for depression may reflect impaired differentiation or maintenance of OPCs, consistent with reports of widespread white matter abnormalities and disrupted oligodendrocyte function in depression [36]. Schizophrenia was associated not only with OPCs within a narrow window (0-4 years) but also subsequently with mature oligodendrocytes. These findings highlight a critical developmental period during which disrupted myelination may compromise long-range connectivity, consistent with the neurodevelopmental model

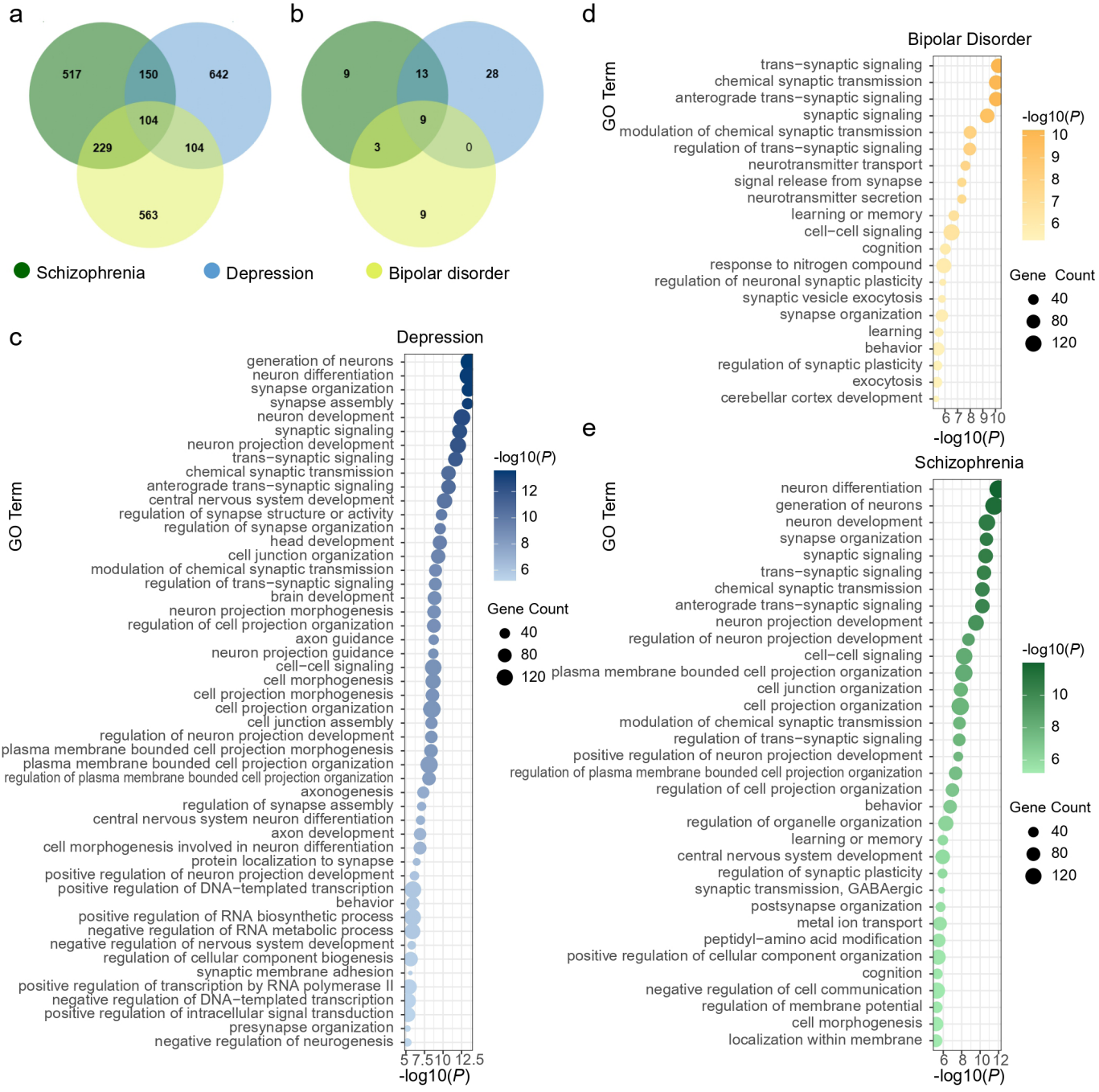

Figure 1. Gene- and pathway-level analyses of three psychiatric disorders. a. Venn diagram shows the number of genes identified by gene-based association tests and their overlap among the three psychiatric disorders. **b.** Venn diagram shows the number of pathways identified by statistical over-representation analysis and their overlap among the three disorders. **c-e**, Bubble plots display the enriched Gene Ontology (GO) biological process terms (Bonferroni-corrected $P < 0.05$) for depression (**c**), bipolar disorder (**d**), and schizophrenia (**e**). The x-axis represents the significance level of each term, while the y-axis lists the GO terms. Bubble color indicates significance, and bubble size represents the number of genes enriched in each term.

of schizophrenia [37, 38]. Together, these results suggest that depression may be characterized by chronic deficits in OPCs function, while schizophrenia reflects postnatal developmental failures in oligodendrocyte maturation and myelination. This distinction underscores the importance of temporally resolved glial mechanisms in contributing to disorder-specific pathophysiology.

Disorder-specific scDRS trajectories across cell types and developmental windows

We next compared average scDRS scores for schizophrenia, depression, and bipolar disorder across developmental

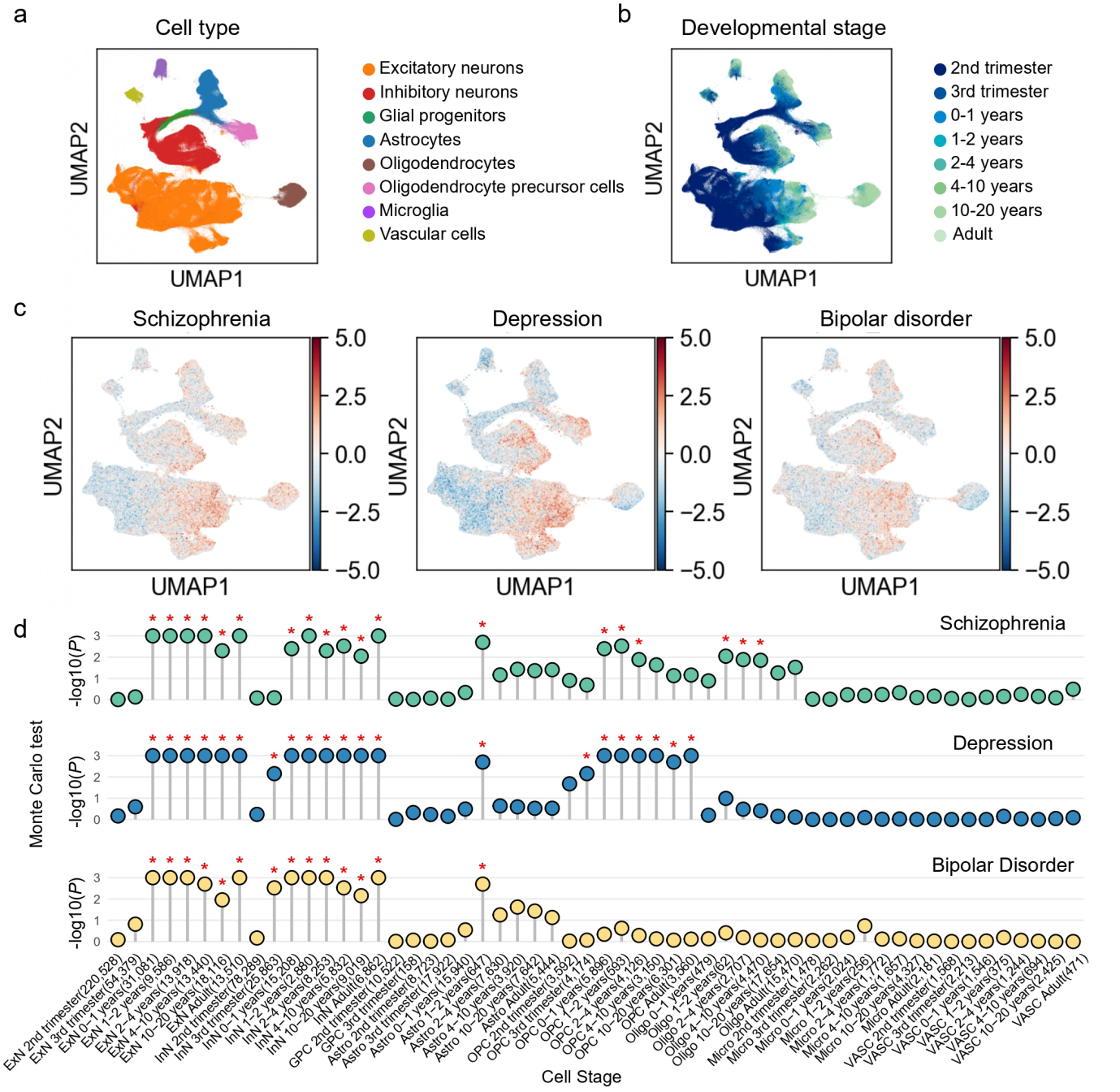

Figure 2. Associations of human cortical cells with risk genes for schizophrenia, depression, and bipolar disorder. a-b, UMAP (uniform manifold approximation and projection) visualization of human cortical cells, with cluster labels indicating annotated cell types (**a**) and developmental stages (**b**). **c**, UMAP visualizations display the disease relevance score for schizophrenia, depression and bipolar disorder assigned to each cell. d, Cell type-level scDRS analysis for the three psychiatric disorders. The y-axis represents the -$\log_{10}$ (*P* values) of the cell type-level analyses of human cortical cells for the three psychiatric disorders, grouped by cell types and developmental stages (x-axis, with number of cells indicated in parentheses). Asterisks denote significant cell type-disease associations (FDR < 0.05 across 56 cell types in different developmental stages). ExN, excitatory neuron; InN, inhibitory neuron; GPC, glial progenitor cell; Astro, astrocyte; OPC, oligodendrocyte precursor cell; Oligo, oligodendrocyte; Micro, microglia; VASC, vascular cell.

stages in the associated cell types (Figure 3). In both excitatory and inhibitory neurons, depression exhibited the highest postnatal scDRS scores, with a pronounced peak during the 1-2 years stage. In astrocytes, all three disorders demonstrated scDRS peaks during 1-2 years. Striking differences were observed in OPCs, where depression consistently showed the highest scores across the lifespan, followed by schizophrenia and then bipolar disorder, highlighting more persistent OPCs vulnerability in depression. By contrast, in mature oligodendrocytes, schizophrenia exhibited the highest scores, providing strong support for the established model of myelination deficits and white matter abnormalities as central pathophysiological features of schizophrenia [37, 38].

Robustness of disease-cell associations to gene set size

To evaluate the robustness of our findings to the choice of gene selection threshold in scDRS, we performed a sensitivity analysis using the top 2,000 MAGMA-prioritized genes. The developmental trajectories of scDRS derived from top 2,000 MAGMA-prioritized genes were highly consistent with our primary analysis based on the top 1,000 genes (Figure 4). Although the larger gene set yielded slightly attenuated calibration, the developmental trajectories of scDRS and the distinctions between disorders remained largely consistent, indicating that our findings are robust to variations in gene selection strategy.

Discussion

Our integrative analysis provides novel insights into the cell type- and developmental stage-specific mechanisms underlying schizophrenia, depression, and bipolar disorder. At the gene and pathway level, we observed a substantial overlap of associated genes and convergent enrichment in synaptic processes, consistent with the view that synaptic dysfunction is a core feature across major psychiatric disorders [39]. At the same time, disorder-specific enrichments, such as metal ion transport for schizophrenia, point to unique pathophysiological features.

At the cellular level, excitatory neurons were consistently implicated across disorders from postnatal stages through adulthood, underscoring glutamatergic dysfunction as a shared substrate of psychiatric illness. Inhibitory neurons also showed significant associations, but with broader temporal vulnerability in depression and bipolar disorder, extending back to the fetal period. This aligns with prior studies reporting a widespread excitatory-inhibitory imbalance in these conditions

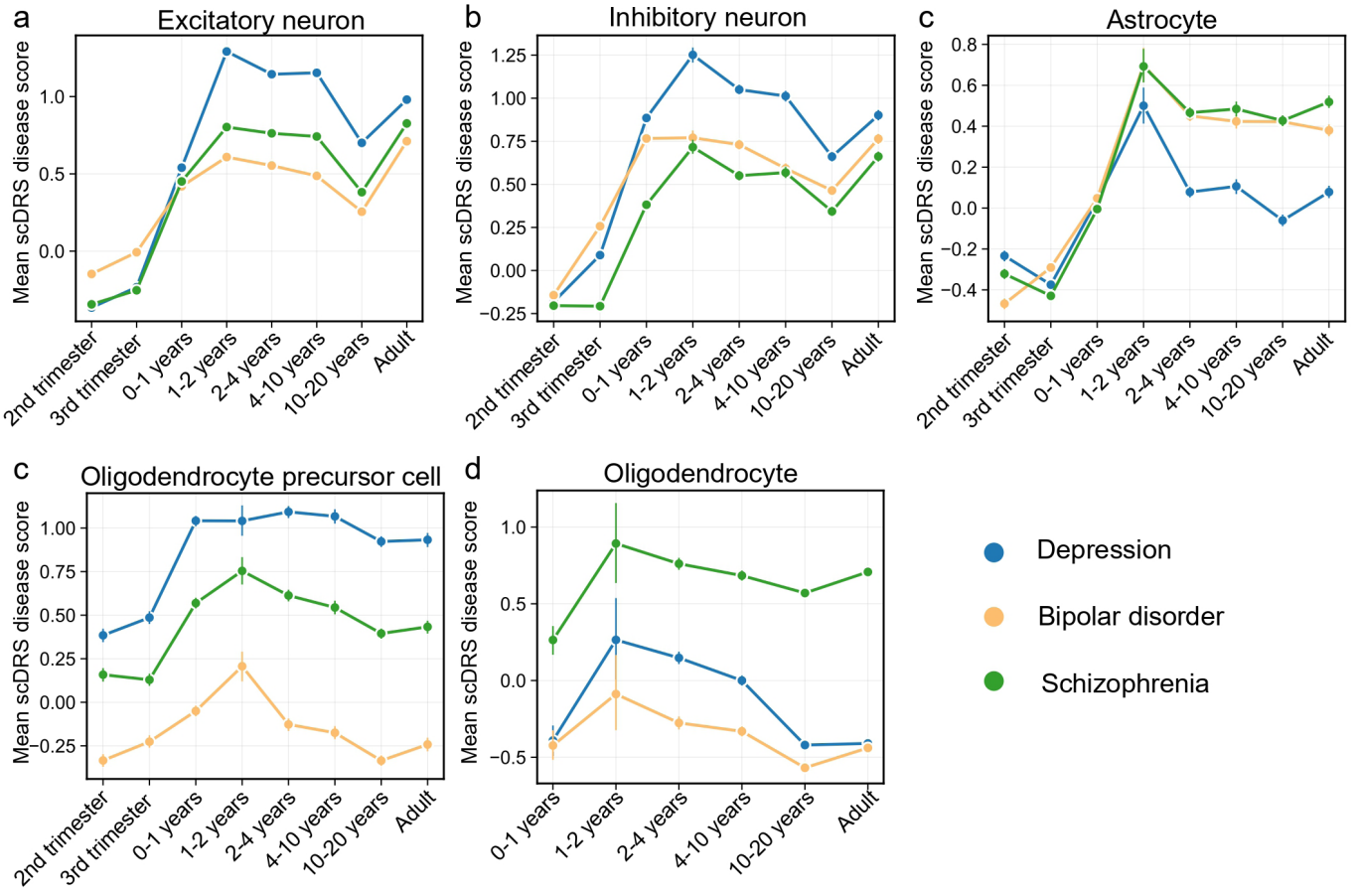

Figure 3. Developmental trajectories of scDRS in human cortical cells for three psychiatric disorders. These plots display the average scDRS (y-axis) for schizophrenia, depression, and bipolar disorder in five major cortical cell types: excitatory neuron (**a**), inhibitory neuron (**b**), astrocyte (**c**), oligodendrocyte precursor cell (OPCs, **d**), and oligodendrocyte (**e**). The developmental window spans from the second trimester of gestation to adulthood (x-axis). Prenatal stages for oligodendrocyte were excluded due to low cell counts (n < 50).

[40-42]. Together, these results emphasize that excitatory-inhibitory imbalance is a unifying mechanism, but with disorder-specific developmental timing.

Glial cell associations demonstrated greater disorder specificity. Astrocytes were consistently implicated across disorders during the 1-2 years, coinciding with peaks in synaptogenesis and gliogenesis [32-35]. OPCs showed prolonged associations in depression, suggesting persistent progenitor dysfunction, whereas schizophrenia was linked to a narrower early childhood window, with mature oligodendrocytes uniquely implicated. This distinction suggests that depression may involve chronic impairments in OPC differentiation or maintenance, while schizophrenia reflects postnatal developmental failures in oligodendrocyte maturation and myelination, consistent with white matter abnormalities observed in these disorders [36, 43].

A key limitation of our study is that we rely on snRNA-seq data from healthy human brains to annotate disease risk. This approach assumes that the transcriptional and regulatory relationships captured in healthy tissues largely reflect those in disease states, an assumption commonly adopted due to the limited availability of high-quality disease-specific single-cell datasets resources. However, disease-related changes, such as altered cell composition, cell-state transitions, and regulatory network remodeling, may influence the generalizability of our findings. Accordingly, our findings should be interpreted as reflecting putative risk-enriched cell types under baseline conditions rather than direct causal effects in disease states. Future studies incorporating disease-specific single-cell datasets will be essential to refine these interpretations. Furthermore, although a smaller number of cells should not substantially affect the scDRS power, the imbalance in the number of cells captured across cell types and developmental stages may introduce potential biases in estimating disease-associated cell types. These proportions not only reflect the intrinsic cellular composition of the human cerebral cortex at different developmental stages but are also influenced by variation in the number of donors contributing to each stage.

Overall, our findings highlight both convergent and distinct neurodevelopmental trajectories across psychiatric disorders, emphasizing the importance of temporally resolved analyses to disentangle shared and disorder-specific mechanisms. This cellular and developmental mapping of polygenic risk may inform strategies for targeted interventions at critical windows of vulnerability.

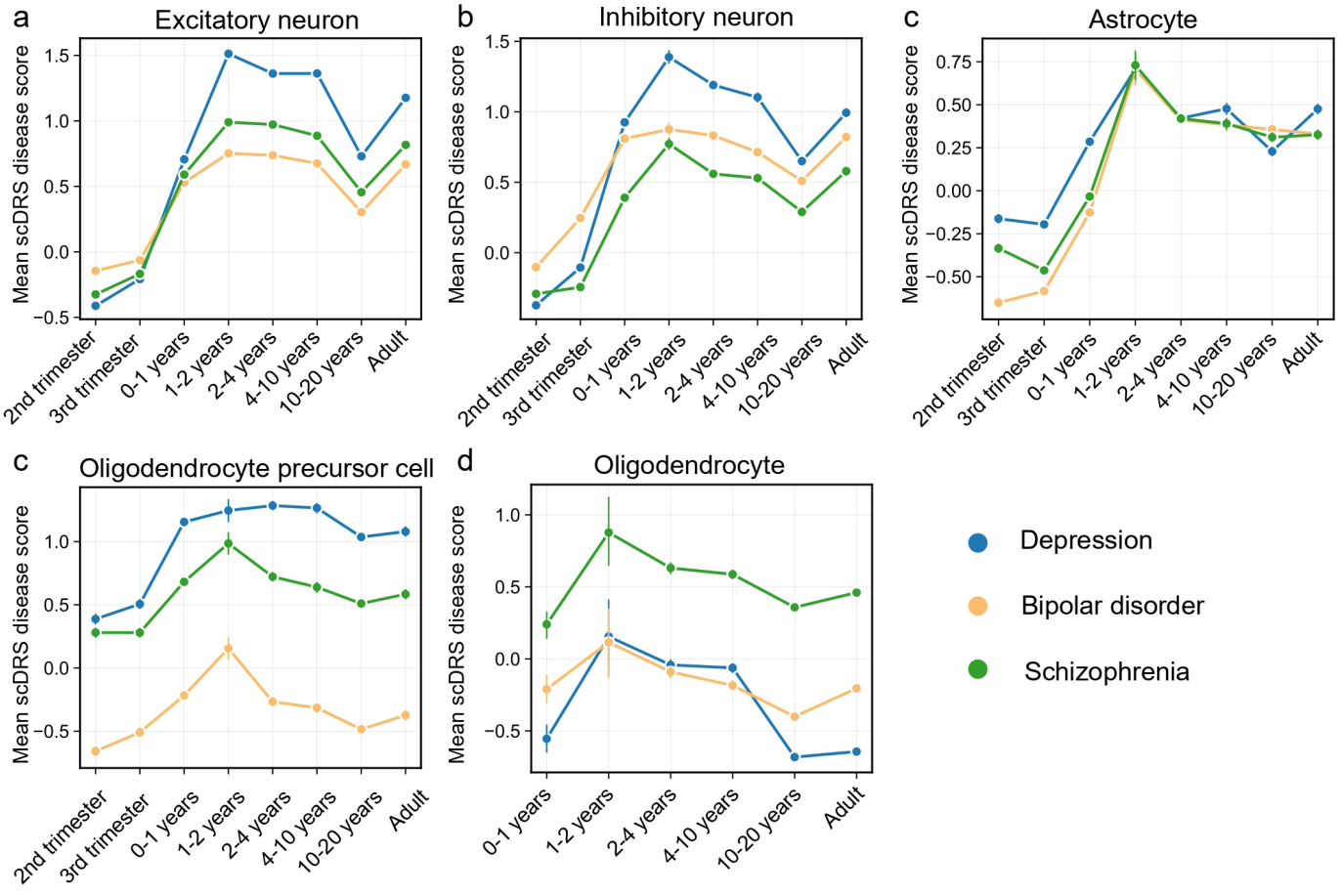

Figure 4. Developmental trajectories of scDRS across human cortical cell types for three psychiatric disorders using the top 2,000 disease-related genes. These plots display the average scDRS (y-axis) for schizophrenia, depression, and bipolar disorder in five major cortical cell types: excitatory neuron (**a**), inhibitory neuron (**b**), astrocyte (**c**), oligodendrocyte precursor cell (OPCs, **d**), and oligodendrocyte (**e**). The developmental window spans from the second trimester of gestation to adulthood (x-axis). Prenatal stages for oligodendrocyte were excluded due to low cell counts (n < 50).

Abbreviations

DSM: Diagnostic and Statistical Manual of Mental Disorders; FDR: False Discovery Rate; FWER: Family-Wise Error Rate; GO: Gene Ontology; GRCh37: Genome Reference Consortium Human Build 37; GWAS: Genome-Wide Association Study; ICD: International Classification of Diseases; OPCs: Oligodendrocyte Precursor Cells; scDRS: Single-Cell Disease Relevance Score; snRNA-seq: Single-Nucleus RNA Sequencing; SNP: Single Nucleotide Polymorphism; UMAP: Uniform Manifold Approximation and Projection.

Author Contributions

N.L. conceived and designed the study. Y.L. and S.W. performed data preprocessing and statistical analyses. J.T. contributed to data interpretation and manuscript revision. N.L. drafted the manuscript with input from all authors. All authors read and approved the final manuscript.

Acknowledgements

We are grateful to the Psychiatric Genomics Consortium for providing GWAS summary statistics of schizophrenia, depression, and bipolar disorder. We thank Dmitry Velmeshev et al. for generating and sharing the single-nucleus RNA sequencing dataset of prenatal and postnatal human cortical development, which was essential for this study.

Funding Information

This work was supported by the Tianjin Municipal Health Commission Science and Technology Project (Grant No. TJWJ2025QN006).

Ethics Approval and Consent to Participate

This study used publicly available GWAS summary statistics and previously published single-nucleus RNA sequencing datasets. No new human participants or animal subjects were recruited, and therefore no additional ethics approval or informed consent was required.

Competing Interests

The authors declare no competing interests.

Data Availability

The GWAS summary statistics for schizophrenia, depression, and bipolar disorder are available from the Psychiatric Genomics Consortium (https://pgc.unc.edu/). The single-nucleus RNA sequencing dataset of prenatal and postnatal human cortical development is available from the original publication (Velmeshev et al., Science, 2019).

References

[1] Charlson F, van Ommeren M, Flaxman A, Cornett J, Whiteford H, & Saxena S. (2019). New WHO prevalence estimates of mental disorders in conflict settings: a systematic review and meta-analysis. Lancet, 394(10194), 240-248. https://doi.org/10.1016/s0140-6736(19)30934-1

[2] Li W, Yang Y, An FR, Zhang L, Ungvari GS, Jackson T, et al. (2020). Prevalence of comorbid depression in schizophrenia: A meta-analysis of observational studies. J Affect Disord, 273, 524-531. https://doi.org/10.1016/j.jad.2020.04.056

[3] Laursen TM, Agerbo E, & Pedersen CB. (2009). Bipolar disorder, schizoaffective disorder, and schizophrenia overlap: a new comorbidity index. J Clin Psychiatry, 70(10), 1432-1438. https://doi.org/10.4088/JCP.08m04807

[4] Waddington JL. (2024). From operational diagnostic to dimensional-continuum concepts of psychotic and non-psychotic illness: Embracing catatonia across psychopathology and intrinsic movement disorder in neural network dysfunction. Schizophr Res, 263, 99-108. https://doi.org/10.1016/j.schres.2022.10.001

[5] Schottner Sieler M, Golay P, Vieira S, Alameda L, Conus P, Klauser P, et al. (2025). A dimensional approach to psychosis: identifying cognition, depression, and thought disorder factors in a clinical sample. Schizophrenia (Heidelb), 11(1), 97. https://doi.org/10.1038/s41537-025-00641-x

[6] Li J, Long Z, Ji GJ, Han S, Chen Y, Yao G, et al. (2025). Major depressive disorder on a neuromorphic continuum. Nat Commun, 16(1), 2405. https://doi.org/10.1038/s41467-025-57682-0

[7] Trubetskoy V, Pardinas AF, Qi T, Panagiotaropoulou G, Awasthi S, Bigdeli TB, et al. (2022). Mapping genomic loci implicates genes and synaptic biology in schizophrenia. Nature, 604(7906), 502-508. https://doi.org/10.1038/s41586-022-04434-5

[8] Als TD, Kurki MI, Grove J, Voloudakis G, Therrien K, Tasanko E, et al. (2023). Depression pathophysiology, risk prediction of recurrence and comorbid psychiatric disorders using genome-wide analyses. Nat Med, 29(7), 1832-1844. https://doi.org/10.1038/s41591-023-02352-1

[9] Mullins N, Forstner AJ, O'Connell KS, Coombes B, Coleman JRI, Qiao Z, et al. (2021). Genome-wide association study of more than 40,000 bipolar disorder cases provides new insights into the underlying biology. Nat Genet, 53(6), 817-829. https://doi.org/10.1038/s41588-021-00857-4

[10] Cross-Disorder Group of the Psychiatric Genomics Consortium. Electronic address pmhe, & Cross-Disorder Group of the Psychiatric Genomics C. (2019). Genomic Relationships, Novel Loci, and Pleiotropic Mechanisms across Eight Psychiatric Disorders. Cell, 179(7), 1469-1482 e1411. https://doi.org/10.1016/j.cell.2019.11.020

[11] Lee PH, Feng YA, & Smoller JW. (2021). Pleiotropy and Cross-Disorder Genetics Among Psychiatric Disorders. Biol Psychiatry, 89(1), 20-31. https://doi.org/10.1016/j.biopsych.2020.09.026

[12] Cross-Disorder Group of the Psychiatric Genomics C.

(2013). Identification of risk loci with shared effects on five major psychiatric disorders: a genome-wide analysis. Lancet, 381(9875), 1371-1379. https://doi.org/10.1016/S0140-6736(12)62129-1
[13] Sullivan PF, & Geschwind DH. (2019). Defining the Genetic, Genomic, Cellular, and Diagnostic Architectures of Psychiatric Disorders. Cell, 177(1), 162-183. https://doi.org/10.1016/j.cell.2019.01.015
[14] van Erp TG, Hibar DP, Rasmussen JM, Glahn DC, Pearlson GD, Andreassen OA, et al. (2016). Subcortical brain volume abnormalities in 2028 individuals with schizophrenia and 2540 healthy controls via the ENIGMA consortium. Mol Psychiatry, 21(4), 547-553. https://doi.org/10.1038/mp.2015.63
[15] Schmaal L, Pozzi E, T CH, van Velzen LS, Veer IM, Opel N, et al. (2020). ENIGMA MDD: seven years of global neuroimaging studies of major depression through worldwide data sharing. Transl Psychiatry, 10(1), 172. https://doi.org/10.1038/s41398-020-0842-6
[16] Hibar DP, Westlye LT, Doan NT, Jahanshad N, Cheung JW, Ching CRK, et al. (2018). Cortical abnormalities in bipolar disorder: an MRI analysis of 6503 individuals from the ENIGMA Bipolar Disorder Working Group. Mol Psychiatry, 23(4), 932-942. https://doi.org/10.1038/mp.2017.73
[17] Rootes-Murdy K, Panta S, Kelly R, Romero J, Quidé Y, Cairns MJ, et al. (2024). Cortical similarities in psychiatric and mood disorders identified in federated VBM analysis via COINSTAC. Patterns (N Y), 5(7), 100987. https://doi.org/10.1016/j.patter.2024.100987
[18] Birnbaum R, & Weinberger DR. (2017). Genetic insights into the neurodevelopmental origins of schizophrenia. Nat Rev Neurosci, 18(12), 727-740. https://doi.org/10.1038/nrn.2017.125
[19] Cameron D, Mi D, Vinh NN, Webber C, Li M, Marin O, et al. (2023). Single-Nuclei RNA Sequencing of 5 Regions of the Human Prenatal Brain Implicates Developing Neuron Populations in Genetic Risk for Schizophrenia. Biol Psychiatry, 93(2), 157-166. https://doi.org/10.1016/j.biopsych.2022.06.033
[20] Li M, Santpere G, Imamura Kawasawa Y, Evgrafov OV, Gulden FO, Pochareddy S, et al. (2018). Integrative functional genomic analysis of human brain development and neuropsychiatric risks. Science, 362(6420). https://doi.org/10.1126/science.aat7615
[21] Schork AJ, Won H, Appadurai V, Nudel R, Gandal M, Delaneau O, et al. (2019). A genome-wide association study of shared risk across psychiatric disorders implicates gene regulation during fetal neurodevelopment. Nat Neurosci, 22(3), 353-361. https://doi.org/10.1038/s41593-018-0320-0
[22] Herring CA, Simmons RK, Freytag S, Poppe D, Moffet JJD, Pflueger J, et al. (2022). Human prefrontal cortex gene regulatory dynamics from gestation to adulthood at single-cell resolution. Cell, 185(23), 4428-4447 e4428. https://doi.org/10.1016/j.cell.2022.09.039
[23] Velmeshev D, Perez Y, Yan Z, Valencia JE, Castaneda-Castellanos DR, Wang L, et al. (2023). Single-cell analysis of prenatal and postnatal human cortical development. Science, 382(6667), eadf0834. https://doi.org/10.1126/science.adf0834
[24] Bryois J, Skene NG, Hansen TF, Kogelman LJA, Watson HJ, Liu Z, et al. (2020). Genetic identification of cell types underlying brain complex traits yields insights into the etiology of Parkinson's disease. Nat Genet, 52(5), 482-493. https://doi.org/10.1038/s41588-020-0610-9
[25] Jagadeesh KA, Dey KK, Montoro DT, Mohan R, Gazal S, Engreitz JM, et al. (2022). Identifying disease-critical cell types and cellular processes by integrating single-cell RNA-sequencing and human genetics. Nat Genet, 54(10), 1479-1492. https://doi.org/10.1038/s41588-022-01187-9
[26] Zhang MJ, Hou K, Dey KK, Sakaue S, Jagadeesh KA, Weinand K, et al. (2022). Polygenic enrichment distinguishes disease associations of individual cells in single-cell RNA-seq data. Nat Genet, 54(10), 1572-1580. https://doi.org/10.1038/s41588-022-01167-z
[27] Wolf FA, Angerer P, & Theis FJ. (2018). SCANPY: large-scale single-cell gene expression data analysis. Genome Biol, 19(1), 15. https://doi.org/10.1186/s13059-017-1382-0
[28] de Leeuw CA, Mooij JM, Heskes T, & Posthuma D. (2015). MAGMA: generalized gene-set analysis of GWAS data. PLoS Comput Biol, 11(4), e1004219. https://doi.org/10.1371/journal.pcbi.1004219
[29] Auton A, Brooks LD, Durbin RM, Garrison EP, Kang HM, Korbel JO, et al. (2015). A global reference for human genetic variation. Nature, 526(7571), 68-74. https://doi.org/10.1038/nature15393
[30] Chen J, Bardes EE, Aronow BJ, & Jegga AG. (2009). ToppGene Suite for gene list enrichment analysis and candidate gene prioritization. Nucleic Acids Res, 37(Web Server issue), W305-311. https://doi.org/10.1093/nar/gkp427
[31] Healy J, & McInnes L. (2024). Uniform manifold approximation and projection. Nature Reviews Methods Primers, 4(1), 82. https://doi.org/10.1038/s43586-024-00363-x
[32] Petanjek Z, Judas M, Simic G, Rasin MR, Uylings HB, Rakic P, et al. (2011). Extraordinary neoteny of synaptic spines in the human prefrontal cortex. Proc Natl Acad Sci U S A, 108(32), 13281-13286. https://doi.org/10.1073/pnas.1105108108
[33] Huttenlocher PR, & Dabholkar AS. (1997). Regional differences in synaptogenesis in human cerebral cortex. J Comp Neurol, 387(2), 167-178. https://doi.org/10.1002/(sici)1096-9861(19971020)387:2<167::aid-cne1>3.0.co;2-z
[34] Clarke LE, & Barres BA. (2013). Emerging roles of astrocytes in neural circuit development. Nat Rev Neurosci, 14(5), 311-321. https://doi.org/10.1038/nrn3484
[35] Molofsky AV, & Deneen B. (2015). Astrocyte development: A Guide for the Perplexed. Glia, 63(8), 1320-1329. https://doi.org/10.1002/glia.22836
[36] Zhou B, Zhu Z, Ransom BR, & Tong X. (2021). Oligodendrocyte lineage cells and depression. Mol Psychiatry, 26(1), 103-117. https://doi.org/10.1038/s41380-020-00930-0
[37] Douaud G, Smith S, Jenkinson M, Behrens T, Johansen-Berg H, Vickers J, et al. (2007). Anatomically related grey and white matter abnormalities in adolescent-onset schizophrenia. Brain, 130(Pt 9), 2375-2386. https://doi.org/10.1093/brain/awm184
[38] Takahashi N, Sakurai T, Davis KL, & Buxbaum JD. (2011). Linking oligodendrocyte and myelin dysfunction to neurocircuitry abnormalities in schizophrenia. Prog Neurobiol, 93(1), 13-24. https://doi.org/10.1016/j.pneuro-

bio.2010.09.004
[39] Lin YC, & Koleske AJ. (2010). Mechanisms of synapse and dendrite maintenance and their disruption in psychiatric and neurodegenerative disorders. Annu Rev Neurosci, 33, 349-378. https://doi.org/10.1146/annurev-neuro-060909-153204
[40] Howes OD, & Shatalina E. (2022). Integrating the Neurodevelopmental and Dopamine Hypotheses of Schizophrenia and the Role of Cortical Excitation-Inhibition Balance. Biol Psychiatry, 92(6), 501-513. https://doi.org/10.1016/j.biopsych.2022.06.017
[41] Hu YT, Tan ZL, Hirjak D, & Northoff G. (2023). Brain-wide changes in excitation-inhibition balance of major depressive disorder: a systematic review of topographic patterns of GABA- and glutamatergic alterations. Mol Psychiatry, 28(8), 3257-3266. https://doi.org/10.1038/s41380-023-02193-x
[42] Lee Y, Zhang Y, Kim S, & Han K. (2018). Excitatory and inhibitory synaptic dysfunction in mania: an emerging hypothesis from animal model studies. Exp Mol Med, 50(4), 1-11. https://doi.org/10.1038/s12276-018-0028-y
[43] Kelly S, Jahanshad N, Zalesky A, Kochunov P, Agartz I, Alloza C, et al. (2018). Widespread white matter microstructural differences in schizophrenia across 4322 individuals: results from the ENIGMA Schizophrenia DTI Working Group. Mol Psychiatry, 23(5), 1261-1269. https://doi.org/10.1038/mp.2017.170

Review Article

Brain Conflux

Multiscale Modeling of Transcranial Alternating Current Stimulation: Induced Electric Field and Cellular Responses

Authors

Guosheng Yi, Xinbo Hou, Xuelin Huang, Fu Zhang, Jintao Chen, Shen Li

Correspondence

lishen@tmu.edu.cn (S. Li)

Graphical Abstract

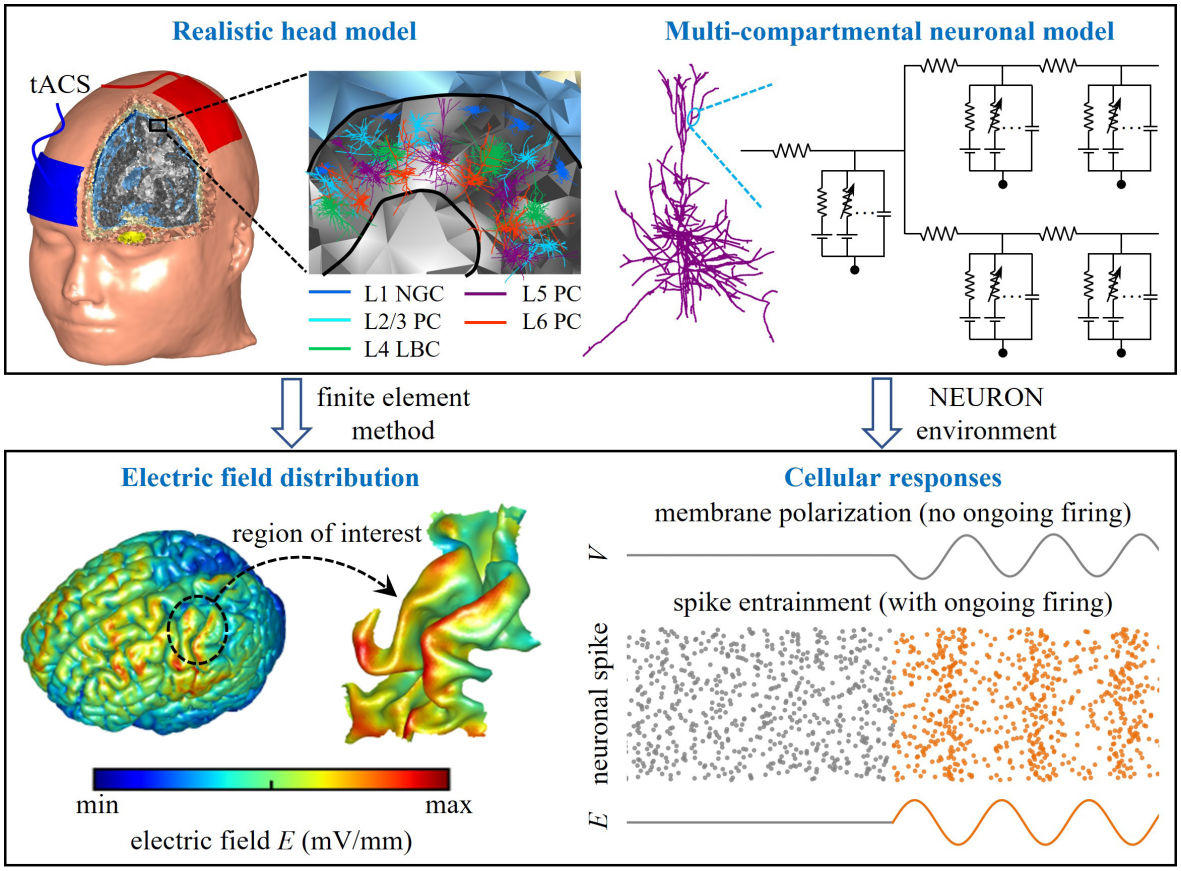

https://doi.org/10.71321/wyq6hf65

 B. Conflux. Vol. 1, No. 3 (2025)

Review Article Brain Conflux

Multiscale Modeling of Transcranial Alternating Current Stimulation: Induced Electric Field and Cellular Responses

Guosheng Yi [1] **,** Xinbo Hou [1] , Xuelin Huang [1] , Fu Zhang [1] , Jintao Chen [1] , Shen Li [2,3*]

Received: 2025-09-20 | Accepted: 2025-10-19 | Published online: 2025-11-11

Abstract

Transcranial alternating current stimulation (tACS) is a non-invasive neuromodulation technique that generates weak oscillatory electric fields (EFs) in the brain and has shown promise for probing neural oscillations and treating neuropsychiatric disorders. However, its effects on neural activity remain highly variable across studies, and controversies persist regarding whether conventional tACS intensities can genuinely entrain neuronal firing. Experimental approaches alone have limited capacity to resolve these inconsistencies. Computational modeling provides a powerful complementary framework to quantify induced EFs, predict cellular responses, and generate mechanistic hypotheses. In this review, we focus on multiscale models spanning from macroscopic realistic head models to microscopic multi-compartmental neuronal models. Head models elucidate how anatomy, tissue conductivity, stimulation parameters, and electrode montage shape the spatial distribution of tACS-induced fields, while multi-compartmental models reveal how EFs, neuronal morphology, biophysics, and synaptic inputs govern cell-type-specific polarization and spike entrainment. We highlight key insights, unresolved controversies, and emerging trends, including the integration of head and neuronal models, network-level simulations, and the use of artificial intelligence to bridge scales. By critically synthesizing advances in multiscale modeling, we argue that coupling computational frameworks with experimental recordings is essential for explaining the diversity of tACS effects and for translating mechanistic insights into individualized, clinically effective interventions.

Keywords: Transcranial alternating current stimulation; computational modeling; induced electric field; multi-compartmental neuronal models; membrane polarization; spike entrainment.

Introduction

Transcranial alternating current stimulation (tACS) uses scalp electrodes to apply low-intensity current (typically no more than 2 mA) at a specific frequency to modulate neural activity in a noninvasive and tolerable manner [1, 2]. By targeting endogenous oscillations, tACS provides a unique opportunity to probe the causal relationship between neural oscillations, cognition, and behavior [3, 4], and it is increasingly explored as a therapeutic strategy for neuropsychiatric disorders [5-7]. Despite rapid growth in experimental and clinical applications, the mechanisms by which tACS shapes neural dynamics remain incompletely understood.

At the core of tACS action are oscillatory electric fields (EFs) generated within the brain [8]. Such field is the acting force for driving its effects on neural activity [3]. The weak oscillatory field induced by tACS is not strong enough to activate action potentials in resting neurons, which is traditionally categorized as a subthreshold stimulation. Experimental recordings in rats [9-13], ferrets [14, 15], nonhuman primates [16-20], and humans [13] showed that such weak EFs can modulate spike timing and entrain neural activity. The above interventions are determined by EF strength and frequency, which also depend on cell type and ongoing oscillations. Particularly, tACS-induced effects on neural activity are highly variable across studies, and some findings are not fully reliable and difficult to replicate. This inconsistency has fueled ongoing debate over whether conventional tACS intensities, commonly 1-2 mA at the scalp, can genuinely entrain neural firing *in vivo* [21-24].

Computational modeling has emerged as a powerful complement to experimental approaches for addressing these controversies. Models can quantify EF distributions across tissues, test mechanistic hypotheses at the cellular level, and guide experimental design and clinical protocols [25-26]. In particular, realistic head models allow estimation of EF distribution across brain regions based on individual anatomy, while

1 School of Electrical and Information Engineering, Tianjin University, Tianjin, 300072, China.

2 Brain Assessment & Intervention Laboratory, Tianjin Anding Hospital, Mental Health Center, Tianjin Medical University, Tianjin, 300222, China

3 Institute of Mental Health, Tianjin Anding Hospital, Mental Health Center, Tianjin Medical University, Tianjin, 300222, China

* Corresponding Author.

multi-compartmental neuronal models capture the morphology- and biophysics-dependent responses of single cells to applied fields. Integrating these scales enables mechanistic insights into how tACS affects neural activity, from the distribution of currents in the brain to the entrainment of individual neurons.

Previous studies [2-5, 8, 27-31] summarized the neurophysiological and cognitive effects of tACS and discussed methodological challenges. In contrast, our review focuses specifically on multiscale computational modeling. We first outline advances in realistic head models that predict EF distributions, then examine multi-compartmental neuronal models that characterize cellular polarization and spiking entrainment. Finally, we discuss how integrating these approaches can resolve current controversies, highlight emerging directions such as network-level and artificial intelligence-assisted modeling, and consider the implications for translating tACS into individualized, clinically effective neuromodulation.

Realistic Head Models of tACS

tACS generates oscillating EFs across brain tissues, which are usually measured in units of voltage per meter (V/m) or millivolts per millimeter (mV/mm) [3, 32]. As noted, the fluctuating EF is the acting force of tACS. Therefore, calculation of EF in the target region is a first step to mechanistically understand cellular responses via modeling. Measured EFs can also be used to facilitate electrode montage selection and individualized dosing [3, 33, 34], and to predict inter-individual variability in tACS effects [35].

Realistic head models are powerful tools for predicting EF distribution induced in the brain during tACS [36, 37], which are often impractical to measure using experimental methods alone. These head models are created from anatomical magnetic resonance imaging (MRI), segmented into different tissue types such as scalp, skull, cerebrospinal fluid, gray matter, and white matter. The typical workflow includes MRI segmentation, 3D-surface tissue reconstruction, electrode placement, volume mesh generation, assignment of electrical conductivity and permittivity, specification of physics settings and boundary conditions, and finite element method (FEM) calculation [36, 38]. Common toolboxes used for simulating EF in realistic head models include SimNIBS [39, 40], COMETS2 [41], ROAST [38], SCIRun [42], and SimBio [43]. These toolboxes use FEM to numerically calculate EFs. Note that when calculating tACS-induced fields, it is usually assumed that the coupling between electric and magnetic fields is negligible, i.e., the quasi-static approximation [44]. This approximation is valid in the frequency range currently used for tACS [45].

The calculation of EF induced by tACS depends on the electrical conductivity of brain tissues. Since tissue conductivity varies between individuals, it is necessary to validate the predictions of a head model with *in vivo* measurements. Huang et al [46] directly measured EF in ten epilepsy patients generated by tACS and calibrated individual head models by adjusting skull, scalp, and brain conductivities to match recorded EFs. The resulting individualized models predicted EF spatial distribution with high accuracy for all subjects. Their validation results were later confirmed by Opitz et al [47], which consistently showed that realistic brain models using standard conductivities slightly misestimate the measured EF strength, suggesting the need for individual adjustments of tissue conductivities. Further, tissue conductivity exhibits inter-individual variability, and accounting for this variation is crucial for gaining better insights into stimulation mechanisms. However, many tACS modeling studies are based on a single exemplary head model. To capture anatomical and tissue variabilities, Berger et al [48] recently created a comprehensive dataset of 100 quality-assured realistic head models with variable tissue conductivities based on individual imaging data from the Human Connectome Project s1200 release. To reflect inter-individual variability, the scalp, skull, and grey matter tissue conductivities for each model were assigned pseudo-randomly from biologically plausible distributions [49]. The cerebrospinal fluid, white matter, and eye tissue conductivities were fixed at the default setting. To assess the quality of each head mesh, the authors performed a semi-manual correction for tissue accuracy and quality measurements of finite-element analysis. They also provided the simulation results of exemplary tACS montage based on a desynchronized montage outlined by Alekseichuk et al [50]. The dataset of their head models can assist in population variability analysis, meta-modeling techniques, and stimulation target optimization.

Other factors affecting tACS-induced EF distribution include stimulation current intensity, frequency, phase, electrode placement, and head anatomy. Recordings in surgical epilepsy patients [46] showed that the maximum EF exhibits approximately linear dependence on stimulation current intensity, which is about 0.4-0.5 V/m in human when current intensity is 1 mA from peak-to-baseline. Recordings in monkeys [32] showed that there is a small attenuation (up to 10%) in EF intensity as stimulation frequency increases. Alekseichuk et al [51] combined direct invasive recordings with computational models to characterize the dependence of EF magnitude and phase on stimulation phase during multi-electrode tACS. Their work demonstrated that specific phase configurations can create a “traveling wave” stimulation pattern, in which the location of maximum EF shifts over time. Subsequently, Lee et al [52] used phasor algebra and detailed head models to develop a simulation framework for predicting the phase gradient of EFs during multi-channel tACS. Their simulations precisely predicted *in vivo* recordings in monkeys when the return electrode was placed within a small radius (< 5 mm) from its actual location. They individually calibrated the overestimation in EF amplitude through optimization of tissue conductivity, which enhanced the correspondence between simulated and measured field amplitudes. Using validated head models, Opitz et al [47] determined the tolerance limits for variation in electrode placement, recommending that a placement accuracy of within 1 cm is required for reliable tACS application. In a following comparative modeling study involving mice, monkeys, and humans [53], the same research group revealed that head size is another factor influencing EF strength. Moreover, Ma et al [54] identified skull thickness, scalp thickness, and epidural cerebrospinal fluid thickness as key anatomical factors that contribute to the inter-individual variability of EF intensity.

Multi-Compartmental Neuronal Models of Cellular Responses to tACS

The oscillatory EF generated by tACS with conventional intensities (i.e., 1-2 mA) can periodically polarize the transmembrane potential. *In vitro* recordings in rats showed that such polarization response almost linearly increases with EF strength and decreases substantially as field frequency is varied from 10 Hz to 100 Hz [10]. The mean sensitivity of membrane potential to applied field exhibits an exponential decay function of frequency. However, other *in vitro* experiments in rats [9, 13] and humans [13] reported there is no frequency dependence in membrane polarization by weak EFs. Additionally, consistent evidence from *in vitro* studies in rats [9, 10, 12, 13], ferrets [14], and humans [13], as well as *in vivo* recordings in rats [11], ferrets [14, 15] and nonhuman primates [16-20] showed that the weak EF can alter neural spike timing and cause entrainment. Yet, the degree of entrainment is highly variable within and across cell types. Some *in vivo* experiments in humans [23, 24] even revealed that the current intensities commonly used may not be sufficient to genuinely entrain neural activity. These contradictory findings underscore the necessity of using computational models to quantify and understand the variable effects of tACS on cellular activity.

Multi-Compartmental Neuronal Models

The neural response to tACS is not only determined by the induced EF but also depends on cell properties, including biophysics, morphology, orientation, and ongoing brain activity. Using EF distribution alone is not sufficient to predict all cellular effects of tACS, which should be coupled to single-neuron models. Multi-compartmental models are powerful tools for predicting cellular responses to spatially distributed EF. This type of model discretizes the complex cell morphology into small compartments. Each compartment includes its specific membrane capacitance, resistance, ionic channel, and morphological features (i.e., length and diameter). Adjacent compartments are connected by an intracellular (axial) resistance. The membrane potential gradient along the neurites generates axial currents flowing between compartments. The branch points in the dendrites or axon connect to at least three neighboring compartments. The conductance-based models introduced by Hodgkin and Huxley [55] provide powerful tools for describing the relationship between electrical activity and underlying ionic currents in each compartment. According to Hodgkin-Huxley (HH) formalism, an ionic current is calculated as the product of its conductance and driving force. See reference [56] for a more comprehensive description of such models.

The multi-compartmental conductance-based neuronal models with realistic morphologies have been developed and validated for a wide range of cell types across animal species and humans, which are publicly available through repositories such as ModelDB, GitHub, and the library of Blue Brain models. A common software for simulating compartmental models is the NEURON environment [57], which offers a user-friendly graphical interface. It also allows users to develop custom models, execute simulations, and optimize parameters using Python, MATLAB or its specific programming language based on hoc.

tACS is modeled by applying the induced EF to each cell compartment as its extracellular voltage using NEURON's *extracellular* mechanism [58-60]. The spatial morphologies of multi-compartmental models allow them to effectively describe the biophysical effects of EF on cell membrane. Since large current sources generated by the electrode placed at the scalp are distant from underlying cells, the induced EF has a low spatial gradient at the scale of individual neurons [61, 62]. Thus, when introducing the EF generated by a scalp electrode to a neuronal model, the field is often assumed to be uniform, i.e., the quasi-uniform assumption [59, 61-63].

According to the HH framework, transmembrane potential dynamics emerge from the interactions of intrinsic membrane properties, which include passive capacitance-resistance and voltage-gated ionic conductances [56]. These properties collectively govern cellular filtering behaviors over a range of stimulation frequencies. When an oscillatory EF is applied, it modulates transmembrane voltage by altering the extracellular potential in each neuronal compartment. Such periodic perturbations interact with the membrane time constant and ion channel kinetics, thereby conferring an inherent frequency dependence on cellular response to oscillatory EFs.

Modeling Studies on Membrane Polarization

Membrane polarization is the subthreshold response of resting neurons to weak EFs, which significantly depends on cell morphology and stimulation frequency. Multi-compartmental HH-type models have been used to simulate tACS-induced membrane polarization (summarized in Table 1). Under the quasi-uniform assumption, these studies directly apply weak sinusoidal EFs to isolated neuronal models without synaptic input or other external stimuli.

Computational studies have examined the frequency-dependent polarization response in subcellular elements of neocortical layer 5 pyramidal cells (L5 PCs), including dendrites, soma, and axon. Toloza et al [59] applied weak sinusoidal EFs to a multi-compartmental PC model, and field intensity is limited to 5 mV/mm peak-to-peak to make sure cellular response is subthreshold. They found that the membrane polarization in the apical dendrites is opposite to the soma and basal dendrites. When the apical region is depolarized, the basal region is hyperpolarized, and vice versa. Membrane polarization depends on field orientation relative to the cell, and the maximal polarization occurs when the EF is parallel to the soma-to-dendritic axis. These simulations are consistent with earlier modeling [64] and *in vitro* [65] results. Membrane response is also shaped by EF frequency. The polarization in the apical tuft exhibits a frequency resonance at 20 ± 4 Hz, corresponding to a band-pass behavior. The polarization in other cell compartments decreases monotonically with increasing stimulation frequency, exhibiting a low-pass filter behavior. The hyperpolarization-activated cation current (I_h) is the primary ionic mechanism that leads to the resonance response in distal dendrites, and its conductance density controls the resonance frequency. Subsequently, Aspart et al [66] used multi-compartmental models to quantify the frequency-dependent polarization profile in the dendrites and soma of a L5b PC to AC fields of sinusoidal waveform. They calculated cell sensitivity to AC fields by the ratio of polarization amplitude to field amplitude. In their simulations, the field sensitivity in apical dendrites exhibits a frequency resonance around 10-20 Hz, which is not

observed in the soma or basal dendrites. They related these differential frequency-dependent polarization profiles to cell morphology and active channels. The former increases field sensitivity in the apical dendrites, while the presence of high density of h-type channels decreases field sensitivity at low field frequencies. We recently used two-compartment models to analyze the membrane polarization induced by oscillating EFs in the frequency domain [67]. We applied linear system analysis to compute the transfer functions of the models, which were then used to understand the frequency-dependent patterns of membrane polarization. We showed that the presence of I_h introduces a new zero and pole to dendritic transfer function, reducing polarization amplitude at low frequencies and causing a visible frequency resonance. We also found that the compartment geometry, internal coupling conductance, and other ionic currents affect the polarization response mainly by altering the gain and poles of transfer functions.

Membrane polarization has also been quantified in different types of cells. Tran et al [60] examined somatic polarization in L1 neurogliaform cell (NGC), L2/3 PC, L4 large basket cell (LBC), L5 PC, and L6 PC using multi-compartmental models with oscillatory EFs. They applied polarization length to quantify cell sensitivity to applied EF, which was computed by somatic polarization per unit field. They showed that there is a linear relationship between somatic polarization and EF strength, and the mean coefficient of determination R^2 is 0.9818 over the set of all neurons. L5 PC exhibits the highest polarization lengths, followed by L6 PC and L2/3 PC. L1 NGC and L4 LBC have lower values than PCs. Recently, we used a set of multi-compartmental models to examine the polarization response in the subcellular elements of above five cell types to sinusoidal EFs [68]. For each cell type, we included five virtual clones with random variations in their dendritic and axonal morphologies, which were previously validated to replicate cellular responses to weak fields [61]. Our simulations showed that membrane polarization varies by cell type and subcellular element. The somatic polarization in PCs is sensitive to sinusoidal EF that is oriented roughly parallel to the cortical column, while the polarization sensitivity to field direction for non-pyramidal cells varies between clones. Axon usually exhibits the highest polarization, followed by the dendrites and soma. For PCs, the polarization in the apical dendrites exhibits a visible frequency resonance, while the other subcellular elements primarily exhibit low-pass behavior. These findings are consistent with above mentioned studies [59, 66, 67]. The subcellular elements of non-pyramidal cells exhibit complex frequency-dependent polarization profiles. Similarly, Gaugain et al [69] found that somatic polarization in PCs is the highest at direct current and decreases exponentially with AC frequency, which corresponds to a low-pass filter behavior. The polarization in inhibitory neurons exhibits a resonance in the 5-15 Hz range. L5 PCs have the highest polarization lengths, and somatostatin and parvalbumin cells have lower values.

Modeling Studies on Entrainment of Spiking Activity

The subthreshold membrane polarization by tACS can alter spike timing and entrain neural activity. The multi-compartmental HH-type models have also been used to examine these effects on ongoing firing activity (summarized in Table 2). In this scenario, the synaptic inputs are applied to multi-compartmental models to generate spontaneous firing. The neural entrainment is commonly quantified by phase locking value (PLV), which measures spike timing synchronization relative to tACS waveform [60, 69]. The minimum PLV is 0, which means the spike timings are uniformly distributed over all phases. The maximum value is 1, which means the spike timing is perfectly synchronized to a specific phase of tACS.

Computational studies have investigated spike entrainment by tACS in different types of cortical cells. In these studies, tACS was modeled by directly applying a spatially uniform EF with sinusoidal waveform to an isolated multi-compartmental model. Using this method, Tran et al [60] systematically examined the effects of tACS on firing activity in L1 NGC, L2/3 PC, L4 LBC, L5 PC, and L6 PC. To generate spontaneous firing activity, an excitatory synaptic input was added to each cell at a random location on the apical dendrite for PCs or the basal dendrite for interneurons. A stochastic Poisson process was used to model the presynaptic input. The synaptic conductance

Table 1. Summary of Multi-compartmental Modeling Studies on Membrane Polarization.

Reference	Cortical Cell Type	Main Results
Toloza et al [59]	L5 PC	I_h is the primary ionic mechanism that leads to the resonance response to tACS in the apical dendrites.
Aspart et al [66]	L5 PC	Cell morphology and I_h contribute to the resonance in the apical dendrites.
Huang et al [67]	PC	Passive membrane properties and I_h underlie frequency-dependent polarization by altering the model's transfer function.
Tran et al [60]	L1 NGC, L2/3 PC, L4 LBC, L5 PC, L6 PC	L5 PC exhibits the highest polarization lengths, followed by L6 PC and L2/3 PC. L1 NGC and L4 LBC have lower values than PCs.
Huang et al [68]	L1 NGC, L2/3 PC, L4 LBC, L5 PC, L6 PC	Membrane polarization varies by cell type and subcellular element. Axon usually exhibits the highest polarization, followed by the dendrites and soma.
Gaugain et al [69]	L2/3 PC, L5 PC, L6 PC, VIP interneurons, SST interneurons, PV interneurons	Somatic polarization in PCs decreases with frequency, which exhibits a resonance in inhibitory neurons. L5 PCs have the highest polarization lengths, and SST and PV cells have lower values.

was modeled using a two-exponential function. They found that sine-wave EF does not alter the firing rate of cortical cells when field intensity is in the range of human experiments (i.e., < 1 V/m). However, such weak fields can entrain the spiking activity in L5 PC and L4 LBC. L2/3 and L6 PCs exhibit weaker entrainment than L5 PC and L4 LBC, and no entrainment is observed in L1 NGC. The cell-type-specific entrainment is related to neuronal morphology and cell biophysics. Recently, Gaugain et al [69] found that the phase entrainment of cortical cells is dependent on EF intensity and frequency. In their simulations, the presynaptic spike train was also generated by a stochastic Poisson distribution. The multiple synapses and their parameters were determined to generate reproducible firing activity with a mean rate at 10 Hz in each cell. They showed that there is a linear increase in entrainment to tACS frequency with EF intensity. When EF intensity is 10 V/m, L5 PCs exhibit the highest entrainment at their intrinsic firing frequency, which decays with stimulus frequency. The entrainment in inhibitory neurons increases with frequency. They also developed three-compartment PC model and single-compartment inhibitory neuron model to replicate above simulations. These simplified models can be used for faster computation of network-level dynamics with tACS.

To mechanistically understand the morphology-dependent effects of tACS, several studies [70, 71] employed integrate-and-fire (IF) models to approximate neural activity generated in a biophysically more sophisticated ball-and-stick (BS) model. The BS model consists of a lumped somatic compartment attached to a passive dendritic cable with a specified length. The IF model provides a simple phenomenological description of spike generation while retaining biologically plausibility of HH-type dynamics [72]. In IF models, a spike is generated when membrane potential exceeds a predefined threshold. Aspart et al [70] developed extended IF models to reflect the morphology-dependent EF effects extracted from a BS model. The *in vivo* like noisy synaptic inputs were used to generate spontaneous spiking, which were modeled as Ornstein-Uhlenbeck processes. They found that an oscillatory EF causes spike rate resonance and the resonance frequency depends on synaptic input location, which is related to the dendritic filter of synaptic inputs. With the similar technique, Ladenbauer and Obermayer [71] analytically determined the parameters of a two-compartment model to reproduce somatic voltage dynamics in a BS model. The IF formalism was used to model the spike dynamics in each compartment. They found that the oscillatory EF (1 V/m) causes a clear resonance in spike rate when its frequency is in the beta and low gamma bands. They further showed that the weak field effectively reflects anti-correlated inputs at the soma and dendrite, which modulate firing activity and lead to spike rate resonance. Using the two-compartment models described above, we recently investigated the effects of oscillatory EFs on spike train correlations between pairs of unconnected neurons driven by shared fluctuating dendritic inputs [73]. We observed that output correlation increases with EF intensity while exhibits resonance at specific field frequencies. This correlation resonance is influenced by the morphological differences between the somatic and dendritic compartments, with increased structural asymmetry resulting in more pronounced resonant behavior. These findings were further validated using morphologically detailed PC models.

An isolated multi-compartmental model cannot account for all cellular effects of tACS, and it is necessary to examine cellular responses to stimulation in a neuronal network with synaptic connections. Multi-compartmental models incorporate numerous variables, parameters, and nonlinearities. Incorporating these models into networks with synaptic connections to simulate cellular responses thus significantly increases computational cost. For this reason, simpler neuronal models are often appropriate for network-scale simulations of tACS. The relevant HH-type model usually includes two compartments, which is the minimal individual neuronal unit to capture the spatial polarization by EFs [71, 73, 74]. One compartment represents the apical dendrite, and the other compartment is the soma. Particularly, they are still computationally efficient when simulating network dynamics. The method for coupling EF to a two-compartment model is the same as that used in multi-compartmental models. With the network of two-compartmental models, Zhao et al [75] found that low intensity tACS (< 0.3 V/m) desynchronizes neural firing relative to ongoing endogenous oscillations, while higher intensity stimulation (> 0.3 V/m) directly entrains neural firing. These are consistent with experimental recordings in the nonhuman primate brain [20]. Compared to isolated single cells, tACS-induced entrainment is amplified by synaptic coupling and network effects. Their simulations also revealed that oscillatory EFs directly entrain pyramidal cell and then drive the interneurons. Note that the two-compartment models do not include realistic cell morphology, which is an important factor that may lead to variability in single neuron responses to tACS [60, 66, 70]. Importantly, such simplified models are unable to simulate membrane polarization in dendritic and axonal terminals as well as their arbors, and thus neglect tACS effects on presynaptic and postsynaptic compartments [61]. All these factors can affect their predictions on input-output properties in single neurons and further alter network-level activity. Simulation of tACS effects on large-scale networks with morphologically detailed neuronal models can be executed on the supercomputers [61, 76]. Further, there were studies using networks of phenomenological models (such as, Izhikevich or IF models) to simulate the entrainment of cortical oscillations by tACS, which were reviewed in reference [27] and not covered here.

Above studies use a uniform EF to describe tACS, which do not consider the anatomical distribution of EFs. Wischnewski et al [19] integrated multi-compartmental models of L5 thick-tufted PCs with a realistic head model to simulate tACS effects on spiking activities. Alternating currents were applied to the scalp anterior and posterior of motor cortex through two electrodes. The head model predicts that the EF is strongest at crown of the precentral gyrus, which is 0.31 mV/mm and decreases with depth into the sulcus. Such EF significantly entrains L5 PCs without altering firing rates. The neural entrainment by tACS depends on the orientation of cortical cells. Since the locations of PCs in anterior and posterior wall of the precentral gyrus are along electric current direction, they are more entrained than those at the crown and the bottom of the sulcus. Further, the anterior wall and posterior wall are entrained at different phases. Wischnewski et al [19] also developed a simplified microcircuit model with two PCs and one interneuron, and each neuron was described by a two-compartment model consisting of a soma and a dendrite. Combined with the realistic head model, they replicated the phase shifts

over time observed in experimental recordings, suggesting that N-methyl-D-aspartate (NMDA)-mediated synaptic plasticity is a factor that drives above phase precession. We recently used multiscale modeling to examine how L5 PCs in primary motor cortex respond to conventional M1-SO tACS [77]. The simulations of an anatomically accurate head model showed that the induced EFs distribute heterogeneously across the L5 surface of interest. By calculating PLV and preferred phase of morphologically realistic neuronal models, we found that the direction and intensity of heterogeneous EF and cell morphology are factors that contribute to the diverse entrainments. Our simulations also validated the quasi-uniform assumption used for modeling tACS effects on spike entrainment. The synaptic inputs in above two studies are modeled using a similar approach to Tran et al [60]. Note that such multiscale models were also applied to quantify the axonal and dendritic

Table 2. Summary of Multi-compartmental Modeling Studies on Entrainment of Spiking Activity.

Reference	Neuronal Model	tACS Model	Main Results
Tran et al [60]	isolated multi-compartmental model with realistic morphology	uniformly distributed sinusoidal EF	Weak fields (< 1 V/m) entrain spiking activity in L5 PC and L4 LBC. L2/3 and L6 PCs exhibit weaker entrainment than L5 PC and L4 LBC, and no entrainment is observed in L1 NGC. Cell-type-specific entrainment is related to neuronal morphology and biophysics.
Gaugain et al [69]	isolated multi-compartmental model with realistic morphology	uniformly distributed sinusoidal EF	Phase entrainment depends on EF intensity and frequency. L5 PCs exhibit the highest entrainment at 10 Hz when field intensity is 10 V/m, which decays with stimulus frequency. The entrainment in inhibitory cells increases with frequency.
Aspart et al [70]	extended IF model developed based on a BS model	uniformly distributed sinusoidal EF	An oscillatory EF causes spike rate resonance and the resonance frequency depends on synaptic input location, which is related to the dendritic filter for synaptic inputs.
Ladenbauer and Obermayer [71]	two-compartment IF model developed based on a BS model	uniformly distributed sinusoidal EF	An oscillatory EF (1 V/m) effectively reflects anti-correlated inputs at the soma and dendrite, which modulate firing activity and lead to spike rate resonance.
Huang et al [73]	two-compartment IF model developed based on a BS model	uniformly distributed sinusoidal EF	Spike train correlation increases with EF intensity while exhibits resonance at specific field frequencies. This correlation resonance is influenced by the morphological differences between the somatic and dendritic compartments.
Zhao et al [75]	cortical network consisting of 800 PCs and 200 interneurons, and each neuron is described by a two-compartment HH-type model	uniformly distributed sinusoidal EF	Low intensity EF (< 0.3 V/m) desynchronizes neural firing relative to ongoing endogenous oscillations, while higher intensity field (> 0.3 V/m) directly entrains neural firing. tACS-induced entrainment is amplified by synaptic coupling and network effects. The oscillatory EFs directly entrain PCs and then drive the interneurons.
Wischnewski et al [19]	isolated multi-compartmental model with realistic morphology	EFs calculated in a realistic head model	EF entrains L5 PCs without altering firing rates, which depends on the orientation of cortical cells. The PCs in anterior and posterior wall of the precentral gyrus are more entrained than those at the crown and the bottom of the sulcus.
Wischnewski et al [19]	a microcircuit with two PCs and one interneuron, and each neuron is described by a two-compartment HH-type model	EFs calculated in a realistic head model	NMDA-mediated synaptic plasticity is a factor that drives the phase shifts over time observed in experimental recordings.
Huang et al [77]	isolated multi-compartmental model with realistic morphology	EFs calculated in a realistic head model	EF heterogeneity and cell morphology are factors that contribute to diverse entrainments. The quasi-uniform assumption used for modeling tACS effects on spike entrainment is validated.

polarization by transcranial direct current stimulation [61] and cortical neuron activation by transcranial magnetic stimulation [78]. These studies collectively indicate that the multiscale modeling is a promising approach for understanding cellular response to noninvasive brain stimulation.

Conclusions

tACS offers a noninvasive means to probe and modulate neural oscillations, yet fundamental questions remain about its ability to entrain neuronal activity at conventionally applied intensities. Multiscale computational models provide a critical framework for resolving these controversies by linking macroscopic EF distributions to cell-type-specific polarization and spike entrainment. Realistic head models have clarified how anatomy, tissue conductivity, stimulation parameters, and electrode montage shape field strength, while multi-compartmental neuronal models have demonstrated how cell morphology, ionic currents, and synaptic inputs govern cellular responsiveness.

Data-driven methods have been applied to develop multiscale models to reproduce and integrate experimental data. Markram et al [76] used a multi-objective optimization to constrain the vector of ion channel conductance densities in neocortical microcircuitry to reproduce recorded spike features. Dura-Bernal et al [79] applied a hyperparameter optimization framework to tune synaptic weights in auditory thalamocortical circuits to produce physiological firing rates. The resulting data-driven multiscale models were used to interpret the cellular and circuit mechanisms underlying experimental observations. Therefore, the data-driven integration of multiscale models with experimental recordings across species and human neuroimaging will be essential for identifying cell- and region-specific mechanisms of tACS, reconciling translational differences, and capturing excitatory-inhibitory network interactions.

Further, the convolutional neural networks were previously used to rapidly predict EF distribution in brain tissues [80-81] and activation threshold in cortical cells [82] during transcranial magnetic stimulation. The temporal convolutional networks were applied to predict the subthreshold dynamics and spike timing in L5 PCs with synaptic inputs [83]. The hierarchical convolutional neural networks were used to model neural single-unit and population responses in higher visual cortical areas [84]. These studies suggest that artificial neural networks could be introduced to assist in multiscale tACS modeling and bridge the data at different scales. By advancing toward individualized, validated, and clinically informed modeling frameworks, potentially enhanced by artificial intelligence technologies, future work can transform tACS from a variable experimental tool into a precise neuromodulation strategy with robust therapeutic applications.

Abbreviations

VIP: vasoactive intestinal peptide; SST: somatostatin; PV: parvalbumin.

Author Contributions

GSY contributed to conceptualization, literature review, supervision, manuscript writing, and revision. XBH and XLH contributed to literature review, manuscript writing, and revision. FZ and JTC contributed to literature review and revision. SL contributed to conceptualization, literature review, manuscript writing, and revision.

Acknowledgements

Not applicable.

Ethics Approval and Consent to Participate

Not applicable.

Funding information

This work was sponsored by National Natural Science Foundation of China (82371512), Natural Science Foundation of Tianjin (24JCYBJC01000), Tianjin Health Research Project (TJWJ2024MS037) and Tianjin Key Medical Discipline Construction Project (TJYXZDXK-3-015B). All funding had no role in study design, data analysis, paper submission and publication.

Competing Interests

The authors declare that they have no existing or potential commercial or financial relationships that could create a conflict of interest at the time of conducting this study.

Data Availability

All data needed to evaluate the conclusions in the paper are present in the paper or the Supplementary Materials. Additional data related to this paper may be requested from the authors.

References

[1] Antal A, Paulus W. (2013). Transcranial alternating current stimulation (tACS). Front Hum Neurosci, 7, 317. http://doi.org/10.3389/fnhum.2013.00317

[2] Van Hoornweder S, Stagg CJ, Wischnewski M. (2025). Personalizing transcranial electrical stimulation. Trends Neurosci, 48(9), 663-678. https://doi.org/10.1016/j.tins.2025.07.007

[3] Wischnewski M, Alekseichuk I, Opitz A. (2023). Neurocognitive, physiological, and biophysical effects of transcranial alternating current stimulation. Trends Cogn Sci, 27(2),189-205. https://doi.org/10.1016/j.tics.2022.11.013

[4] Riddle J, Frohlich F. (2021). Targeting neural oscillations

with transcranial alternating current stimulation. Brain Res, 1765, 147491. https://doi.org/10.1016/j.brainres.2021.147491
[5] Agboada D, Zhao Z, Wischnewski M. (2025). Neuroplastic effects of transcranial alternating current stimulation (tACS): from mechanisms to clinical trials. Front Hum Neurosci, 19, 1548478. https://doi.org/10.3389/fnhum.2025.1548478
[6] Gholamali Nezhad F, Martin J, Tassone VK, Swiderski A, Demchenko I, Khan S, et al. (2024). Transcranial alternating current stimulation for neuropsychiatric disorders: a systematic review of treatment parameters and outcomes. Front Psychiatry, 15, 1419243. https://doi.org/10.3389/fpsyt.2024.1419243
[7] Biačková N, Adamová A, Klírová M. (2024). Transcranial alternating current stimulation in affecting cognitive impairment in psychiatric disorders: a review. Eur Arch Psychiatry Clin Neurosci, 274(4), 803-826. https://doi.org/10.1007/s00406-023-01687-7
[8] Liu A, Vöröslakos M, Kronberg G, Henin S, Krause MR, Huang Y, et al. (2018). Immediate neurophysiological effects of transcranial electrical stimulation. Nat Commun, 9(1), 5092. https://doi.org/10.1038/s41467-018-07233-7
[9] Anastassiou CA, Perin R, Markram H, Koch C. (2011). Ephaptic coupling of cortical neurons. Nat Neurosci, 14(2), 217-23. https://doi.org/10.1038/nn.2727
[10] Deans JK, Powell AD, Jefferys JG. (2007). Sensitivity of coherent oscillations in rat hippocampus to AC electric fields. J Physiol, 583(Pt 2), 555-65. https://doi.org/10.1113/jphysiol.2007.137711
[11] Ozen S, Sirota A, Belluscio MA, Anastassiou CA, Stark E, Koch C, et al. (2010). Transcranial electric stimulation entrains cortical neuronal populations in rats. J Neurosci, 30(34), 11476-85. https://doi.org/10.1523/JNEUROSCI.5252-09.2010
[12] Francis JT, Gluckman BJ, Schiff SJ. (2003). Sensitivity of neurons to weak electric fields. J Neurosci, 23(19), 7255-61. https://doi.org/10.1523/JNEUROSCI.23-19-07255.2003
[13] Lee SY, Kozalakis K, Baftizadeh F, Campagnola L, Jarsky T, Koch C, et al. (2024). Cell-class-specific electric field entrainment of neural activity. Neuron, 112(15), 2614-2630.e5. https://doi.org/10.1016/j.neuron.2024.05.009
[14] Fröhlich F, McCormick DA. (2010). Endogenous electric fields may guide neocortical network activity. Neuron, 67(1), 129-43. https://doi.org/10.1016/j.neuron.2010.06.005
[15] Huang WA, Stitt IM, Negahbani E, Passey DJ, Ahn S, Davey M, et al. (2021). Transcranial alternating current stimulation entrains alpha oscillations by preferential phase synchronization of fast-spiking cortical neurons to stimulation waveform. Nat Commun, 12(1), 3151. https://doi.org/10.1038/s41467-021-23021-2
[16] Krause MR, Vieira PG, Csorba BA, Pilly PK, Pack CC. (2019). Transcranial alternating current stimulation entrains single-neuron activity in the primate brain. Proc Natl Acad Sci U S A, 116(12), 5747-5755. https://doi.org/10.1073/pnas.1815958116
[17] Vieira PG, Krause MR, Pack CC. (2020). tACS entrains neural activity while somatosensory input is blocked. PLoS Biology, 18(10), e3000834. https://doi.org/10.1371/journal.pbio.3000834
[18] Johnson L, Alekseichuk I, Krieg J, Doyle A, Yu Y, Vitek J, et al. (2020). Dose-dependent effects of transcranial alternating current stimulation on spike timing in awake nonhuman primates. Sci Adv, 6(36), eaaz2747. https://doi.org/10.1126/sciadv.aaz2747
[19] Wischnewski M, Tran H, Zhao Z, Shirinpour S, Haigh ZJ, Rotteveel J, et al. (2024). Induced neural phase precession through exogenous electric fields. Nat Commun, 15(1), 1687. https://doi.org/10.1038/s41467-024-45898-5
[20] Krause MR, Vieira PG, Thivierge JP, Pack CC. (2022). Brain stimulation competes with ongoing oscillations for control of spike timing in the primate brain. PLoS Biol, 20(5), e3001650. https://doi.org/10.1371/journal.pbio.3001650
[21] Beliaeva V, Polania R. (2020). Can low-intensity tACS genuinely entrain neural activity in vivo? Brain Stimul, 13(6), 1796-1799. https://doi.org/10.1016/j.brs.2020.10.002
[22] Khatoun A, Asamoah B, Mc Laughlin M. (2019). How does transcranial alternating current stimulation entrain single-neuron activity in the primate brain? Proc Natl Acad Sci U S A, 116(45), 22438-22439. https://doi.org/10.1073/pnas.1912927116
[23] Vöröslakos M, Takeuchi Y, Brinyiczki K, Zombori T, Oliva A, Fernández-Ruiz A, et al. (2018). Direct effects of transcranial electric stimulation on brain circuits in rats and humans. Nat Commun, 9(1), 483. https://doi.org/10.1038/s41467-018-02928-3
[24] Lafon B, Henin S, Huang Y, Friedman D, Melloni L, Thesen T, et al. (2017). Low frequency transcranial electrical stimulation does not entrain sleep rhythms measured by human intracranial recordings. Nat Commun, 8(1), 1199. https://doi.org/10.1038/s41467-017-01045-x
[25] Zuidema W, French RM, Alhama RG, Ellis K, O'Donnell TJ, Sainburg T, et al. (2020). Five ways in which computational modeling can help advance cognitive science: lessons from artificial grammar learning. Top Cogn Sci, 12(3), 925-941. https://doi.org/10.1111/tops.12474
[26] Aberra AS, Peterchev AV, Grill WM. (2018). Biophysically realistic neuron models for simulation of cortical stimulation. J Neural Eng, 15(6), 066023. https://doi.org/10.1088/1741-2552/aadbb1
[27] Madadi Asl M, Valizadeh A. (2025). Entrainment by transcranial alternating current stimulation: Insights from models of cortical oscillations and dynamical systems theory. Phys Life Rev, 53, 147-176. https://doi.org/10.1016/j.plrev.2025.03.008
[28] Bland NS, Sale MV. (2019). Current challenges: the ups and downs of tACS. Exp Brain Res, 237(12), 3071-3088. https://doi.org/10.1007/s00221-019-05666-0
[29] Beliaeva V, Savvateev I, Zerbi V, Polania R. (2021). Toward integrative approaches to study the causal role of neural oscillations via transcranial electrical stimulation. Nat Commun, 12(1), 2243. https://doi.org/10.1038/s41467-021-22468-7
[30] Sasaki R. (2025). Modulating cortico-cortical networks with transcranial alternating current stimulation: a minireview. Phys Ther Res, 28(1), 1-8. https://doi.org/10.1298/ptr.R0035
[31] He Y, Liu S, Chen L, Ke Y, Ming D. (2023). Neurophysiological mechanisms of transcranial alternating current stimulation. Front Neurosci, 17, 1091925. https://doi.

org/10.3389/fnins.2023.1091925
[32] Opitz A, Falchier A, Yan CG, Yeagle EM, Linn GS, Megevand P, et al. (2016). Spatiotemporal structure of intracranial electric fields induced by transcranial electric stimulation in humans and nonhuman primates. Sci Rep, 6, 31236. https://doi.org/10.1038/srep31236
[33] Sadeghihassanabadi F, Misselhorn J, Gerloff C, Zittel S. (2022). Optimizing the montage for cerebellar transcranial alternating current stimulation (tACS): a combined computational and experimental study. J Neural Eng, 19(2), 026060. https://doi.org/10.1088/1741-2552/ac676f
[34] Van Hoornweder S, Cappozzo V, De Herde L, Puonti O, Siebner HR, Meesen RLJ, et al. (2024). Head and shoulders-The impact of an extended head model on the simulation and optimization of transcranial electric stimulation. Imaging Neurosci (Camb), 2, imag-2-00379. https://doi.org/10.1162/imag_a_00379
[35] Kasten FH, Duecker K, Maack MC, Meiser A, Herrmann CS. (2019). Integrating electric field modeling and neuroimaging to explain inter-individual variability of tACS effects. Nat Commun, 10(1), 5427. https://doi.org/10.1038/s41467-019-13417-6
[36] Miranda PC, Callejón-Leblic MA, Salvador R, Ruffini G. (2018). Realistic modeling of transcranial current stimulation: the electric field in the brain. Curr Opin Biomed Eng, 8, 20-27. https://doi.org/10.1016/j.cobme.2018.09.002
[37] Hunold A, Haueisen J, Nees F, Moliadze V. (2023). Review of individualized current flow modeling studies for transcranial electrical stimulation. J Neurosci Res, 101(4), 405-423. https://doi.org/10.1002/jnr.25154
[38] Huang Y, Datta A, Bikson M, Parra LC. (2019). Realistic volumetric-approach to simulate transcranial electric stimulation-ROAST-a fully automated open-source pipeline. J Neural Eng, 16(5), 056006. https://doi.org/10.1088/1741-2552/ab208d
[39] Thielscher A, Antunes A, Saturnino GB. (2015). Field modeling for transcranial magnetic stimulation: a useful tool to understand the physiological effects of TMS? Conf Proc IEEE Eng Med Biol Soc, 2015, 222-225. https://doi.org/10.1109/EMBC.2015.7318340
[40] Nielsen JD, Madsen KH, Puonti O, Siebner HR, Bauer C, Madsen CG, et al. (2018). Automatic skull segmentation from MR images for realistic volume conductor models of the head: Assessment of the state-of-the-art. Neuroimage, 174, 587-598. https://doi.org/10.1016/j.neuroimage.2018.03.001
[41] Lee C, Jung YJ, Lee SJ, Im CH. (2017). COMETS2: An advanced MATLAB toolbox for the numerical analysis of electric fields generated by transcranial direct current stimulation. J Neurosci Methods, 277, 56-62. https://doi.org/10.1016/j.jneumeth.2016.12.008
[42] Dannhauer M, Brooks D, Tucker D, MacLeod R. (2012). A pipeline for the simulation of transcranial direct current stimulation for realistic human head models using SCIRun/BioMesh3D. Annu Int Conf IEEE Eng Med Biol Soc, 2012, 5486-5489. https://doi.org/10.1109/EMBC.2012.6347236
[43] Wagner S, Rampersad SM, Aydin Ü, Vorwerk J, Oostendorp TF, Neuling T, et al. (2014). Investigation of tDCS volume conduction effects in a highly realistic head model. J Neural Eng, 11(1), 016002. https://doi.org/10.1088/1741-2560/11/1/016002
[44] Ruffini G, Wendling F, Merlet I, Molaee-Ardekani B, Mekonnen A, Salvador R, et al. (2013). Transcranial current brain stimulation (tCS): models and technologies. IEEE Trans Neural Syst Rehabil Eng, 21(3), 333-45. https://doi.org/10.1109/TNSRE.2012.2200046
[45] Gaugain G, Quéguiner L, Bikson M, Sauleau R, Zhadobov M, Modolo J, et al. (2023). Quasi-static approximation error of electric field analysis for transcranial current stimulation. J Neural Eng, 20(1), 016027. https://doi.org/10.1088/1741-2552/acb14d
[46] Huang Y, Liu AA, Lafon B, Friedman D, Dayan M, Wang X, et al. (2017). Measurements and models of electric fields in the in vivo human brain during transcranial electric stimulation. Elife, 6, e18834. https://doi.org/10.7554/eLife.18834
[47] Opitz A, Yeagle E, Thielscher A, Schroeder C, Mehta AD, Milham MP. (2018). On the importance of precise electrode placement for targeted transcranial electric stimulation. Neuroimage, 181, 560-567. https://doi.org/10.1016/j.neuroimage.2018.07.027
[48] Berger TA, Wischnewski M, Opitz A, Alekseichuk I. (2025). Human head models and populational framework for simulating brain stimulations. Sci Data, 12(1), 516. https://doi.org/10.1038/s41597-025-04886-0
[49] McCann H, Pisano G, Beltrachini L. (2019). Variation in reported human head tissue electrical conductivity values. Brain Topogr, 32(5), 825-858. https://doi.org/10.1007/s10548-019-00710-2
[50] Alekseichuk I, Pabel SC, Antal A, Paulus W. (2017). Intrahemispheric theta rhythm desynchronization impairs working memory. Restor Neurol Neurosci, 35(2), 147-158. https://doi.org/10.3233/RNN-160714
[51] Alekseichuk I, Falchier AY, Linn G, Xu T, Milham MP, Schroeder CE, et al. (2019). Electric field dynamics in the brain during multi-electrode transcranial electric stimulation. Nat Commun, 10(1), 2573. https://doi.org/10.1038/s41467-019-10581-7
[52] Lee S, Shirinpour S, Alekseichuk I, Perera N, Linn G, Schroeder CE, et al. (2023). Predicting the phase distribution during multi-channel transcranial alternating current stimulation in silico and in vivo. Comput Biol Med, 166, 107516. https://doi.org/10.1016/j.compbiomed.2023.107516
[53] Alekseichuk I, Mantell K, Shirinpour S, Opitz A. (2019). Comparative modeling of transcranial magnetic and electric stimulation in mouse, monkey, and human. Neuroimage, 194, 136-148. https://doi.org/10.1016/j.neuroimage.2019.03.044
[54] Ma WW, Wang FX, Yi YY, Huang Y, Li XY, Liu YO, et al. (2024). Mapping the electric field of high-definition transcranial electrical stimulation across the lifespan. Sci Bull, 69(24), 3876-3888. https://doi.org/10.1016/j.scib.2024.10.001
[55] Hodgkin AL, Huxley AF. (1952). A quantitative description of membrane current and its application to conduction and excitation in nerve. J Physiol, 117(4), 500-44. https://doi.org/10.1113/jphysiol.1952.sp004764
[56] David S, Bruce G, Andrew G, editor. Principles of computational modelling in neuroscience. 1st ed. New York: Cambridge University Press; 2011.
[57] Hines ML, Carnevale NT. (1997). The NEURON simulation environment. Neural Comput, 9(6), 1179-209. https://doi.

org/10.1162/neco.1997.9.6.1179
[58] Anastassiou CA, Montgomery SM, Barahona M, Buzsáki G, Koch C. (2010). The effect of spatially inhomogeneous extracellular electric fields on neurons. J Neurosci, 30(5), 1925-1936. https://doi.org/10.1523/JNEUROSCI.3635-09.2010
[59] Toloza EHS, Negahbani E, Fröhlich F. (2018). Ih interacts with somato-dendritic structure to determine frequency response to weak alternating electric field stimulation. J Neurophysiol, 119(3), 1029-1036. https://doi.org/10.1152/jn.00541.2017
[60] Tran H, Shirinpour S, Opitz A. (2022). Effects of transcranial alternating current stimulation on spiking activity in computational models of single neocortical neurons. Neuroimage, 250, 118953. https://doi.org/10.1016/j.neuroimage.2022.118953
[61] Aberra AS, Wang R, Grill WM, Peterchev AV. (2023). Multiscale model of axonal and dendritic polarization by transcranial direct current stimulation in realistic head geometry. Brain Stimul, 16(6), 1776-1791. https://doi.org/10.1016/j.brs.2023.11.018
[62] Bikson M, Dmochowski J, Rahman A. (2013). The "quasi-uniform" assumption in animal and computational models of non-invasive electrical stimulation. Brain Stimul, 6(4), 704-705. https://doi.org/10.1016/j.brs.2012.11.005
[63] Jackson MP, Rahman A, Lafon B, Kronberg G, Ling D, Parra LC, et al. (2016). Animal models of transcranial direct current stimulation: Methods and mechanisms. Clin Neurophysiol, 127(11), 3425-3454. https://doi.org/10.1016/j.clinph.2016.08.016
[64] Radman T, Ramos RL, Brumberg JC, Bikson M. (2009). Role of cortical cell type and morphology in subthreshold and suprathreshold uniform electric field stimulation in vitro. Brain Stimul, 2(4), 215-228.e3. https://doi.org/10.1016/j.brs.2009.03.007
[65] Bikson M, Inoue M, Akiyama H, Deans JK, Fox JE, Miyakawa H, et al. (2004). Effects of uniform extracellular DC electric fields on excitability in rat hippocampal slices in vitro. J Physiol, 557(Pt 1), 175-190. https://doi.org/10.1113/jphysiol.2003.055772
[66] Aspart F, Remme MWH, Obermayer K. (2018). Differential polarization of cortical pyramidal neuron dendrites through weak extracellular fields. PLoS Comput Biol, 14(5), e1006124. https://doi.org/10.1371/journal.pcbi.1006124
[67] Huang X, Wang J, Yi G. (2024). Frequency-domain analysis of membrane polarization in two-compartment model neurons with weak alternating electric fields. Cogn Neurodyn, 18(3), 1245-1264. https://doi.org/10.1007/s11571-023-09980-w
[68] Huang X, Wei X, Wang J, Yi G. (2024). Frequency-dependent membrane polarization across neocortical cell types and subcellular elements by transcranial alternating current stimulation. J Neural Eng, 21(1), 016034. https://doi.org/10.1088/1741-2552/ad2b8a
[69] Gaugain G, Al Harrach M, Yochum M, Wendling F, Bikson M, Modolo J, et al. (2025). Frequency-dependent phase entrainment of cortical cell types during tACS: computational modeling evidence. J Neural Eng, 22(1), 016028. https://doi.org/10.1088/1741-2552/ad9526
[70] Aspart F, Ladenbauer J, Obermayer K. (2016). Extending integrate-and-fire model neurons to account for the effects of weak electric fields and input filtering mediated by the dendrite. PLoS Comput Biol, 12(11), e1005206. https://doi.org/10.1371/journal.pcbi.1005206
[71] Ladenbauer J, Obermayer K. (2019). Weak electric fields promote resonance in neuronal spiking activity: Analytical results from two-compartment cell and network models. PLoS Comput Biol, 15(4), e1006974. https://doi.org/10.1371/journal.pcbi.1006974
[72] Brette R. (2015). What is the most realistic single-compartment model of spike initiation?. PLoS Comput Biol, 11(4), e1004114. https://doi.org/10.1371/journal.pcbi.1004114
[73] Huang X, Wei X, Wang J, Yi G. (2025). Effects of transcranial alternating current stimulation on spike train correlation in two-compartment model neurons. Biol Cybern, 119(4-6), 26. https://doi.org/10.1007/s00422-025-01025-1
[74] Yi GS, Wang J, Wei XL, Tsang KM, Chan WL, Deng B, et al. (2014). Exploring how extracellular electric field modulates neuron activity through dynamical analysis of a two-compartment neuron model. J Comput Neurosci, 36(3), 383-399. https://doi.org/10.1007/s10827-013-0479-z
[75] Zhao Z, Shirinpour S, Tran H, Wischnewski M, Opitz A. (2024). Intensity- and frequency-specific effects of transcranial alternating current stimulation are explained by network dynamics. J Neural Eng, 21(2), 026024. https://doi.org/10.1088/1741-2552/ad37d9
[76] Markram H, Muller E, Ramaswamy S, Reimann MW, Abdellah M, Sanchez CA, et al. (2015). Reconstruction and simulation of neocortical microcircuitry. Cell, 163, 456-92. https://doi.org/10.1016/j.cell.2015.09.029
[77] Huang X, Wei X, Wang J, Yi G. (2025). Multi-scale model of neural entrainment by transcranial alternating current stimulation in realistic cortical anatomy. J Comput Neurosci. https://doi.org/10.1007/s10827-025-00912-7
[78] Aberra AS, Wang B, Grill WM, Peterchev AV. (2020). Simulation of transcranial magnetic stimulation in head model with morphologically-realistic cortical neurons. Brain Stimul, 13(1), 175-189. https://doi.org/10.1016/j.brs.2019.10.002
[79] Dura-Bernal S, Griffith EY, Barczak A, O'Connell MN, McGinnis T, Moreira JVS, et al. (2023). Data-driven multiscale model of macaque auditory thalamocortical circuits reproduces in vivo dynamics. Cell Rep, 42(11), 113378. https://doi.org/10.1016/j.celrep.2023.113378
[80] Yokota T, Maki T, Nagata T, Murakami T, Ugawa Y, Laakso I, et al. (2019). Real-time estimation of electric fields induced by transcranial magnetic stimulation with deep neural networks. Brain Stimul, 12(6), 1500-1507. https://doi.org/10.1016/j.brs.2019.06.015
[81] Li H, Deng ZD, Oathes D, Fan Y. (2022). Computation of transcranial magnetic stimulation electric fields using self-supervised deep learning. Neuroimage, 264, 119705. https://doi.org/10.1016/j.neuroimage.2022.119705
[82] Aberra AS, Lopez A, Grill WM, Peterchev AV. (2023). Rapid estimation of cortical neuron activation thresholds by transcranial magnetic stimulation using convolutional neural networks. Neuroimage, 275, 120184. https://doi.org/10.1016/j.neuroimage.2023.120184
[83] Beniaguev D, Segev I, London M. (2021). Single cortical neurons as deep artificial neural networks. Neuron, 109(17), 2727-2739.e3. https://doi.org/10.1016/j.neuron.2021.07.002

[84] Yamins DL, DiCarlo JJ. (2016). Using goal-driven deep learning models to understand sensory cortex. Nat Neurosci, 19(3), 356-65. https://doi.org/10.1038/nn.4244

Case Report Brain Conflux

Middle Meningeal Artery Embolization for Chronic Subdural Hematoma: A 3-Case Series and Literature Review

Authors

Xingguo Xu, Cunxin Zhu, Zhenxing Yang, Ji Yin, Xianhao Huo, Dejun Huang

Correspondence

hdj1225@163.com (D. Huang), neurohuo@163.com (X. Huo)

Graphical Abstract

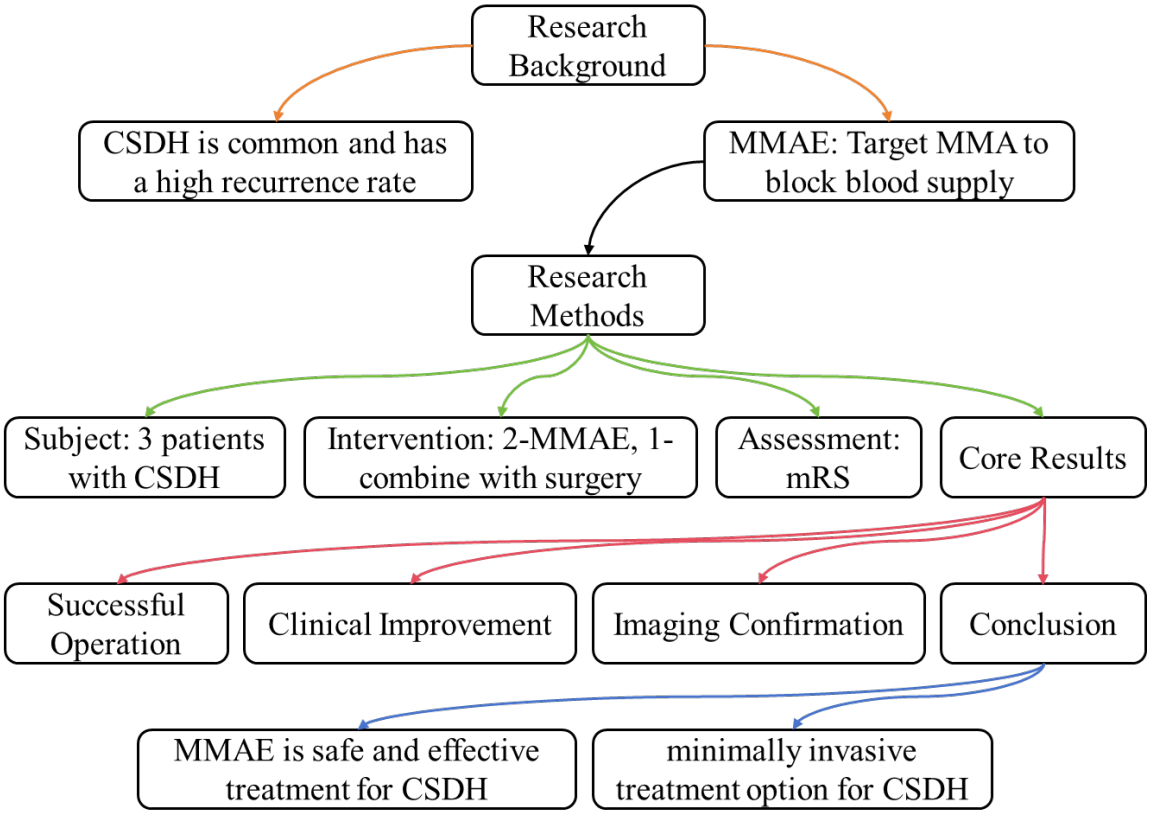

https://doi.org/10.71321/dp20z404

Middle Meningeal Artery Embolization for Chronic Subdural Hematoma: A 3-Case Series and Literature Review

Xingguo Xu[1†], Cunxin Zhu[2†], Zhenxing Yang[1], Ji Yin[1], Xianhao Huo[1*], Dejun Huang[1*]

Received: 2025-09-07 | Accepted: 2025-09-11 | Published online: 2025-11-15

Abstract

Objective: To explore the efficacy of middle meningeal artery embolization (MMAE) in the treatment of chronic subdural hematoma (CSDH).
Methods: We retrospectively analyzed clinical data of 3 patients (with 4-sided hematomas) diagnosed with CSDH who were admitted to the Department of Neurosurgery, General Hospital of Ningxia Medical University in December 2021. Two patients underwent MMAE (one with bilateral MMA embolization), and one patient received MMAE combined with subdural burr hole drainage. All patients were embolized using Onyx glue. Clinical efficacy was evaluated using the modified Rankin Scale (mRS), with a ≥1-point decrease post-treatment defined as symptom improvement. Hematoma absorption was assessed via imaging.
Results: Successful superselective catheterization of the middle meningeal artery (MMA) was achieved in all 3 patients (4-sided hematomas), with complete occlusion of the frontoparietal trunk of the MMA and its main branches. No procedure-related complications occurred. During a 2–4 month follow-up, all patients showed clinical improvement (mRS decreased by 1–2 points). Imaging confirmed complete absorption of all 4-sided hematomas, resolution of clinical symptoms, and no recurrence.
Conclusion: MMAE is a safe, effective, and promising treatment for CSDH.
Keywords: MMAE; CSDH; mRS; Case Series.

Introduction

Chronic subdural hematoma (CSDH) is a common neurosurgical condition, predominantly affecting elderly patients, and is associated with significant morbidity and mortality [1-3]. Current treatment modalities include conservative management, burr hole drainage, and hematoma evacuation [4]. Pharmacological options for CSDH primarily consist of steroids, platelet-activating factor antagonists, and statins [5]. However, conservative treatment success rates vary widely, with failure rates requiring surgical intervention ranging from 15% to 90% [4], and non-surgical approaches are only effective in select patient subgroups [6-10]. Thus, surgical evacuation remains the mainstay for most CSDH cases [11]. Nevertheless, 5%–30% of surgical cases experience hematoma recurrence [12-17], partly because conventional surgery does not address the underlying pathophysiological mechanisms of CSDH formation [18-20].
In recent years, middle meningeal artery embolization (MMAE) has emerged as a minimally invasive approach to target the vascular supply of CSDH, aiming to improve treatment outcomes [21]. This study evaluates the efficacy of MMAE in treating CSDH through a case series and literature review.

Materials and Methods

Clinical Data

Three patients with CSDH were included: 2 males (1 with bilateral hematomas) and 1 female, aged 58–59 years (mean 58.3 years). All had a history of head trauma, with disease duration ranging from 23 to 60 days (mean 37.67 days) (Table 1).

Imaging Data

All patients were diagnosed with CSDH via preoperative cranial CT. One patient had bilateral hematomas, and 2 had unilateral hematomas. Hematoma types included 2 cases (3 sides) of isodense hematomas and 1 case (1 side) of mixed-type hematomas.

1 Department of Neurosurgery, Ningxia Medical University General Hospital
2 Department of Nursing, Qilu Medical University
† These authors contributed equally to this work.
* Corresponding Author.

Table 1. Clinical details of the three patients

Age (years)	Gender	Time from Onset (days)	Symptoms	Hematoma Location	Comorbidities	Surgical Method	Follow-up (months)
59	Male	23	Headache	Left frontal, parietal, temporal, occipital lobes	None	MMAE	4
59	Male	30	Headache	Bilateral frontal and temporal lobes	Hypertension (1 year)	MMAE	2
58	Female	60	Headache, left limb weakness	Right frontal and temporal lobes	None	MMAE + Burr hole drainage	2

Treatment Method

Patients were placed in the supine position, with routine disinfection and draping. The right femoral artery was punctured using the Seldinger technique, and a 6F arterial sheath was inserted. Cerebral angiography was performed, followed by systemic heparinization. Under fluoroscopic guidance, a 6F guiding catheter was advanced into the affected external carotid artery using a 150 cm guidewire. A microcatheter was then navigated into the external carotid artery → maxillary artery → MMA under microguidewire guidance. After injecting DMSO as a solvent, 0.5 mL of Onyx glue was administered to embolize the affected MMA. The procedure was completed by withdrawing the microcatheter and guiding catheter.

Postoperative Management

All patients received postoperative fluid replacement. D-dimer levels were monitored on postoperative day 2:

- If D-dimer levels were not significantly elevated, patients were allowed early ambulation for rehabilitation.
- If D-dimer was elevated, lower extremity Doppler ultrasound was performed; ambulation was permitted if no deep vein thrombosis was detected.

Two patients underwent standalone MMAE with normal postoperative D-dimer levels and ambulated on postoperative day 1. One patient (MMAE + burr hole drainage) had elevated D-dimer but no deep vein thrombosis; the surgical drain was removed at 30 hours, and ambulation was initiated thereafter.

Follow-up

Patients were followed up via outpatient visits and telephone calls for 2–5 months. Neurological function was assessed using the mRS:

- 0: Asymptomatic
- 1: Symptomatic but no disability; able to perform all daily activities
- 2: Mild disability; independent in self-care but unable to resume previous activities
- 3: Moderate disability; walks unassisted but requires help with daily activities
- 4: Severe disability; unable to walk or self-care without assistance
- 5: Bedridden, incontinent, requiring long-term care
- 6: Death

Results

All 3 patients (4-sided hematomas) achieved successful superselective MMA catheterization, with complete occlusion of the frontoparietal trunk of the MMA and its main branches. No procedure-related complications occurred. During follow-up (2–5 months):

- All patients showed clinical improvement: 2 patients had mRS scores decrease from 2 to 0, and 1 patient improved from 3 to 0.
- Imaging confirmed complete absorption of all 4-sided hematomas, resolution of symptoms, and no recurrence (Figures 1–3).

Discussion

CSDH incidence is rising annually [22]. With population aging and increased use of anticoagulants/antiplatelets, the U.S. is projected to see >60,000 new cases yearly by 2030, making CSDH the most common adult neurosurgical diagnosis [1].

The pathophysiology of CSDH involves complex processes. Historically attributed to traumatic bridging vein rupture [23, 24], inflammation is now recognized as a key driver [25, 26], explaining CSDH development in trauma-negative patients or those with delayed onset. Inflammation, membrane formation, angiogenesis, and fibrinolysis synergistically promote hematoma expansion [25]. Conventional surgery relieves mass effect but does not address these mechanisms, leading to recurrence [11, 21]. MMAE targets the vascular supply of CSDH, overcoming this limitation [21].

MMAE is applicable to all CSDH types, complementing drug therapy and burr hole drainage. It is particularly valuable for patients on long-term antiplatelets/anticoagulants, or with thrombocytopenia/coagulation disorders, except those with severe contrast allergies or renal insufficiency. Studies support MMAE's efficacy: Fiorella et al. reported lower treatment failure rates with MMAE vs. standard therapy [27]; multicenter studies highlight its safety as a minimally invasive alternative [28-30].

In our series, 2 patients underwent MMAE (1 bilateral), and 1 received MMAE + burr hole drainage, with complete hematoma resolution and symptom improvement. MMAE works by occluding the MMA (a key blood supply to CSDH capsules) with Onyx glue, cutting off hematoma perfusion and preventing recurrence. Compared to conventional surgery, it reduces infection, rebleeding, and brain tissue damage, enabling faster recovery—critical for elderly patients to minimize bedridden complications.

Limitations include the small sample size (3 patients, 4-sided hematomas) and short follow-up (2–4 months), which restrict generalizability and long-term efficacy assessment. Future

https://doi.org/10.71321/dp20z404

Figure 1. Preoperative CT showing left frontal, parietal, temporal, and occipital CSDH (**A**); left MMA embolization (**B**); 4-month follow-up CT showing complete hematoma absorption (**C**).

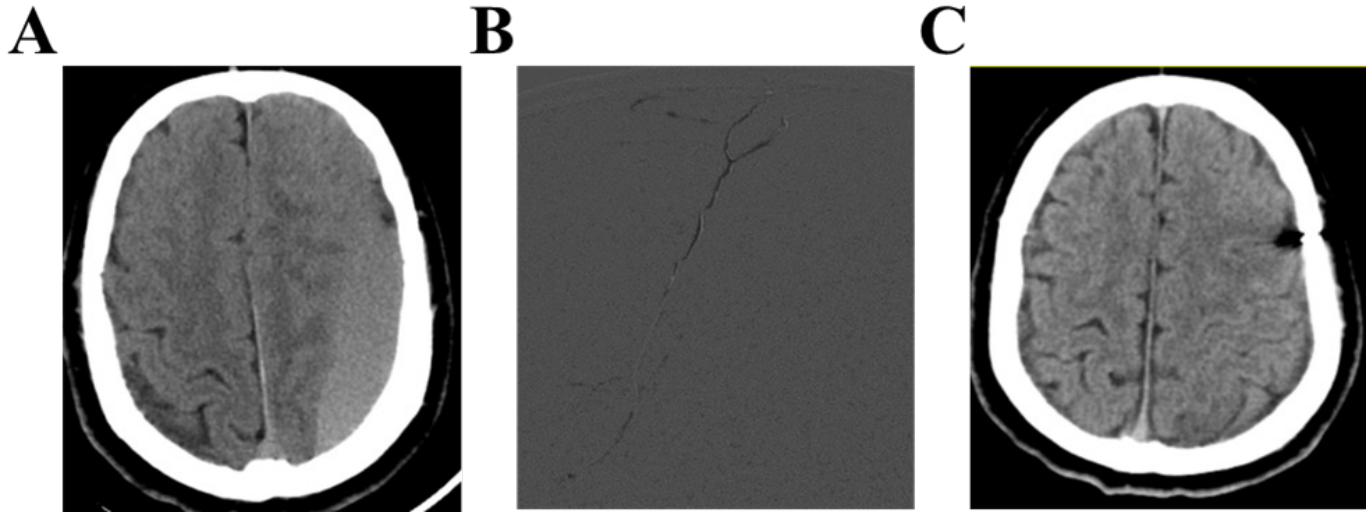

Figure 2. Preoperative CT showing bilateral frontal and temporal CSDH (**A**); bilateral MMA embolization (**B**); 2-month follow-up CT showing complete hematoma absorption (**C**).

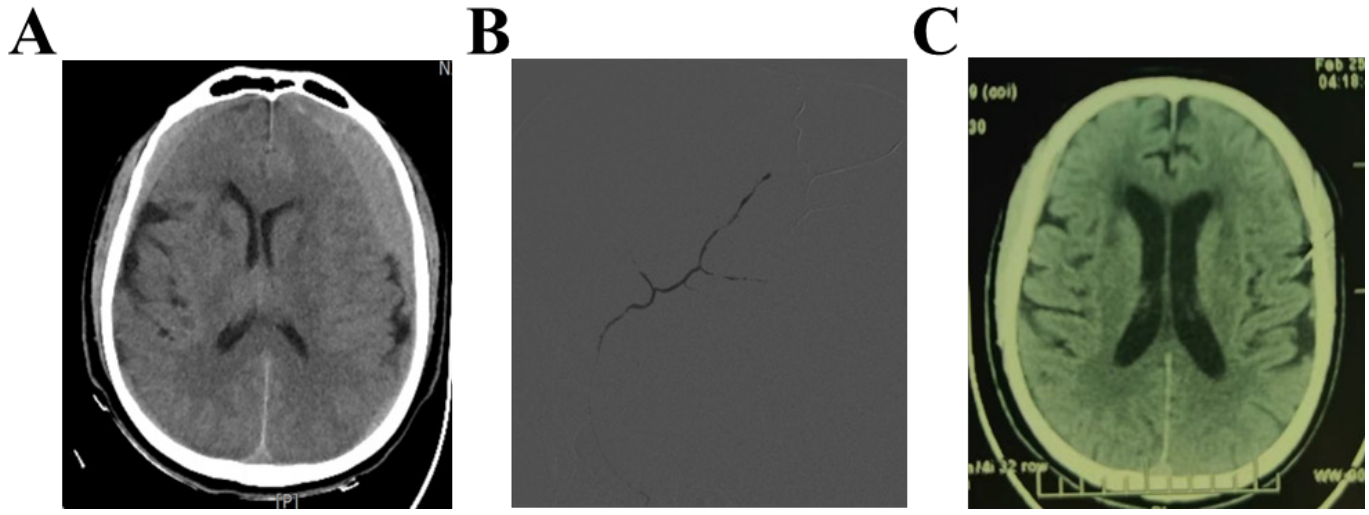

Figure 3. Preoperative CT showing right frontal and temporal CSDH (**A**); right MMA embolization (**B**); 2-month follow-up CT showing complete hematoma absorption (**C**).

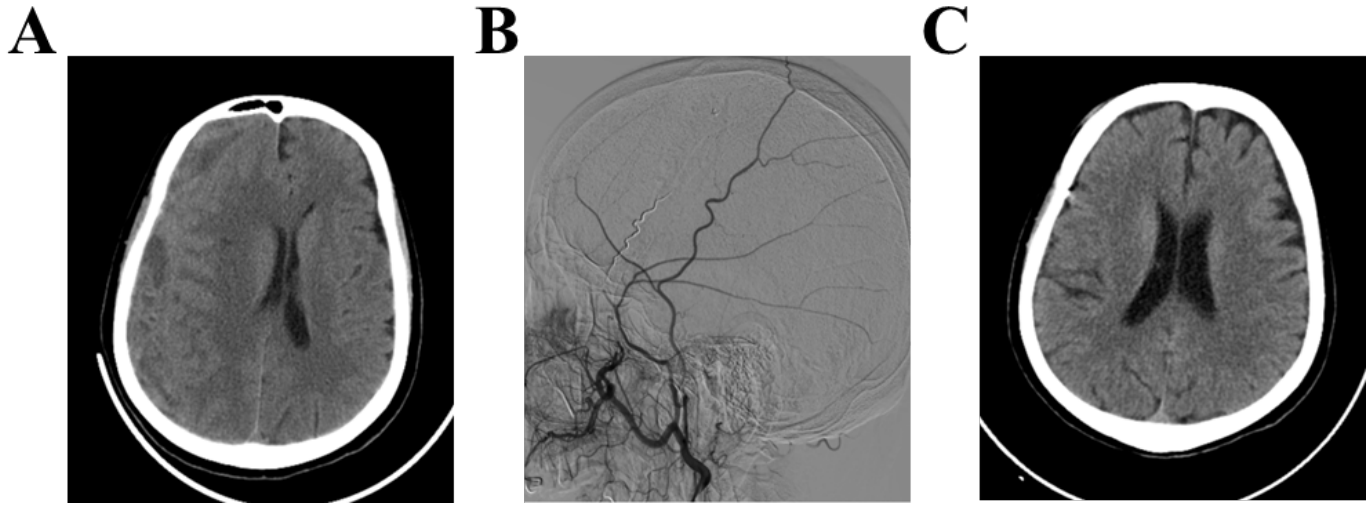

multicenter, large-cohort studies with extended follow-up are needed to validate MMAE's safety and optimize protocols.

Conclusion

MMAE or MMAE combined with burr hole drainage achieved successful occlusion of the MMA, complete hematoma absorption, symptom resolution, and no recurrence in 3 CSDH patients. Supported by literature, MMAE blocks hematoma blood supply, addressing limitations of traditional treatments, and is a safe, effective CSDH therapy. Further research with larger cohorts and longer follow-up is warranted to confirm its broader applicability and long-term outcomes.

Abbreviations

MMAE: Middle Meningeal Artery Embolization; CSDH: Chronic Subdural Hematoma; MMA: Middle Meningeal Artery; mRS: modified Rankin Scale; DMSO: Dimethyl Sulfoxide.

Author Contributions

Dejun Huang and Xianhao Huo conceived the study. Xingguo Xu and Cunxin Zhu collected data, drafted the manuscript, and conducted literature reviews. Zhenxing Yang and Ji Yin revised imaging data. All authors contributed to discussions and final manuscript revisions.

Acknowledgements

Not applicable.

Funding Information

None.

Ethics Approval and Consent to Participate

This study was approved by the Ethics Committee of Ningxia Medical University General Hospital (No. XJS2021120).

Competing Interests

The authors declare no competing interests.

Data Availability

The raw data supporting this study are available from the corresponding authors upon reasonable request.

References

[1] Balser, D., Farooq, S., Mehmood, T., Reyes, M., & Samadani, U. (2015). Actual and projected incidence rates for chronic subdural hematomas in United States Veterans Administration and civilian populations. Journal of neurosurgery, 123(5), 1209–1215. https://doi.org/10.3171/2014.9.JNS141550

[2] Foreman, P., Goren, O., Griessenauer, C. J., Dalal, S. S., Weiner, G., & Schirmer, C. M. (2019). Middle Meningeal Artery Embolization for Chronic Subdural Hematomas: Cautious Optimism for a Challenging Pathology. World neurosurgery, 126, 528–529. https://doi.org/10.1016/j.wneu.2019.03.160

[3] Miranda, L. B., Braxton, E., Hobbs, J., & Quigley, M. R. (2011). Chronic subdural hematoma in the elderly: not a benign disease. Journal of neurosurgery, 114(1), 72–76. https://doi.org/10.3171/2010.8.JNS10298

[4] Ironside, N., Nguyen, C., Do, Q., Ugiliweneza, B., Chen, C. J., Sieg, E. P., James, R. F., & Ding, D. (2021). Middle meningeal artery embolization for chronic subdural hematoma: a systematic review and meta-analysis. Journal of neurointerventional surgery, 13(10), 951–957. https://doi.org/10.1136/neurintsurg-2021-017352

[5] Soleman, J., Nocera, F., & Mariani, L. (2017). The conservative and pharmacological management of chronic subdural haematoma. Swiss medical weekly, 147, w14398. https://doi.org/10.57187/smw.2017.14398

[6] Berghauser Pont, L. M., Dirven, C. M., Dippel, D. W., Verweij, B. H., & Dammers, R. (2012). The role of corticosteroids in the management of chronic subdural hematoma: a systematic review. European journal of neurology, 19(11), 1397–1403. https://doi.org/10.1111/j.1468-1331.2012.03768.x

[7] Sun, T. F., Boet, R., & Poon, W. S. (2005). Non-surgical primary treatment of chronic subdural haematoma: Preliminary results of using dexamethasone. British journal of neurosurgery, 19(4), 327–333. https://doi.org/10.1080/02688690500305332

[8] Qiu, S., Zhuo, W., Sun, C., Su, Z., Yan, A., & Shen, L. (2017). Effects of atorvastatin on chronic subdural hematoma: A systematic review. Medicine, 96(26), e7290. https://doi.org/10.1097/MD.0000000000007290

[9] Poulsen, F. R., Munthe, S., Søe, M., & Halle, B. (2014). Perindopril and residual chronic subdural hematoma volumes six weeks after burr hole surgery: a randomized trial. Clinical neurology and neurosurgery, 123, 4–8. https://doi.org/10.1016/j.clineuro.2014.05.003

[10] Thotakura, A. K., & Marabathina, N. R. (2015). Nonsurgical Treatment of Chronic Subdural Hematoma with Steroids. World neurosurgery, 84(6), 1968–1972. https://doi.org/10.1016/j.wneu.2015.08.044

[11] Ban, S. P., Hwang, G., Byoun, H. S., Kim, T., Lee, S. U., Bang, J. S., Han, J. H., Kim, C. Y., Kwon, O. K., & Oh, C. W. (2018). Middle Meningeal Artery Embolization for Chronic Subdural Hematoma. Radiology, 286(3), 992–999. https://doi.org/10.1148/radiol.2017170053

[12] Amirjamshidi, A., Abouzari, M., Eftekhar, B., Rashidi, A., Rezaii, J., Esfandiari, K., Shirani, A., Asadollahi, M., & Aleali, H. (2007). Outcomes and recurrence rates in chronic sub-

dural haematoma. British journal of neurosurgery, 21(3), 272–275. https://doi.org/10.1080/02688690701272232
[13] Jung, Y. G., Jung, N. Y., & Kim, E. (2015). Independent predictors for recurrence of chronic subdural hematoma. Journal of Korean Neurosurgical Society, 57(4), 266–270. https://doi.org/10.3340/jkns.2015.57.4.266
[14] Torihashi, K., Sadamasa, N., Yoshida, K., Narumi, O., Chin, M., & Yamagata, S. (2008). Independent predictors for recurrence of chronic subdural hematoma: a review of 343 consecutive surgical cases. Neurosurgery, 63(6), 1125–1129. https://doi.org/10.1227/01.NEU.0000335782.60059.17
[15] Leroy, H. A., Aboukaïs, R., Reyns, N., Bourgeois, P., Labreuche, J., Duhamel, A., & Lejeune, J. P. (2015). Predictors of functional outcomes and recurrence of chronic subdural hematomas. Journal of clinical neuroscience : official journal of the Neurosurgical Society of Australasia, 22(12), 1895–1900. https://doi.org/10.1016/j.jocn.2015.03.064
[16] Oh, H. J., Lee, K. S., Shim, J. J., Yoon, S. M., Yun, I. G., & Bae, H. G. (2010). Postoperative course and recurrence of chronic subdural hematoma. Journal of Korean Neurosurgical Society, 48(6), 518–523. https://doi.org/10.3340/jkns.2010.48.6.518
[17] Santarius, T., Kirkpatrick, P. J., Ganesan, D., Chia, H. L., Jalloh, I., Smielewski, P., Richards, H. K., Marcus, H., Parker, R. A., Price, S. J., Kirollos, R. W., Pickard, J. D., & Hutchinson, P. J. (2009). Use of drains versus no drains after burr-hole evacuation of chronic subdural haematoma: a randomised controlled trial. Lancet (London, England), 374(9695), 1067–1073. https://doi.org/10.1016/S0140-6736(09)61115-6
[18] D'Abbondanza, J. A., & Loch Macdonald, R. (2014). Experimental models of chronic subdural hematoma. Neurological research, 36(2), 176–188. https://doi.org/10.1179/1743132813Y.0000000279
[19] Stanisic, M., Aasen, A. O., Pripp, A. H., Lindegaard, K. F., Ramm-Pettersen, J., Lyngstadaas, S. P., Ivanovic, J., Konglund, A., Ilstad, E., Sandell, T., Ellingsen, O., & Sæhle, T. (2012). Local and systemic pro-inflammatory and anti-inflammatory cytokine patterns in patients with chronic subdural hematoma: a prospective study. Inflammation research : official journal of the European Histamine Research Society ... [et al.], 61(8), 845–852. https://doi.org/10.1007/s00011-012-0476-0
[20] Kalamatianos, T., Stavrinou, L. C., Koutsarnakis, C., Psachoulia, C., Sakas, D. E., & Stranjalis, G. (2013). PlGF and sVEGFR-1 in chronic subdural hematoma: implications for hematoma development. Journal of neurosurgery, 118(2), 353–357. https://doi.org/10.3171/2012.10.JNS12327
[21] Kan, P., Maragkos, G. A., Srivatsan, A., Srinivasan, V., Johnson, J., Burkhardt, J. K., Robinson, T. M., Salem, M. M., Chen, S., Riina, H. A., Tanweer, O., Levy, E. I., Spiotta, A. M., Kasab, S. A., Lena, J., Gross, B. A., Cherian, J., Cawley, C. M., Howard, B. M., Khalessi, A. A., … Thomas, A. J. (2021). Middle Meningeal Artery Embolization for Chronic Subdural Hematoma: A Multi-Center Experience of 154 Consecutive Embolizations. Neurosurgery, 88(2), 268–277. https://doi.org/10.1093/neuros/nyaa379
[22] Ducruet, A. F., Grobelny, B. T., Zacharia, B. E., Hickman, Z. L., DeRosa, P. L., Andersen, K. N., Sussman, E., Carpenter, A., & Connolly, E. S., Jr (2012). The surgical management of chronic subdural hematoma. Neurosurgical review, 35(2), 155–169. https://doi.org/10.1007/s10143-011-0349-y
[23] Gelabert-González, M., Iglesias-Pais, M., García-Allut, A., & Martínez-Rumbo, R. (2005). Chronic subdural haematoma: surgical treatment and outcome in 1000 cases. Clinical neurology and neurosurgery, 107(3), 223–229. https://doi.org/10.1016/j.clineuro.2004.09.015
[24] Stroobandt, G., Fransen, P., Thauvoy, C., & Menard, E. (1995). Pathogenetic factors in chronic subdural haematoma and causes of recurrence after drainage. Acta neurochirurgica, 137(1-2), 6–14. https://doi.org/10.1007/BF02188772
[25] Edlmann, E., Giorgi-Coll, S., Whitfield, P. C., Carpenter, K. L. H., & Hutchinson, P. J. (2017). Pathophysiology of chronic subdural haematoma: inflammation, angiogenesis and implications for pharmacotherapy. Journal of neuroinflammation, 14(1), 108. https://doi.org/10.1186/s12974-017-0881-y
[26] Hamou, H. A., Clusmann, H., Schulz, J. B., Wiesmann, M., Altiok, E., & Höllig, A. (2022). Chronic Subdural Hematoma. Deutsches Arzteblatt international, 119(12), 208–213. https://doi.org/10.3238/arztebl.m2022.0144
[27] Fiorella, D., Monteith, S. J., Hanel, R., Atchie, B., Boo, S., McTaggart, R. A., Zauner, A., Tjoumakaris, S., Barbier, C., Benitez, R., Spelle, L., Pierot, L., Hirsch, J. A., Froehler, M., Arthur, A. S., & STEM Investigators (2025). Embolization of the Middle Meningeal Artery for Chronic Subdural Hematoma. The New England journal of medicine, 392(9), 855–864. https://doi.org/10.1056/NEJMoa2409845
[28] Sattari, S. A., Yang, W., Shahbandi, A., Feghali, J., Lee, R. P., Xu, R., Jackson, C., Gonzalez, L. F., Tamargo, R. J., Huang, J., & Caplan, J. M. (2023). Middle Meningeal Artery Embolization Versus Conventional Management for Patients With Chronic Subdural Hematoma: A Systematic Review and Meta-Analysis. Neurosurgery, 92(6), 1142–1154. https://doi.org/10.1227/neu.0000000000002365
[29] Liu, J., Ni, W., Zuo, Q., Yang, H., Peng, Y., Lin, Z., Li, Z., Wang, J., Zhen, Y., Luo, J., Lin, Y., Chen, J., Hua, X., Lu, H., Zhong, M., Liu, M., Zhang, J., Wang, Y., Wan, J., Li, Y., … MAGIC-MT Investigators (2024). Middle Meningeal Artery Embolization for Nonacute Subdural Hematoma. The New England journal of medicine, 391(20), 1901–1912. https://doi.org/10.1056/NEJMoa2401201
[30] Davies, J. M., Knopman, J., Mokin, M., Hassan, A. E., Harbaugh, R. E., Khalessi, A., Fiehler, J., Gross, B. A., Grandhi, R., Tarpley, J., Sivakumar, W., Bain, M., Crowley, R. W., Link, T. W., Fraser, J. F., Levitt, M. R., Chen, P. R., Hanel, R. A., Bernard, J. D., Jumaa, M., … EMBOLISE Investigators (2024). Adjunctive Middle Meningeal Artery Embolization for Subdural Hematoma. The New England journal of medicine, 391(20), 1890–1900. https://doi.org/10.1056/NEJMoa2313472